NSWC TR 89-170

AD-A223 048

SONAR PERFORMANCE ESTIMATION MODEL WITH SEISMO-ACOUSTIC EFFECTS ON UNDERWATER SOUND PROPAGATION

BY JUAN I. ARVELO, JR.

UNDERWATER SYSTEMS DEPARTMENT

27 JUNE 1989

DTIC
ELECTE
JUN 20 1990
S
B
D

NAVAL SURFACE WARFARE CENTER

Dahlgren, Virginia 22448-5000 ● Silver Spring, Maryland 20903-5000

90 06 18 238

REPORT DOCUMENTATION PAGE

1a. REPORT SECURITY CLASSIFICATION UNCLASSIFIED			1b. RESTRICTIVE MARKINGS		
2a. SECURITY CLASSIFICATION AUTHORITY			3. DISTRIBUTION/AVAILABILITY OF REPORT Approved for public release; distribution is unlimited.		
2b. DECLASSIFICATION/DOWNGRADING SCHEDULE					
4. PERFORMING ORGANIZATION REPORT NUMBER(S) NSWC TR 89-170			5. MONITORING ORGANIZATION REPORT NUMBER(S)		
6a. NAME OF PERFORMING ORGANIZATION Naval Surface Warfare Center	6b. OFFICE SYMBOL (If applicable) U25		7a. NAME OF MONITORING ORGANIZATION		
6c. ADDRESS (City, State, and ZIP Code) 10901 New Hampshire Ave. Silver Spring, MD 20903-5000			7b. ADDRESS (City, State, and ZIP Code)		
8a. NAME OF FUNDING/SPONSORING ORGANIZATION	8b. OFFICE SYMBOL (If applicable)		9. PROCUREMENT INSTRUMENT IDENTIFICATION NUMBER		
8c. ADDRESS (City, State, and ZIP Code)			10. SOURCE OF FUNDING NOS		

	PROGRAM ELEMENT NO.	PROJECT NO.	TASK NO.	WORK UNIT NO.
	61152N	R00N0	11	

11. TITLE (Include Security Classification) Sonar Performance Estimation Model with Seismo-Acoustic Effects on Underwater Sound Propagation

12. PERSONAL AUTHOR(S)
Arvelo, Juan I., Jr.

13a. TYPE OF REPORT Technical Review	13b. TIME COVERED FROM TO	14. DATE OF REPORT (Yr., Mo., Day) 1989, June, 27	15. PAGE COUNT 166

16. SUPPLEMENTARY NOTATION

17.	COSATI CODES		18. SUBJECT TERMS (Continue on reverse if necessary and identify by block number)
FIELD	GROUP	SUB GR	Normal Mode Range-Dependent
20	01		Propagation Loss Bottom Elasticity
			Low-Frequency Shear Waves

19. ABSTRACT (Continue on reverse if necessary and identify by block number)

The correct estimation of the performance of any sonar system depends on the accurate computation of the propagation loss of the signal. In underwater acoustics, low-frequency sound is less attenuated and the easiest signal to detect at large distances.

Hence, the theory of normal modes has been modified to incorporate the effects of shear waves from the elastic ocean floor. The effects of absorption have also been included as the imaginary component of the shear and compressional wave numbers. The eigenvalues of the multilayered wave guide are searched in the complex K-plane by the Levenberg-Marquardt minimization of the magnitude of the complex characteristic equation. The liquid layers of the water column are represented by a linear wave number squared with depth to better simulate the sound speed profile. It has been found that the compressional sound speed of an elastic layer can also have a linear wave number squared and that the density in a liquid layer can be a (Cont.)

20. DISTRIBUTION/AVAILABILITY OF ABSTRACT X UNCLASSIFIED/UNLIMITED SAME AS RPT DTIC USERS	21. ABSTRACT SECURITY CLASSIFICATION UNCLASSIFIED	
22a. NAME OF RESPONSIBLE INDIVIDUAL Juan I. Arvelo, Jr.	22b. TELEPHONE NUMBER (Include Area Code) (202) 394-3428	22c. OFFICE SYMBOL U25

DD FORM 1473, 84 MAR   83 APR edition may be used until exhausted   UNCLASSIFIED
All other editions are obsolete   SECURITY CLASSIFICATION OF THIS PAGE

19. variable with depth and still obtain solvable wave equations.

A semi-infinite elastic bottom basement layer with compressional and shear absorption has been included to the normal mode model and it has been found that the absorption causes the wave number spectrum of the radiating modes to be inherently discrete, hence the number of radiating modes are drastically reduced.

The range dependence of the acoustic properties and the boundaries of the ocean have been included by a modified version of the adiabatic normal mode theory. This newly developed version handles the shear wave contribution and the fact that the eigenvalues and depth functions are complex.

The coherent transmission loss in the elastic layers is computed using the magnitude of the acoustic intensity vector and its value in decibels is vastly used in determining the performance of active and passive sonar systems.

Comparisons are made with experimental measurements of the transmission loss of underwater explosives producing very good agreement for frequencies above 100 Hz. At lower frequencies, sound penetrates deeper into the bottom where no data on the acoustic properties is available. Hence, this model is used for inverse scattering predictions of the unknown properties.

FOREWORD

This report incorporates the effects of shear wave from the elastic ocean floor to the normal mode transmission loss model. The possible range dependence of the acoustic properties of the ocean is modeled with a modified version of the adiabatic approximation for slow variations. This newly developed model proves itself very useful for performance estimation of acoustic mines and sonar systems that operate at low frequencies. This work was funded by the Independent Research Board of the Naval Surface Warfare Center.

Approved by:

C. A. KALIVRETENOS, Head
Sensors and Electronics Division

DTIC
COPY
INSPECTED
6

Accession For	
NTIS GRA&I	☑
DTIC TAB	☐
Unannounced	☐
Justification	
By	
Distribution/	
Availability Codes	
Dist	Avail and/or Special
A-1	

CONTENTS

ILLUSTRATIONS

ILLUSTRATIONS (Cont.)

ILLUSTRATIONS (Cont.)

ILLUSTRATIONS (Cont.)

ILLUSTRATIONS (Cont.)

ILLUSTRATIONS (Cont.)

TABLES

CHAPTER 1

INTRODUCTION

An electromagnetic wave in vacuum travels a distance of nearly 300,000 kilometers in just one second. At the same time sound has only traveled about 340 meters. However, the electromagnetic wave attenuates very rapidly in water.[1] Also, the attenuation coefficient of both waves varies significantly with frequency, but low-frequency sound is the best form of underwater radiation known to man.[2]

An acoustic wave incident from the water to the solid sediments of the bottom create a compressional (longitudinal) wave and a shear (transverse) wave as shown by the use of the plane wave approximation of sound.[3-6] This, so called, *birefraction* phenomena is also observed with electromagnetic waves in calcite and it is described by a medium with two indices of refraction. The same phenomenon applies to seismo-acoustics.

With the use of explosive sound sources with a broad frequency band, Pekeris[7] found that the effects of shear waves on the propagation of sound in the water increases with decreasing depth of the water and with decreasing frequency of the propagated sound. Since the attenuation coefficient of sound is directly proportional to its frequency,[2] this and the low-frequency absorption caused by the shear waves makes the ocean wave guide a band-pass filter of the sound emitted by the source.[8]

If the acoustic properties of this ocean wave guide are well known, then it is possible to calculate the optimum frequency of sound propagation.[9,10] It has been observed that sound with frequency below the optimum frequency highly depends on the acoustic properties of the bottom sediments because of the relatively small absorptive effects of low frequency sound, while the transmission of sound with frequency greater than the optimum frequency depends mostly on the acoustic properties of the water column.[11]

Since the optimum frequency of most ocean environments is smaller than

one kilohertz, an underwater acoustic model for the propagation of sound in this frequency band is needed. This model must contain the effects of the acoustic properties of the water column and the seismo-acoustic properties of the bottom sediments.[12]

The ray theory is highly satisfactory to predict and explain some electromagnetic phenomena, and it is very useful in predicting the transmission loss of high-frequency sound. However, this asymptotic approximation cannot explain wave-type phenomena such as diffraction and interference.[13] Pedersen[14] pointed out that approximating the ocean's sound speed profile by layers of constant sound speed gradients causes erroneous transmission loss computations where acoustic interference occurs. However, his transmission loss calculations are made using ray theory which is the greater cause of errors.

The normal mode theory represents the exact solution to the perfect wave guide and it is used mostly in low-frequency underwater sound predictions.[15] This model could also be used to predict the behavior of the transmitted high-frequency sound with the expense of more computation time and memory. With some assumptions and approximations, the normal mode theory can be expanded to include the effects of layers with linear acoustic properties, shear waves from elastic layers, and range dependence of the ocean wave guide.

Various underwater acoustic models have been developed which treat some of these properties. Each model has its virtues and limitations. For high-frequency sound propagation the ray theory can handle all the mentioned properties but we are interested in the low frequency region.

The *parabolic equation* (PE) method was originated by Frederick Tappert[16] in the late 70's where he approximated the wave equation in order to obtain a parabolic differential equation which has the mathematical property of a closed form solution which can be solved by calculating the transmission loss while incrementing in range without iterations. This approximation involves neglecting the incoming solution of the wave equation and the use of the large-range asymptotic approximation of the Hankel functions. This method was adopted by Jensen and Kuperman[17] to study the propagation of sound in an up-slope wedge-shaped wave guide with a fluid-type bottom. Their results showed that as the depth of the water gets shallower, the trapped modes reach their cutoff frequency and become part of the continuous spectrum. Later, Ding

2

Lee[18,19] used an implicit finite-difference model to solve the parabolic equation. McDaniel[20] made comparisons between normal mode and the parabolic approximation concluding that the latter displays errors in the computation of the phase and group velocities. The limitations of the parabolic approximation are that it applies only to sound propagation at small angles with respect to the horizontal, it does not handle the horizontally reflected waves, and it is incapable of handling the shear waves created in the elastic bottom layers.[21,22] Many acousticians[23-27] have included shear waves in their PE models, but their theory is based on approximations and lacks the rigorous derivation of elastic effects.

The *fast field* method developed by Schmidt[28] is made to include the elasticity of the bottom layers, but it may only be used in range-independent environments.

Porter and Reiss[29,30] have also included the shear waves by incorporating the impedance condition as a boundary condition to the *normal mode* computations. However, this is also a range-independent model which uses the plane-wave approximation to calculate the acoustic impedances.

The *coupled normal mode* method was implicitly originated by Allan Pierce[31,32] in the mid 60s as an adiabatic-mode theory, with eigenray calculations to estimate the coupling coefficients, to simplify the solution to the propagation in a range-dependent environment. In this adiabatic mode theory, he assumes an isovelocity wave guide and a weak coupling between the natural modes of the wedge-like wave guide. He found that compressional waves refract into the basement until they get completely attenuated. McDaniel[33-35] used the coupled wave equations to calculate the energy transferred between normal modes as a result from bottom scattering of the ocean, and has shown that randomly rough sea bed layering can increase the transmission loss depending upon the degree of penetration of the acoustic field into the sediment. Evans[36-38] modeled the axisymmetric range-dependent medium as N range-independent segments with a pressure-release false bottom suitably deep to convert the continuous spectrum into a discrete form. The eigenvalues and eigenfunctions of each range-independent segment was solved by taking into account only the absorption of the basement layer to avoid the reflected energy from the pressure-release false bottom. The group made up of by Graves, Chwieroth, Miller, Nagl, Überall, and Zarur[39-43] have used a similar method

3

for solving the set of coupled range equations, but they included water layers with linear pressure wave number squared. This gives a betters approximation of the sound speed profile and the solution for each layer is given by Airy functions. Comparisons of the PE model and the coupled normal mode model have been made for some up-slope range-dependent wave guides[44,45] which gives the best agreement if the environment slowly varies with range. However, it has not been possible to define how slow the range dependent wave guide must be.

Even though the elastic effects were not incorporated in the coupled normal mode method, there is no reason why this method cannot be applied to the elastic wave equation. The objective of this report is to expand the normal mode theory in order to predict the transmission loss of low-frequency underwater sound with the effects of a depth-dependent sound speed in the water column and the elastic effects of the solid sediments of the bottom. Since some range dependence of the acoustic properties and the boundaries between the layers has been experimentally observed, this property will be included using an adiabatic approach assuming slowly range-dependent acoustic properties. Another feature of the model to be presented here is that the unrealistic false boundary used by Evans and Miller to convert the continuous spectrum into a discrete form has been removed because the absorptive effects of the elastic layers causes the radiating spectrum to be discrete.

The derivation of the wave equation and theory of normal modes in a liquid wave guide is developed in the second chapter. Since the attenuation coefficient of low-frequency sound in water is negligible compared to the loss in the bottom elastic sediments, this property will not be included. However, each layer of the horizontally stratified water column will have a constant density and sound speed gradient.

In the next chapter, the general elastic wave equation will be derived and solved by dividing the ocean floor into layers of constant acoustic properties and separating the solution into a divergent (pressure) and a rotational (shear) term. Each solid sediment will be described by a layer thickness, a density, a compressional sound speed, a compressional attenuation coefficient, a shear sound speed, and a shear attenuation coefficient.

The liquid-solid boundary conditions are derived in the next chapter in order to match the solutions for each adjacent layer. The ocean wave guide has a set of *trapped* modes which are evanescent in the bottom and a set of

4

radiating modes which are the major contributor to the sound propagation into the bottom of the ocean and they become damped by absorption.

A complex characteristic equation is derived where the complex eigenvalues can be found by searching for the complex zeros. The most challenging part of this normal mode method is to find the best method of determining these complex roots of the characteristic equation, since "There are *no* good, general methods for solving systems of more than one nonlinear equation"[46] The Newton-Raphson Method for Nonlinear Systems of Equations[46] and the Muller Method with Deflation used in the subroutine "DZANLY" from the IMSL Library[47] were used to converge into the complex zeros, but severe divergence has been experienced for some of the roots. Therefore, the Levenberg-Marquardt minimization algorithm for the magnitude of the complex determinant has been adopted for the uniform convergence to the nearest minima[48]

The adiabatic approximation for slowly range-dependent ocean wave guides is finally used to obtain the range-dependent sound propagation model with the effects of the elastic and absorptive properties of the ocean floor. With such a model, it will be possible to better understand the various propagation phenomena related to low-frequency sound and to predict the transmission loss of sound in realistic ocean conditions.

CHAPTER 2

DERIVATION OF THE WAVE EQUATION FOR FLUID LAYERS

The wave equation is a mathematical description of the reaction of the media due to a disturbance from an external force caused by a source or sources. The media can be in the state of gas, liquid, or a solid, and the source may be electromagnetic or mechanical. In this chapter, the mechanical (acoustic) propagation of the disturbance in a fluid medium is treated. The fluid medium is the ocean environment modeled as a horizontally stratified acoustic wave guide where the surface is treated as a pressure-release, or soft, or resilient, boundary. The bottom is modeled as elastic layers in the next chapter.

The disturbance created by the acoustic source may be expressed as a change in the total pressure, relative to the undisturbed pressure, as a function of the density fluctuation created by this external force. If the density fluctuation is much smaller than the undisturbed density of the environment, then the total disturbed pressure may be expanded in the following Taylor series:

$$P(\rho) = P_0 + \left(\frac{\partial P}{\partial \rho}\right)_{\rho_0} (\rho - \rho_0) + \frac{1}{2}\left(\frac{\partial^2 P}{\partial \rho^2}\right)_{\rho_0}(\rho - \rho_0)^2 + \ldots \tag{1}$$

where the partial derivatives are constants determined for the adiabatic compression and expansion of the fluid about its equilibrium density ρ_0, the equilibrium pressure is P_0, and the instantaneous total density is ρ.

If the magnitude of the condensation is much smaller than unity, i.e.,

$$s \equiv (\rho - \rho_0)/\rho_0 \equiv \rho_\sim/\rho_0 \tag{2}$$

6

then the first two terms in the Taylor expansion are of greatest contribution and an acoustic pressure caused by the disturbance may be defined as

$$p \equiv P(\rho) - P_0 \cong \left(\frac{\partial P}{\partial \rho}\right)_{\rho_0} \rho_\sim \tag{3}$$

where by thermodynamic arguments[49] it is found that, in an adiabatic media, the sound speed is given by

$$c^2 \equiv \left(\frac{\partial P}{\partial \rho}\right)_{\rho_0} \tag{4}$$

and the adiabatic bulk modulus is given by

$$B = \rho_0 c^2 \tag{5}$$

therefore, the acoustic pressure is simplified to

$$p \simeq c^2 \rho_\sim \tag{6}$$

which is called the *state equation*.

An equation for the motion of the particles in the fluid is also necessary for the proper environmental description. Consider an infinitesimal cubic volume in the medium where the disturbance is taking place as shown in Figure 1(a) for the one-dimensional derivation in cartesian coordinates. Equating forces in a continuous medium gives

$$F_{external} + A [P(x) - P(x+dx)] = \frac{d}{dt}\left(\rho\ A\ dx\ \frac{dx}{dt}\right) \tag{7}$$

where the external force is the disturbance created by the sound source and can be written in terms of a "force density" with the expression

$$F_{external} \equiv X_e \, A \, dx \tag{8}$$

and using the definition of a derivative

$$\frac{\partial P}{\partial x} = \frac{P(x+dx)-P(x)}{dx} \tag{9}$$

Equation (7) becomes

$$X_e - \frac{\partial P}{\partial x} = V_x \frac{\partial}{\partial x}(V_x\rho) + \frac{\partial}{\partial t}(V_x\rho) \tag{10}$$

which in three dimensions is given by

$$X_e - \vec{\nabla}P = \vec{V} \; (\vec{\nabla}\cdot\rho\vec{V}) + \frac{\partial}{\partial t}(\rho\vec{V}) \tag{11}$$

where the density is a function of space and time, and the equation is in a non-linear form. The total pressure is P and the total instantaneous particle velocity is $\vec{V}$. Dividing the instantaneous density, pressure, and particle velocity into an undisturbed part and an acoustic part, Equation (11) simplifies to the linear form

$$\vec{\nabla}p + \rho_0\frac{\partial\vec{v}}{\partial t} \simeq X_e \tag{12}$$

where the acoustic pressure is p and the particle velocity is $\vec{v}$.

Since the fluid of interest is continuous throughout the infinitesimal volume, Figure 1(b) will be helpful in deriving a continuity equation under the argument that the mass moving into the volume, $\rho(x) \, A \, V_x(x) \, dt$, must be the same as the mass coming out, $\rho(x+dx) \, A \, V_x(x+dx) \, dt$. There may be a change

in mass inside the volume due to the compressibility of the fluid, $\frac{\partial \rho}{\partial t}$ A dx dt, and there may exist a source of mass inside the volume represented by Q A dx dt. Taking the definition of the derivative in Equation (9) gives

$$- \frac{d}{dx}(\rho \vec{V}) \text{ A dx dt} = \frac{\partial \rho}{\partial t} \text{ A dx dt} + \text{Q A dx dt} \qquad (13)$$

which is rewritten in three dimensions as

$$\vec{\nabla} \cdot (\rho \vec{V}) + \frac{\partial \rho}{\partial t} + Q = 0 \qquad (14)$$

or in a linearized form as

$$\rho_0 \vec{\nabla} \cdot \vec{v} + \frac{\partial \rho}{\partial t} \sim = 0 \qquad (15)$$

where Q = 0 when the source is external.

Substituting Equation (6) into Equation (15) for the acoustic density, taking its partial derivative in time, and dropping the subscript 0 of the undisturbed density of the medium, gives

$$\rho \frac{\partial}{\partial t}(\vec{\nabla} \cdot \vec{v}) + c^{-2} \frac{\partial^2}{\partial t^2} p = 0 \qquad (16)$$

and taking the divergence of Equation (12) yields

$$\rho \vec{\nabla} \cdot (1/\rho \ \vec{\nabla} p) + \rho \frac{\partial}{\partial t}(\vec{\nabla} \cdot \vec{v}) = \rho \ \vec{\nabla} \cdot (\vec{X}/\rho) \qquad (17)$$

which subtracted from Equation (16) provides the inhomogeneous wave equation

$$\rho \vec{\nabla} \cdot (1/\rho \ \vec{\nabla} p) + k^2 p = \rho \ \vec{\nabla} \cdot (1/\rho \ \vec{\nabla} U) \qquad (18)$$

where the external force has been written in terms of an external potential energy, time harmonic behavior has been assumed where $k=\omega/c$, and the undisturbed density of the fluid is taken as space dependent. This equation can also be written as

$$\nabla^2 p + k^2 p - \rho^{-1}(\vec{\nabla}\rho) \cdot (\vec{\nabla}p) = \nabla^2 U - \rho^{-1}(\vec{\nabla}\rho) \cdot (\vec{\nabla}U) \tag{19}$$

which is simplified under the change of variables

$$p = \sqrt{\rho}\ \Pi \tag{20}$$

and

$$U = \sqrt{\rho}\ \nu \tag{21}$$

to obtain

$$\nabla^2 \Pi + (k^2 + K^2)\Pi = \nabla^2 \nu + K^2 \nu \tag{22}$$

where

$$K^2 \equiv \frac{1}{2\rho} \nabla^2 \rho - \frac{3}{4} \left(\frac{1}{\rho} \vec{\nabla}\rho \right)^2. \tag{23}$$

If the density is taken as a linear function of depth, then Equation (23) simplifies. However, the inhomogeneous equation to solve also has a depth dependent wave number to worry about due to the depth dependence of the sound speed. The changes in density with depth only occurs in the surface of the Arctic Ocean where water has been solidified and at regions where the water from rivers merge into the salty ocean waters. It is concluded that, for simplicity, the ocean environment can be divided into horizontal layers with constant density. It is understood that the bottom's solid sediments may have layers of large density gradients[50] In this case, Equation (22) must be solved. However, it is also possible to divide this layer into smaller constant-density layers. Then Equation (18) becomes

$$\nabla^2 p + k^2 p = \nabla^2 U \tag{24}$$

which, in an unbounded medium, has a general homogeneous solution consisting of an outgoing and an incoming wave, and an inhomogeneous solution caused by the external force. Since a sound source in a fluid can only produce a scalar potential (no shear waves), the curl of Equation (12) gives the property

$$\vec{\nabla} \times \vec{v} = \text{constant} \equiv \text{vorticity} \tag{25}$$

the vorticity in the medium does not change. Therefore, if initially there has been no rotational component of the particle velocity then the vorticity will always be null and this particle velocity can be written in terms of a velocity potential

$$\vec{v} \equiv \vec{\nabla}\varphi \tag{26}$$

which substituted back into Equation (12) gives

$$p = -\rho \, \frac{\partial \varphi}{\partial t} \tag{27}$$

and assuming harmonic time dependence yields

$$p = -i\omega\rho \, \varphi \tag{28}$$

or

$$\vec{v} = \frac{-i\vec{\nabla}p}{\omega\rho}. \tag{29}$$

Substitution of Equation (28) into Equation (24) provides the inhomogeneous Helmholtz equation

$$\nabla^2 \varphi + k^2 \varphi = \frac{i}{\omega \, \rho} \, \nabla^2 U \tag{30}$$

which must be solved for the velocity potential. If the medium is bounded,

11

the solution must satisfy the appropriate boundary conditions.

The conservation of energy is obtained by the scalar product of Equation (12) with the particle velocity and substituting the continuity equation, Equation (15), providing the law of conservation of energy:

$$\frac{\partial \mathcal{E}}{\partial t} + \vec{\nabla} \cdot \vec{I} = 0 \tag{31}$$

where

$$\mathcal{E} \equiv \frac{1}{2} \rho \, v^2 + \frac{p^2}{2\rho c^2} \tag{32}$$

is the acoustic energy density, and

$$\vec{I} = p \, \vec{v} \tag{33}$$

is the acoustic energy flux or acoustic intensity in SI units of Watts per square meter. Integrating Equation (31) throughout a volume in the fluid medium provides the acoustic power

$$\Pi \equiv \frac{d}{dt} \int_v \mathcal{E} \, dV = - \oint_s \vec{I} \cdot \hat{n} \, dS \tag{34}$$

in terms of a closed surface integral around the volume where all the energy is contained.

To obtain these important measurable quantities, it is necessary and sufficient to solve Equation (30) for the velocity potential. To solve this equation by separation of variables, it has been proven that the sound speed must be a function of only one variable.[51] This variable is taken to be the vertical direction since temperature and the total pressure of the ocean highly depends on depth. Based on experimental measurements, numerical fits have been made to determine the sound speed and its attenuation coefficient in the sea.

A simplified version of Wilson's formula for the sound speed as a function of temperature, salinity, and depth is given by

$$c(z) = 1492.9 + 3(T-10) - 6 \times 10^{-3}(T-10)^2 - 4 \times 10^{-2}(T-18)^2 + 1.2(S-35) -$$
$$10^{-2}(T-18)(S-35) + z/61 \tag{35}$$

where the temperature T is in celsius, the salinity S is in parts per thousand, and the depth z is in meters. The formula is accurate to 0.1 m/s for a temperature less than 20°C and for depths less than 8.0 kilometers[2]. A sound speed profile, with its salinity and temperature profiles, is displayed in Figure 2 as a function of depth in the Arctic Ocean. Note the variability of the data which is caused by currents. Sound speeds in the oceans may vary anywhere between 1400 m/s and 1600 m/s.

The attenuation coefficient has been fitted by Thorp as a function of frequency, temperature, and pressure. A simplified version of the formula is

$$\alpha(f) = 0.003 + 0.1f^2/(1+f^2) + 40f^2/(4100+f^2) + 0.000275f^2 \tag{36}$$

where f is the frequency in kilohertz, α is the attenuation coefficient in decibels per kiloyard, and the relationship holds for frequencies greater than ten hertz but lower than one megahertz. This attenuation coefficient is included in the environmental properties as the imaginary part of the wave number. However, it must be converted to units of nepers per meter. The conversion is given by

$$\alpha(\text{nepers/meter}) = \alpha(\text{dB/kyd}) / [20 \log(e)] / 914.4. \tag{37}$$

Note that the attenuation coefficient is directly proportional to the frequency, therefore low frequency sound travels farther than its counterpart.

CHAPTER 3

THE GENERAL ELASTIC WAVE EQUATION

Consider two infinitesimal volume elements, P and Q, at a distance $\Delta \vec{r}$ from each other in an elastic medium. An external disturbance moves these elements to the position P' and Q', respectively.

Strain, a dimensionless quantity, is defined as the change in position of a point, say Q, with respect to a reference neighboring point, say P, divided by the distance between these points, i.e. $/\Delta \vec{r}/$. Therefore, expand each component of the $\vec{\zeta}$ displacement in a Taylor series relative to the $\vec{\xi}$ displacement as follows:

$$\zeta_x = \xi_x + \frac{\partial \xi_x}{\partial x} \Delta x + \frac{\partial \xi_x}{\partial y} \Delta y + \frac{\partial \xi_x}{\partial z} \Delta z + \ldots \tag{38}$$

and combine them to obtain the expansion,

$$\vec{\zeta} = \vec{\xi} + (\Delta \vec{r} \cdot \vec{\nabla}) \vec{\xi} + \ldots \tag{39}$$

where the higher order terms are nonlinear and may be neglected if we assume the maximum amplitude of the displacement vectors, ξ and ζ, to be much smaller than the wavelength of the disturbance (Hooke's law). This assumption is valid at low frequencies and at distances greater than a wavelength from the external source.

Adding and subtracting the terms $\frac{\partial \xi_z}{\partial x} \Delta z$ and $\frac{\partial \xi_y}{\partial x} \Delta y$ in Equation (38) gives,

$$\zeta_x = \xi_x + \Omega_y \Delta z - \Omega_z \Delta y + S_{xx} \Delta x + S_{xy} \Delta y + S_{xz} \Delta z + \ldots \tag{40}$$

with

14

$$\vec{\Omega} = \frac{1}{2} \vec{\nabla} \times \vec{\xi} \tag{41}$$

and

$$\overset{\leftrightarrow}{S} = \frac{1}{2} \left[\vec{\nabla} \vec{\xi} + \left(\vec{\nabla} \vec{\xi} \right)^{\dagger} \right] \tag{42}$$

where $\dagger$ stands for the transpose of the tensor matrix in the parenthesis and where $\leftrightarrow$ identifies a tensor of second rank. Although there are no units for strain, engineers sometimes use implied multiples, e.g. microinches/inch, a number which is strain x 10^6, or percent strain, a number which is strain x 10^2. Where strain is displacement per unit of length in the direction of displacement, it is referred to as a normal strain. Where the strain is displacement per unit of length in a direction perpendicular to the direction of displacement, it is referred to as a shear strain. In a three-dimensional strain field the strain can be resolved into an isotropic component (or volumetric strain), representing change in volume (and density) of an element, and a deviatoric component, representing change in the shape of an element.

In vector form we get,

$$\vec{\zeta} = \vec{\xi} + \vec{\Omega} \times \Delta\vec{r} + \overset{\leftrightarrow}{S} \cdot \Delta\vec{r} + \dots \tag{43}$$

where ζ is expressed in terms of the rotational and divergent behavior relative to ξ.

In an elastic medium, the linearized Euler equation becomes,

$$\vec{\nabla} \cdot \overset{\leftrightarrow}{P} + \rho \frac{\partial \vec{v}}{\partial t} = \vec{f} \tag{44}$$

where $\overset{\leftrightarrow}{P}$ is the stress tensor, $\vec{v} = \partial\vec{\xi}/\partial t$ is the particle velocity, ρ is the undisturbed density of the medium, and $\vec{f}$ is the external force that disturbs the medium creating the acoustic field. Stress is force per unit area and may be either normal stress produced by tensile, compressive forces acting perpendicular to the faces of cubic elements, or shear stresses, produced by tangential forces acting parallel to the surfaces of cubic elements. In a three-dimensional stress field, the stress sy. .m can also be resolved into an isotropic component (or bulk stress) and a deviatoric component. By definition, this elastic medium has a rest state in which stresses and strains

15

vanish. Linear elasticity means that stress is directly proportional to strain. If the medium is also isotropic then the relationship between the stress and strain tensors in terms of Lamé constants is given by the constitutive relation

$$-\overset{\leftrightarrow}{P} = \lambda \, \Theta \, \overset{\leftrightarrow}{I} + 2 \, \mu \, \overset{\leftrightarrow}{S} \tag{45}$$

where $\Theta = \vec{\nabla} \cdot \vec{\xi}$ is the divergent component of the displacement vector, $\overset{\leftrightarrow}{I}$ is the unit matrix, and the Lamé constants are given by

$$\lambda = \rho(c^2 - 2 \, b^2) \tag{46}$$

and

$$\mu = \rho \, b^2, \tag{47}$$

where c is the compressional sound speed of the medium and b is its shear speed. Equations (45) through (47) are sufficient to characterize the linear, isotropic, elastic medium. The absorptive nature of the medium is modeled by making both sound speeds complex where the imaginary part of the sound speeds is related to their respective attenuation coefficients. Since the speeds are considered space dependent, the substitution of the stresses into Euler's equation, Equation (44), gives

$$\rho \frac{\partial \vec{v}}{\partial t} = \vec{f} + \vec{\nabla} \cdot (\lambda \, \Theta \, \overset{\leftrightarrow}{I}) + 2 \, \vec{\nabla} \cdot (\mu \, \overset{\leftrightarrow}{S}), \tag{48}$$

and substitution of Equations (41) and (42) provides the elastic wave equation

$$\rho \frac{\partial^2 \vec{\xi}}{\partial t^2} = \vec{f} + (\lambda + \mu) \, \vec{\nabla}\Theta + \Theta \, \vec{\nabla}\lambda + \mu \, \nabla^2\vec{\xi} + 2 \, \vec{\nabla}\mu \cdot \overset{\leftrightarrow}{S} \tag{49}$$

which is a set of three coupled inhomogeneous differential equations where each component of the solution $\vec{\xi}$ depends on the others.

To uncouple this generalized elastic wave equation, it is sufficient to eliminate the last term in the right-hand-side. This is done by assuming a quasi space-independent shear modulus, μ. From Equation (47) this means layers

16

of constant shear speed and density, but note that no restriction is imposed on the compressional speed.

In the case of solid (elastic) layers there is no external force present, $\vec{f} = \vec{0}$, since the source is assumed to be in the water column. Furthermore, layers of constant shear modulus are assumed. Under these conditions Equation (49) simplifies to

$$\rho \, \vec{\xi}'' = (\lambda + \mu) \, \vec{\nabla}\Theta + \Theta \, \vec{\nabla}\lambda + \mu \, \nabla^2\vec{\xi}. \tag{50}$$

Since the displacement vector has been expanded into its rotational and divergent part in Equation (43), the same expansion may be applied to the time derivative of the displacement vector now defined as the particle velocity, i.e.,

$$\vec{v} \equiv \vec{\xi}' = \vec{\nabla}\varphi + \vec{\nabla} \times \vec{A} \tag{51}$$

where the first term in the right-hand-side corresponds to the compressional waves and the second term is the shear wave contribution to the acoustic field. Substituting Equation (51) into Equation (50), and taking into consideration the assumption of isodensity layers with constant shear speed, gives

$$\vec{\nabla} \left[\rho \, \varphi'' - (\lambda + 2\mu) \, \nabla^2\varphi \right] = \vec{\nabla} \times \left[\mu \, \nabla^2\vec{A} - \rho \, \vec{A}'' \right]. \tag{52}$$

The divergence of this vector equation is satisfied if

$$(\nabla^2 + k^2) \, \varphi = 0, \tag{53a}$$

which is the compressional wave equation, and the rotational part is satisfied with the shear wave equations

$$(\nabla^2 + \kappa^2) \, \vec{A} = 0, \tag{53b}$$

17

where $k = \omega / c$ is the compressional wave number, $\kappa = \omega / b$ is the shear wave number, and harmonic time dependence is assumed.

For simplicity, the compressional and shear attenuation coefficients are included as the imaginary part of both wave numbers instead of the sound speeds. In this case, the complex compressional wave number is

$$k \equiv \omega / c + i \, \alpha, \tag{54a}$$

where α is the compressional attenuation coefficient and the complex shear wave number is

$$\kappa \equiv \omega / b + i \, \beta, \tag{54b}$$

where β is the constant shear attenuation coefficient.

For the case of axially symmetric propagation in cylindrical coordinates we write

$$\vec{v} = v_r(r,z) \, \hat{r} + v_z(r,z) \, \hat{z} \tag{55}$$

which will be equated to Equation (51) to obtain the components of the particle velocity in terms of the potentials. However, to obtain range independent boundary conditions the vector potential $\vec{A}$ must be written as the curl of another vector potential, i.e.,

$$\vec{A} = \vec{\nabla} \times \vec{\psi} \tag{56}$$

which gives

$$\vec{v} = \vec{\nabla}\varphi + \vec{\nabla} \, (\vec{\nabla} \cdot \vec{\psi}) - \nabla^2\vec{\psi}. \tag{57}$$

The physical meaning of this new vector potential is obvious when calculating the stress matrix for the boundary conditions. The component ψ_r corresponds to the SH-waves in seismology,[52] ψ_θ vanishes in an axially symmetric medium, and ψ_z corresponds to the SV-waves. However, the stress

18

tensor of the SH-wave has only off-diagonal elements, while the stress tensor in the liquid layers has null off-diagonal elements. Therefore, a source in the liquid layers is incapable of exciting SH-waves in the solid layers. In consequence, we have $\psi_r = 0$ and the particle velocity is given by,

$$\vec{v} = \left[\frac{\partial}{\partial r} \varphi + \frac{\partial}{\partial z} \frac{\partial}{\partial r} \psi_z \right] \hat{r} + \left[\frac{\partial}{\partial z} \varphi - \frac{1}{r} \frac{\partial}{\partial r} \left(r \frac{\partial}{\partial r} \psi_z \right) \right] \hat{z}. \tag{58}$$

The shear wave equations to be satisfied are now reduced to the scalar wave equation,

$$(\nabla^2 + \kappa^2) \, \psi_z = 0. \tag{59}$$

Substituting Equations (59) into Equation (58), equating this result with Equation (55), and assuming axially symmetric cylindrical coordinates provides

$$v_r = \frac{\partial}{\partial r} \left[\varphi + \frac{\partial \psi_z}{\partial z} \right] \tag{60a}$$

and

$$v_z = \frac{\partial}{\partial z} \varphi + \left[\frac{\partial^2}{\partial z^2} + \kappa^2 \right] \psi_z \tag{60b}$$

for the components of the particle velocity.

19

CHAPTER 4

SOLUTION OF THE WAVE EQUATION

The solution of the inhomogeneous compressional Helmholtz equation for the liquid layers can be written as the sum of the homogeneous solution and the particular (transient) solution. The generalized homogeneous solution can be used as the solution of the homogeneous compressional wave equation in the solid layers, Equation (53a). The solution of the homogeneous shear wave equation, Equation (59), however, is different since the shear speed and compressional speed of a sediment are usually unequal.

For simplicity and without loss of generality, we may solve the inhomogeneous wave equation in the water column for the case of a point source of unit source strength which, in the cylindrical coordinate system, becomes

$$\left[\frac{1}{r} \frac{\partial}{\partial r} \left(r \frac{\partial}{\partial r} \right) + \frac{\partial^2}{\partial z^2} + k^2(z) \right] \varphi(r,z) = - \frac{1}{2\pi r} \delta(r) \, \delta(z - z_o) \qquad (61)$$

where the source is at $r = 0$, $z = z_o$, and the wave number is taken to be depth dependent only.

A lengthy but elegant way to solve the wave equation is by the use of the Fourier-Bessel transformation,

$$\varphi(r,z) = \int_0^\infty u(k,z) \, J_0(kr) \, k \, dk, \qquad (62a)$$

and its inverse form,

$$u(k,z) = \int_0^\infty \varphi(r,z) \, J_0(kr) \, r \, dr, \qquad (62b)$$

where the zeroth order Bessel functions satisfy the closure relation,

$$\delta(r - r') = r \int_0^\infty J_0(kr) \, J_0(kr') \, k \, dk, \tag{63}$$

and the Bessel equation,

$$k^2 r^2 \, J_0''(kr) + kr \, J_0'(kr) + k^2 r^2 \, J_0(kr) = 0. \tag{64}$$

Substitution of the above equations and the relation

$$\frac{\partial}{\partial r}\left(r \, \frac{\partial}{\partial r} \right) J_0(kr) = k \, J_0'(kr) + k^2 r \, J_0''(kr) = -k^2 r \, J_0(kr) \tag{65}$$

into Equation (61) converts the partial differential equation to the ordinary differential equation

$$\left[\frac{d^2}{dz^2} + k^2(z) - k^2 \right] u(k,z) = - \frac{\delta(z - z_0)}{2\pi} \tag{66}$$

where k^2 is the continuous eigenvalue and $u(k,z)$ is the continuous eigenfunction of the inhomogeneous equation. In the case of a discrete wave number spectrum the eigenequation becomes

$$\left[\frac{d^2}{dz^2} + k^2(z) - k_n^2 \right] u_n(z) = - \frac{\delta(z - z_0)}{2\pi} \tag{67}$$

where $n = 1, 2, 3, \ldots, N$ is the mode index, k_n^2 are the discrete eigenvalues and $u_n(z)$ are the discrete eigenfunctions. These eigenequations are similar to the Schrödinger equation in quantum mechanics. A sound speed profile taken in

the Arctic is shown in Figure 2. The sound speed as a function of depth is contained in $k^2(z) = \omega^2/c^2(z)$ and the minimum sound speed is defined as c_{min} which represents a maximum wave number in the eigenequation k_{max}. Define the "equivalent potential" as $V(z) \equiv k_{max}^2 - k^2(z)$ and the "equivalent eigenvalues" as $E_n \equiv k_{max}^2 - k_n^2$, then the eigenequation becomes

$$u_n''(z) + [E_n - V(z)] u_n(z) = - \delta(z - z_o)/2\pi \qquad (68)$$

which is equivalent to the time-independent Shrödinger wave equation, where the double prime stands for the second derivative with respect to the argument, the minimum potential is zero, and there exists a maximum potential which represents the threshold between the discrete and continuous spectrum. This maximum potential is given by the determination of the sound speed in the limit as $z \rightarrow \infty$. The "propagating modes" are defined by the mode cutoff limit $E_n < \omega^2/c_{min}^2$ and they may be "trapped modes" which are represented by a discrete eigenvalue, or they may be "radiating modes" which are represented by the continuous spectrum. Note that the potential $V(z)$ and the eigenvalues E_n depend on the frequency of the source. Therefore, the number of discrete eigenvalues vary with the frequency of the sound that is disturbing the medium.

Since the ocean floor is not rigid nor soft, the energy spectrum will contain trapped modes which are evanescent in the bottom layers with higher sound speed and radiating modes which represent the energy that radiates into the bottom sediments.

Evans[36-38] and Miller[42-44] have solved the purely real wave equation which gave a discrete eigenvalue spectrum representing the trapped modes and a continuous spectrum representing the radiating modes. The absorptive effects of the fluid-type bottom was later incorporated as the imaginary part of the eigenvalues using the first order perturbation approximation assuming small absorptive effects. The continuous spectrum was forced to be discrete by adding a deep false (pressure-release) boundary. Since this boundary caused reflection of the incident sound, a very large attenuation coefficient must be used in the basement layer, therefore making the first order perturbation approximation an invalid method.

The continuous eigenvalue spectrum is the direct consequence of solving the unrealistic purely real wave equation. If the absorption is incorporated in the wave equation as the imaginary part of the wave number, then the radiating modes will be part of a discrete spectrum. In this case, the Helmholtz equation in Equation (67) becomes

$$\left[\frac{d^2}{dz^2} + k^2(z) - k_n^2 \right] u_n(z) = 0 \tag{69}$$

which is the homogeneous Helmholtz wave equation.

From the continuity of pressure in the liquid layers, which will be discussed in the chapter on the boundary conditions, we shall set the function $\sqrt{\rho(z)} \, u_n(z)$ as the orthonormal eigenfunctions,

$$\int \rho(z) \, u_n(z) \, u_m(z) \, dz = \delta_{nm} \tag{70}$$

which also satisfies Sturm-Louville's Theorem.[51] The closure relation is given by

$$\delta(z - z_0) = \rho(z_0) \sum_{n=1}^{N} u_n(z) \, u_n(z_0), \tag{71}$$

and the eigenfunction is solved by the method of separation of variables for the individual modes which are later added in the form

$$u(k,z) = \sum_{n=1}^{N} a_n(k) \, u_n(z) \tag{72}$$

where $a_n(k)$ is to be determined. The inhomogeneous term is taken into account if we substitute the homogeneous solution in the inhomogeneous equation. The substitution gives

23

$$\left(\frac{d^2}{dz^2} + k^2(z) - k^2 \right) \sum_{n=1}^{N} a_n(k) \, u_n(z) = - \frac{\rho(z_0)}{2\pi} \sum_{n=1}^{N} u_n(z) \, u_n(z_0) \quad (73)$$

and substituting the homogeneous equation provides

$$\sum_{n=1}^{N} \left[a_n(k) \, (k^2 - k_n^2) - \frac{\rho(z_0)}{2\pi} u_n(z_0) \right] u_n(z) = 0 \quad (74)$$

and, to satisfy the equation, the terms inside the brackets are set to zero leading to the relation

$$a_n(k) = \frac{\rho(z_0)}{2\pi} \frac{u_n(z_0)}{k^2 - k_n^2} \quad (75)$$

which substituted into Equation (72) gives

$$u(k,z) = \frac{\rho(z_0)}{2\pi} \sum_{n=1}^{N} \frac{u_n(z_0) \, u_n(z)}{k^2 - k_n^2} \quad (76)$$

and this substituted into Equation (66) gives the scalar potential

$$\varphi(r,z) = \frac{\rho(z_0)}{2\pi} \sum_{n=1}^{N} u_n(z_0) \, u_n(z) \int_0^\infty \frac{J_0(kr) \, k \, dk}{k^2 - k_n^2} \quad (77)$$

where the integral of this equation is better solved by contour integration and it can be defined as

$$I_n(r) = \frac{1}{2} \int_0^\infty \frac{H_0^{(1)}(kr) + H_0^{(2)}(kr)}{k^2 - k_n^2} k \, dk. \qquad (78)$$

A property of the eigenvalues of the problem is that these usually have a smaller imaginary component compared to the real part. Also, both parts of the eigenvalues are positive because outgoing waves from the source are used to satisfy causality. To solve this complex integral, consider the contour integration in the first quadrant of the complex k-plane as displayed in Figure 3, where

$$I_{ni}(r) \equiv \begin{cases} \displaystyle\int_{C_{1i}} \frac{H_0^{(1)}(kr)}{k^2 - k_n^2} k \, dk, & i = 1,2,3 \\[2em] \displaystyle\int_{C_{2i}} \frac{H_0^{(2)}(kr)}{k^2 - k_n^2} k \, dk, & i = 4,5,6 \end{cases} \qquad (79)$$

and, by this definition, the integral to be solved is,

$$I_{ni}(r) \equiv \frac{1}{2} \left[I_{n1}(r) + I_{n4}(r) \right]. \qquad (80)$$

By Jordan's lemma[49] we have

$$I_{n2}(r) = I_{n5}(r) = 0 \qquad (81)$$

also the integrals in Equation (79) show that

$$I_{n3}(r) + I_{n6}(r) = 0 \qquad (82)$$

which means that we may write

$$I_n(r) = \frac{1}{2} \left[\sum_{i=1}^{3} I_{ni}(r) + \sum_{i=4}^{6} I_{ni}(r) \right] = \frac{1}{2} \sum_{i=1}^{6} I_{ni}(r) \qquad (83)$$

where only $I_{n1}(r)$ and $I_{n4}(r)$ contribute to the sum.

Given that the singularities, $k = k_n$, are located in the upper contour we get that

$$\sum_{i=4}^{6} I_{ni}(r) = \oint_{C_2} \frac{H_0^{(2)}(kr)}{k^2 - k_n^2} \, k \, dk = 0 \qquad (84)$$

and

$$\sum_{i=1}^{3} I_{ni}(r) = \oint_{C_1} \frac{H_0^{(1)}(kr)}{k^2 - k_n^2} \, k \, dk = \pi \, i \, H_0^{(1)}(k_n r) \qquad (85)$$

by calculus of residues. Substitution of Equations (84) and (85) in Equation (83) and this one into Equation (77) gives

$$\varphi(r,z) = \frac{i}{4} \, \rho(z_0) \sum_{n=1}^{N} u_n(z_0) \, u_n(z) \, H_0^{(1)}(k_n r) \qquad (86)$$

where the eigenfunctions $u_n(z)$, and eigenvalues k_n, satisfy Equation (69). Note that the solution has been written using a separation of variables.[53]

To solve the characteristic equation for the compressional waves, Equation (69), the sound speed profile is divided into layers where the squared of the index of refraction is a linear function of depth, i.e.,

$$n_j^2(z) = a_j z + b_j \tag{87}$$

where $k_j(z) = \omega\, n_j(z)$, Figure 4 gives the geometry to be used for this mathematical model, and the subscript j is the layer number. To determine a_j and b_j, let the sound speed at the top of the layer to be c_j and that of the bottom to be c_{j+1}. Substituting into our linear equation gives

$$\frac{1}{c_j^2} = a_j\, z_j + b_j, \tag{88a}$$

and

$$-\frac{1}{c_{j+1}^2} = a_j\, z_{j+1} + b_j, \tag{88b}$$

which solved for a_j and b_j results in

$$a_j = \frac{c_j^2 - c_{j+1}^2}{D_j\, c_j^2\, c_{j+1}^2} \tag{89a}$$

and

$$b_j = \frac{1}{c_{j+1}^2} - \frac{z_j(c_j^2 - c_{j+1}^2)}{D_j\, c_j^2\, c_{j+1}^2} \tag{89b}$$

where $D_j = z_{j+1} - z_j$ is the thickness of the layer. The index of refraction is given by $n_j^2 = 1/c_j^2$, and if $\sigma_j \equiv (n_j^2 - n_{j+1}^2)/D_j$, then we have

$$k_j^2(z) = \omega^2\left[n_j^2 + \sigma_j(z_j - z) \right] \equiv k_j^2 + S_j(z - z_j) \tag{90a}$$

where

$$S_j \equiv (k_j^2 - k_{j+1}^2)/D_j \tag{90b}$$

and which substituted into the eigenequation gives

$$\frac{d^2}{dz^2} u_{nj}(z) + \left[k_j^2 + S_j(z - z_j) - k_n^2 \right] u_{nj}(z) = 0 . \tag{91}$$

Define

$$\zeta_{nj}(z) \equiv - S_j^{-2/3} \left[k_j^2 + S_j(z - z_j) - k_n^2 \right] \tag{92}$$

and square its derivative to obtain

$$\frac{d^2}{dz^2} = S_j^{2/3} \frac{d^2}{d\zeta_{nj}^2} \tag{93}$$

which substituted into the new eigenequation gives

$$\left[\frac{d^2}{d\zeta_{nj}^2} - \zeta_{nj} \right] u_{nj}(\zeta_{nj}) = 0. \tag{94}$$

The solutions of this differential equation are the Bessel functions of order 1/3, or more commonly known as the *Airy* functions, i.e.,

$$u_{nj}(\zeta_{nj}) = a_{nj} Ai(\zeta_{nj}) + b_{nj} Bi(\zeta_{nj}). \tag{95}$$

The behavior of the real part of these functions and their derivative is shown in Figure 5 and some of their properties are given in Reference 54. Now that the general solutions are found, we must match the solutions at each boundary with the appropriate boundary conditions in order to find the unknown coefficients and eigenvalues for each mode.

The attenuation coefficient in the water at low frequencies is negligibly

28

small. Therefore, only the shear and compressional attenuation coefficients in the elastic bottom layers are taken into consideration, and only the complex eigenvalue will make the argument of the Airy functions complex.

Using, once more, the method of separation of variables for the solution of the homogeneous shear Helmholtz equation we obtain the general form

$$\psi(r,z) \equiv \sum_{n=1}^{N} A_n \, v_n(z) \, H_n(r) \tag{96}$$

which substituted back in the shear wave equation leads to

$$-\frac{1}{H_n \, r} \frac{d}{dr}\left(r \frac{d}{dr}\right)H_n = \frac{1}{v_n} \frac{d^2}{dz^2} v_n + \kappa^2 \equiv k_n^2 = \text{constant} \tag{97}$$

which gives the ordinary differential equations,

$$\frac{d^2}{dz^2} v_n(z) + [\kappa^2 - k_n^2] \, v_n(z) = 0, \tag{98}$$

and

$$\left(r^2 \frac{d^2}{dz^2} + r \frac{d}{dr} + k_n^2 r^2\right) H_n(r) = 0. \tag{99}$$

The solution of the first equation in the jth layer is

$$v_{nj}(z) = c_{nj} \exp(\gamma_{nj} z) + d_{nj} \exp(-\gamma_{nj} z) \tag{100}$$

where $\gamma_{nj}^2 \equiv k_n^2 - \kappa_j^2$ and the solution can be oscillatory ($\gamma_{nj}^2 < 0$) or exponential ($\gamma_{nj}^2 > 0$). By causality, only the radially outgoing solution of the second equation must be used. The solution to this radial differential equation is the zeroth order Hankel function of the first kind, $H_0^{(1)}(k_n r)$.

Finally, since a_{nj} and b_{nj} are unknowns to be evaluated by the use of the boundary conditions, we are free to choose $A_n \equiv i/4 \, \rho(z_0) \, u_n(z_0)$ which, in the

29

j^{th} layer, gives

$$\psi_j(r,z) = \frac{i}{4} \rho_j(z_0) \sum_{n=1}^{N} u_{nj}(z_0) v_{nj}(z) H_0^{(1)}(k_n r). \qquad (101)$$

This expression simplifies the boundary conditions for the evaluation of the unknown eigenvalues and amplitude of the eigenfunctions.

Note that the nth compressional eigenfunction and the nth shear eigenfunction are represented by the same eigenvalue k_n. The common eigenvalue is necessary to satisfy the general elastic wave equation and to obtain range-independent boundary conditions.

Now that the general solutions are found, these solutions will be matched at each boundary with the appropriate boundary conditions in order to find the unknown coefficients and eigenvalues for each mode.

CHAPTER 5

THE BOUNDARY CONDITIONS

The ocean is modeled as a horizontally stratified wave guide with layers of elastic properties simulating the ocean floor and liquid layers simulating the water column. To match the solutions of adjacent layers, boundary conditions are derived. In this chapter, the boundary conditions for all possible interface are developed.

BOUNDARY BETWEEN LIQUID LAYERS

There are several ways of calculating the boundary conditions. The boundary conditions for the interface between two fluid layers can be obtained when an infinitesimal cylindrical volume is modeled across this boundary. There are two boundary conditions to be satisfied at this interface.

<u>Continuity of the Normal Particle Velocity</u>

The volume integration of Equation (15) in this infinitesimal cylinder provides the expression

$$\rho \oint \vec{v} \cdot \hat{n} \, dA = - \frac{\partial}{\partial t} \int \rho \, dA \, \Delta x \tag{102}$$

where making $\Delta x \rightarrow 0$, the right hand side of the equation vanishes and the surface integral yields the boundary condition

$$\vec{v}_2 \cdot \hat{n} \, \Big|_s = \vec{v}_1 \cdot \hat{n} \, \Big|_s \tag{103}$$

which means that the normal component of the particle velocity is continuous at the interface.

This boundary condition is expressed as $\vec{v} \cdot \hat{n}$ = continuous, and in the case of horizontally stratified layers we may write $\hat{n} = \hat{z}$ to obtain the boundary condition,

$$v_z = \frac{\partial \varphi}{\partial z} = \text{continuous} \tag{104}$$

or using Equation (86) gives

$$\frac{du_n}{dz} = \text{continuous.} \tag{105}$$

Continuity of the Pressure

Assuming that there is no source in the infinitesimal volume of this cylinder, the volume integration of Equation (12) gives

$$-\oint p \, \hat{n} \, dA = \rho \, \frac{\partial}{\partial t} \int \vec{v} \, dA \, \Delta x \tag{106}$$

and letting $\Delta x \rightarrow 0$ yields the pressure boundary condition

$$P_1 \big|_s = P_2 \big|_s \tag{107}$$

which means that the acoustic pressure at the interface is continuous. Substituting Equation (86) into Equation (28) and this one into Equation (107) gives

$$\rho \, u_n = \text{continuous.} \tag{108}$$

32

BOUNDARY BETWEEN LIQUID AND VACUUM

As a very good approximation, we may consider this boundary as pressure-release for acoustic waves in the liquid layer. Therefore, the only boundary condition is that the pressure vanishes at this boundary. Substituting Equation (28) for the pressure, and Equation (86) for the scalar potential gives

$$u_n \big|_{z_o} = 0. \tag{109}$$

The same boundary conditions are obtained using the particle velocity and the stress tensor of an elastic layer by making the shear speed vanish. The particle velocity is given from Equations (55) and (60). From Equations (42) the strain tensor in an axially symmetric environment is given by

$$S = \begin{vmatrix} \dfrac{\partial \xi_r}{\partial r} & 0 & \dfrac{1}{2}\left(\dfrac{\partial \xi_z}{\partial r} + \dfrac{\partial \xi_r}{\partial z} \right) \\ 0 & 0 & 0 \\ \dfrac{1}{2}\left(\dfrac{\partial \xi_r}{\partial z} + \dfrac{\partial \xi_z}{\partial r} \right) & 0 & \dfrac{\partial \xi_z}{\partial z} \end{vmatrix} \tag{110}$$

and using Equation (45) for the stress tensor in terms of the components of the particle velocity gives

$$i\omega \overset{\leftrightarrow}{P} = \begin{vmatrix} (\lambda+2\mu)\dfrac{\partial v_r}{\partial r} + \lambda\left(\dfrac{v_r}{r} + \dfrac{\partial v_z}{\partial z}\right) & 0 & \mu\left(\dfrac{\partial v_r}{\partial z} + \dfrac{\partial v_z}{\partial r}\right) \\ 0 & \lambda\left(\dfrac{\partial v_r}{\partial r} + \dfrac{v_r}{r} + \dfrac{\partial v_z}{\partial z}\right) & 0 \\ \mu\left(\dfrac{\partial v_r}{\partial z} + \dfrac{\partial v_z}{\partial r}\right) & 0 & (\lambda+2\mu)\dfrac{\partial v_z}{\partial z} + \lambda\left(\dfrac{v_r}{r} + \dfrac{\partial v_r}{\partial r}\right) \end{vmatrix}$$

$$(111)$$

which is a Hermitian matrix as expected for being an observable quantity. Now we can calculate the boundary condition for some other cases involving the solid layers.

BOUNDARY BETWEEN LIQUID AND SOLID

In the case of liquid-solid boundaries we have three boundary conditions to satisfy.

Continuity of the Normal Particle Velocity

Using the particle velocity vector in Equations (60) and (55) takes us to the equation

$$\left.\frac{\partial \varphi_1}{\partial z}\right|_{z_0} = \left.\frac{\partial \varphi_s}{\partial z}\right|_{z_0} + \left(\frac{\partial^2}{\partial z^2} + \frac{\omega^2}{b^2}\right)\psi_z\Big|_{z_0} \tag{112}$$

which by substituting Equations (89a), (91), and (94) gives

$$\left.\frac{du_{n1}}{dz}\right|_{z_0} = \left.\frac{du_{ns}}{dz}\right|_{z_0} + k_n^2\, v_n\Big|_{z_0} \tag{113}$$

where z_0 stands for the depth of the boundary to be matched, and these functions must be evaluated at this position. The subscript "1" stands for the depth function in the liquid layer and "s" labels the depth function in the

solid one.

Continuity of the P_{zz} Component of Stress

Extracting the P_{zz} component of the stress matrix in both media gives

$$i\rho_1 \omega \ \varphi_1 \Big|_{z_0} = \frac{1}{i\omega} \left[(\lambda + 2\mu) \frac{\partial v_z}{\partial z} + \lambda \left(\frac{v_r}{r} + \frac{\partial v_r}{\partial r} \right) \right]_{z_0} \tag{114}$$

where by the same equations as used before we obtain

$$\rho_1 u_{n\ell} \Big|_{z_0} = \rho_s u_{ns} \Big|_{z_0} - 2\rho_s (k_n/k_s)^2 \left(u_{ns} + \frac{dv_n}{dz} \right) \Big|_{z_0}. \tag{115}$$

The P_{rz} Component of Stress Vanishes

From Equations (111), and the same equations used before, this boundary condition becomes

$$2 \frac{du_{ns}}{dz} \Big|_{z_0} + (2k_n^2 - k_s^2) \ v_n \Big|_{z_0} = 0. \tag{116}$$

BOUNDARY BETWEEN VACUUM AND SOLID

For a free elastic layer we have two boundary conditions to satisfy. These are,

The P_{zz} Component of Stress Vanishes

$$u_{ns}\Big|_{z_0} - 2(k_n/k_s)^2 \left(u_{ns} + \frac{dv_n}{dz} \right) \Big|_{z_0} = 0. \tag{117}$$

The P_{rz} Component of Stress Vanishes

$$2 \frac{du_{ns}}{dz} \Big|_{z_0} + (2k_n^2 - k_s^2) v_n \Big|_{z_0} = 0. \tag{118}$$

BOUNDARY BETWEEN SOLID LAYERS

In this case we have two boundary conditions from the particle velocity and two from the stress. These are the most general of all boundary conditions given above and are stated as follows:

Continuity of the Normal Particle Velocity

$$\frac{du_n}{dz} + k_n^2 v_n = \text{continuous} \tag{119}$$

Continuity of the Tangential Particle Velocity

$$u_n + \frac{dv_n}{dz} = \text{continuous} \tag{120}$$

Continuity of the P_{zz} Component of Stress

$$\rho u_n - 2\rho(k_n/k)^2 \left(u_n + \frac{dv_n}{dz} \right) = \text{continuous} \tag{121}$$

Continuity of the P_{rz} Component of Stress

$$\rho b^2 \left[2\frac{du_n}{dz} + (2k_n^2 - k^2)\, v_n \right] = \text{continuous} \tag{122}$$

where it is emphasized that the axially symmetric cylindrical coordinate system has been used and the equations are implicitly evaluated at the depth of the boundary interface.

CHAPTER 6

THE PROPAGATION AND MATCHING ALGORITHM

The eigenvalues that characterize the stratified ocean are obtained by satisfying all the boundary conditions simultaneously. The algorithm developed here consist in multiplying all the calculated propagation and matching matrices to obtain the value of the compressional and shear eigenfunctions at some interface where the chosen characteristic equation is to be evaluated. A combination of the up-layer and down-layer evaluation of the eigenfunctions and their derivatives will be used. At the jth interface between two solid layers, the four boundary conditions in Equations (119) through (122) are written in matrix form as

$$
\mathbb{B}_{j-1}
\begin{pmatrix}
u_{nj-1}(z_j) \\
u'_{nj-1}(z_j) \\
v_{nj-1}(z_j) \\
v'_{nj-1}(z_j)
\end{pmatrix}
= \mathbb{B}_j
\begin{pmatrix}
u_{nj}(z_j) \\
u'_{nj}(z_j) \\
v_{nj}(z_j) \\
v'_{nj}(z_j)
\end{pmatrix}
\tag{123}
$$

where

$$
\mathbb{B}_j =
\begin{pmatrix}
1 & 0 & 0 & 1 \\
0 & 1 & k_n^2 & 0 \\
0 & 2\mu_j & -\mu_j T_j/\kappa_j^2 & 0 \\
\rho_j T_j & 0 & 0 & -\rho_j Q_j
\end{pmatrix}
\tag{124}
$$

and it is designated that $Q_j \equiv 2\, k_n^2 / \kappa_j^2$ and $T_j \equiv 1 - Q_j$. For up-layer matching of the eigenfunctions the matrix $\mathbb{B}_{j-1}$ in Equation (123) is taken to the other side and multiplied by $\mathbb{B}_j$ to obtain the matching matrix

$$M_j \equiv B_{j-1}^{-1} B_j = \begin{pmatrix} M_{11} & 0 & 0 & M_{14} \\ 0 & M_{22} & M_{23} & 0 \\ 0 & M_{32} & M_{33} & 0 \\ M_{41} & 0 & 0 & M_{44} \end{pmatrix} \qquad (125)$$

where

$$M_{11} = M_{33} = Q_{j-1} + T_j R_j, \qquad (126a)$$

$$M_{14} = Q_{j-1} - Q_j R_j, \qquad (126b)$$

$$M_{22} = M_{44} = T_{j-1} + Q_{j-1} S_j, \qquad (126c)$$

$$M_{41} = T_{j-1} - T_j R_j, \qquad (126d)$$

$$M_{23} = M_{41} k_n^2, \qquad (126e)$$

and

$$M_{32} = 2 (1 - S_j)/\kappa_{j-1}^2 \qquad (126f)$$

are the elements, and the ratio of densities and shear moduli are defined as $R_j = \rho_j/\rho_{j-1}$ and $S_j = \mu_j/\mu_{j-1}$.

At the liquid-liquid interface the boundary conditions are reduced to two, and the up-layer matching matrix becomes

$$M_j = \begin{pmatrix} R_j & 0 \\ 0 & 1 \end{pmatrix} \qquad (127)$$

at the jth interface.

These matching matrices simply provide the eigenfunctions and their derivatives at the bottom of the j-1 layer when the values at the top of the jth layer are known. Another matrix is needed to propagate the solution from the bottom to the top of the jth layer.

When the values at the bottom of the jth layer has been determined, the solution of the wave equations can be used to propagate the solution to the

39

top of this layer. To create this propagation matrix, Equations (95) and (100) are rewritten in the matrix form

$$
\begin{pmatrix} u_{nj}(z) \\ u'_{nj}(z) \\ v_{nj}(z) \\ v'_{nj}(z) \end{pmatrix} =
$$

$$
\begin{pmatrix} Ai[\zeta_{nj}(z)] & Bi[\zeta_{nj}(z)] & 0 & 0 \\ -S_j^{1/3}Ai'[\zeta_{nj}(z)] & -S_j^{1/3}Bi'[\zeta_{nj}(z)] & 0 & 0 \\ 0 & 0 & \exp(i\gamma_{nj}) & \exp(-i\gamma_{nj}) \\ 0 & 0 & i\gamma_{nj}\exp(i\gamma_{nj}) & -i\gamma_{nj}\exp(-i\gamma_{nj}) \end{pmatrix} \begin{pmatrix} a_{nj} \\ b_{nj} \\ c_{nj} \\ d_{nj} \end{pmatrix}
$$

$$(128)$$

where the banded 4x4 matrix means that the shear and compressional eigenfunctions are propagated independently from each other even though they depend on each other in the matching process. Therefore, the propagation matrix can be divided into a 2x2 compressional propagation matrix and a 2x2 shear propagation matrix. Inverting and evaluating the compressional propagation matrix at the bottom of the jth layer gives

$$
\begin{pmatrix} a_{nj} \\ b_{nj} \end{pmatrix} = \begin{pmatrix} \pi\, Bi'[\zeta_{nj}(z_{j+1})] & \pi\, S_j^{-1/3}Bi[\zeta_{nj}(z_{j+1})] \\ -\pi\, Ai'[\zeta_{nj}(z_{j+1})] & -\pi\, S_j^{-1/3}Ai[\zeta_{nj}(z_{j+1})] \end{pmatrix} \begin{pmatrix} u_{nj}(z_{j+1}) \\ u'_{nj}(z_{j+1}) \end{pmatrix} \quad (129)
$$

where the Wronskian relationship[54]

$$
Bi'(\zeta)\,Ai(\zeta) - Bi(\zeta)\,Ai'(\zeta) = 1/\pi \tag{130}
$$

has been used and the primes denote the derivative with respect to the argument. For the shear propagation matrix we obtain

$$
\begin{pmatrix} c_{nj} \\ d_{nj} \end{pmatrix} = \begin{pmatrix} 1/2\,\exp(-i\gamma_{nj}z_{j+1}) & -i\,\exp(-i\gamma_{nj}z_{j+1})/(2\gamma_{nj}) \\ 1/2\,\exp(i\gamma_{nj}z_{j+1}) & i\,\exp(i\gamma_{nj}z_{j+1})/(2\gamma_{nj}) \end{pmatrix} \begin{pmatrix} v_{nj}(z_{j+1}) \\ v'_{nj}(z_{j+1}) \end{pmatrix}
$$

$$(131)$$

where substituting the unknown coefficients back into Equation (128) and evaluating it at the top of the jth layer gives

$$
\begin{pmatrix} u_{nj}(z_j) \\ u'_{nj}(z_j) \\ v_{nj}(z_j) \\ v'_{nj}(z_j) \end{pmatrix} = \begin{pmatrix} C_{11} & C_{12} & 0 & 0 \\ C_{21} & C_{22} & 0 & 0 \\ 0 & 0 & C_{33} & C_{34} \\ 0 & 0 & C_{43} & C_{44} \end{pmatrix} \begin{pmatrix} u_{nj}(z_{j+1}) \\ u'_{nj}(z_{j+1}) \\ v_{nj}(z_{j+1}) \\ v'_{nj}(z_{j+1}) \end{pmatrix} \tag{132}
$$

where the elements of the compressional eigenfunction are given by

$$
C_{11} = \pi \left[\ \text{Ai}[\zeta_{nj}(z_j)]\ \text{Bi}'[\zeta_{nj}(z_{j+1})] - \text{Ai}'[\zeta_{nj}(z_{j+1})]\ \text{Bi}[\zeta_{nj}(z_j)]\ \right] \tag{133a}
$$

$$
C_{12} = \pi \left[\ \text{Ai}(\zeta_{nj}(z_j))\ \text{Bi}(\zeta_{nj}(z_{j+1})) - \text{Ai}(\zeta_{nj}(z_{j+1}))\ \text{Bi}(\zeta_{nj}(z_j))\ \right]/S_j^{1/3} \tag{133b}
$$

$$
C_{21} = \pi \left[\ \text{Ai}'(\zeta_{nj}(z_{j+1}))\ \text{Bi}'(\zeta_{nj}(z_j)) - \text{Ai}'(\zeta_{nj}(z_j))\ \text{Bi}'(\zeta_{nj}(z_{j+1}))\ \right]S_j^{1/3} \tag{133c}
$$

and

$$
C_{22} = \pi \left[\ \text{Ai}[\zeta_{nj}(z_{j+1})]\ \text{Bi}'[\zeta_{nj}(z_j)] - \text{Ai}'[\zeta_{nj}(z_j)]\ \text{Bi}[\zeta_{nj}(z_{j+1})]\ \right] \tag{133d}
$$

and the elements for the shear eigenfunction are given by

$$
C_{33} = C_{44} = \cos(\gamma_{nj}D_j) \tag{134a}
$$

$$
C_{34} = -\gamma_{nj}^{-1} \sin(\gamma_{nj}D_j) \tag{134b}
$$

and

$$
C_{43} = \gamma_{nj} \sin(\gamma_{nj}D_j) \tag{134c}
$$

where $D_j = z_{j+1} - z_j$ is the thickness of the jth layer and γ_{nj} is given after Equation (100). For trapped compressional modes, only the exponentially

41

decaying solution of the Airy functions must be used since there is no acoustic source in the bottom. If $Ai(\zeta)$ is evaluated at the exponentially decaying part of the function, then $Bi(\zeta)$ cannot be evaluated simultaneously because it is exponentially increasing producing a floating point overflow in the computer. Therefore, an Airy function subroutine that can calculate one of the solutions, instead of both of them simultaneously, must be used. Another serious complication that occurs with the evaluation of Equations (133) is the numerically unstable result when the subtraction of large but very close numbers is performed. In the case where $|\zeta| \gg 10$ and $Arg\ \zeta \cong \pi$ the Airy functions have the asymptotic forms,

$$Bi(\zeta) \longrightarrow i\ Ai(\zeta) \tag{135a}$$

and

$$Bi'(\zeta) \longrightarrow i\ Ai'(\zeta) \tag{135b}$$

which causes precision problems when evaluating the Wronskian and the elements of the propagation matrix. These same propagation matrix coefficients have been encountered by Gordon[55,56] in the area of quantum mechanics and he solved the problem by direct substitution of the series solutions for the Airy functions and its derivatives in Equations (133) to factor out the exponential or sinusoidal functions. However, these where performed under the assumption of purely real arguments of the Airy functions and the series solutions used do not apply to complex arguments. A similar substitution and cancellation technique is obtained by evaluating the numerically stable independent Airy results given by Schulten, Anderson, and Gordon[57] to avoid floating point overflow and other precision problems.

In the water layers the propagation relationship reduces to

$$\begin{pmatrix} u_{nj}(z_j) \\ u'_{nj}(z_j) \end{pmatrix} = \begin{pmatrix} C_{11} & C_{12} \\ C_{21} & C_{22} \end{pmatrix} \begin{pmatrix} u_{nj}(z_{j+1}) \\ u'_{nj}(z_{j+1}) \end{pmatrix} \tag{136}$$

where the unknowns are given in Equations (133).

In the models to be described next, it is further assumed that the acoustic properties of each elastic layer are constant. This is done for simplicity and with the knowledge that it is not easy to determine all the

fine-structure properties of the bottom sediments experimentally, therefore the bottom is usually described as layers of constant properties.[58,59]

CASE A. RIGID FALSE BOTTOM MODEL

The rigid bottom interface is at j=F in Figure 4, the water-bottom interface is at j=J, and the soft surface of the ocean is at j=1. The rigid "false" bottom interface is artificially incorporated only to convert a continuous wave number spectrum into a discrete form. Therefore, the trapped modes will be treated as if the rigid bottom does not exist. Each water layer has two unknowns to be determined, and each solid layer has four. The rigid bottom has null tangential and normal particle velocity. Therefore, the boundary conditions for the radiating modes at the "false" bottom interface are

$$u_{nF-1}(z_F) + v'_{nF-1}(z_F) = 0 \qquad (137a)$$

and

$$u'_{nF-1}(z_F) + \Xi_n v_{nF-1}(z_F) = 0 \qquad (137b)$$

which have four unknowns for any trial value Ξ_n of the eigenvalue squared k_n^2. These equations are conveniently written in the matrix form

$$
\begin{pmatrix} u_{nF-1}(z_F) \\ u'_{nF-1}(z_F) \\ v_{nF-1}(z_F) \\ v'_{nF-1}(z_F) \end{pmatrix} =
\begin{pmatrix} 0 & -1 \\ -\Xi_n & 0 \\ 1 & 0 \\ 0 & 1 \end{pmatrix}
\begin{pmatrix} v_{nF-1}(z_F) \\ v'_{nF-1}(z_F) \end{pmatrix} \qquad (138)
$$

where the special 4x2 matching matrix is represented by M_F.

This set of equations is substituted into the up-layer propagation matrix for the F-1 layer to obtain

$$\begin{pmatrix} u_{nF-1}(z_{F-1}) \\ u'_{nF-1}(z_{F-1}) \\ v_{nF-1}(z_{F-1}) \\ v'_{nF-1}(z_{F-1}) \end{pmatrix} = \mathbb{C}_{F-1} \mathbb{M}_F \begin{pmatrix} v_{nF-1}(z_F) \\ v'_{nF-1}(z_F) \end{pmatrix} \tag{139}$$

where both eigenfunctions and their derivatives are still to be determined. This new recurrence relationship is substituted into the up-layer matching matrix for the F-1 solid-solid boundary to obtain the new relationship

$$\begin{pmatrix} u_{nF-2}(z_{F-1}) \\ u'_{nF-2}(z_{F-1}) \\ v_{nF-2}(z_{F-1}) \\ v'_{nF-2}(z_{F-1}) \end{pmatrix} = \mathbb{M}_{F-1} \mathbb{C}_{F-1} \mathbb{M}_F \begin{pmatrix} v_{nF-1}(z_F) \\ v'_{nF-1}(z_F) \end{pmatrix} \tag{140}$$

and by the same token, the matching and propagating matrices for the solid layers are multiplied to each other until the water-bottom interface is reached with the relationship

$$\begin{pmatrix} u_{nJ}(z_J) \\ u'_{nJ}(z_J) \\ v_{nJ}(z_J) \\ v'_{nJ}(z_J) \end{pmatrix} = \mathbb{C}_J \, \mathbb{M}_{J+1} \, \mathbb{C}_{J+1} \cdots \mathbb{M}_{F-1} \, \mathbb{C}_{F-1} \, \mathbb{M}_F \begin{pmatrix} v_{nF-1}(z_F) \\ v'_{nF-1}(z_F) \end{pmatrix}. \tag{141}$$

The multiplication of the propagating and matching matrices in the solid layers is now given by the 4x2 matrix

$$\mathbb{E} \equiv \mathbb{C}_J \, \mathbb{M}_{J+1} \, \mathbb{C}_{J+1} \cdots \mathbb{M}_{F-1} \, \mathbb{C}_{F-1} \, \mathbb{M}_F. \tag{142}$$

Next is a use of the liquid-solid boundary conditions to evaluate the compressional eigenfunction at the water column. The three boundary conditions are

$$u'_{nJ-1}(z_J) = u'_{nJ}(z_J) + \Xi_n \, v_{nJ}(z_J) \tag{143a}$$

$$\rho_{J-1} u_{nJ-1}(z_J) = \rho_J \, T_J \, u_{nJ}(z_J) - \rho_J \, Q_J \, v'_{nJ}(z_J) \tag{143b}$$

44

and

$$2 \, u'_{nJ}(z_J) + (2 \, \Xi_n - \kappa_J^2) \, v_{nJ}(z_J) = 0 \qquad (143c)$$

where the first two equations are needed to evaluate the compressional eigenfunction in the liquid layer, and the third condition will be used as the characteristic equation of the environment.

The first two equations are rewritten in matrix form as

$$\begin{pmatrix} u_{nJ-1}(z_J) \\ u'_{nJ-1}(z_J) \end{pmatrix} = \begin{pmatrix} T_J/R_J & 0 & 0 & -Q_J/R_J \\ 0 & 1 & \Xi_n & 0 \end{pmatrix} \begin{pmatrix} u_{nJ}(z_J) \\ u'_{nJ}(z_J) \\ v_{nJ}(z_J) \\ v'_{nJ}(z_J) \end{pmatrix} \qquad (144)$$

where the 2x4 special matching matrix will be known as M_J. Substituting Equations (137) into this set of equations gives

$$\begin{pmatrix} u_{nJ-1}(z_J) \\ u'_{nJ-1}(z_J) \end{pmatrix} = M_J \, \mathbb{E} \begin{pmatrix} v_{nF-1}(z_F) \\ v'_{nF-1}(z_F) \end{pmatrix}. \qquad (145)$$

Now comes the propagation and matching in the liquid layers. The method is the same as for the solid layers, except that now the matrices to multiply are 2x2. After propagating and matching up to the surface it is found that

$$\begin{pmatrix} u_{n1}(z_1) \\ u'_{n1}(z_1) \end{pmatrix} = \mathbb{C}_1 \, M_2 \, \mathbb{C}_2 \, M_3 \, \mathbb{C}_3 \ldots M_{J-1} \, \mathbb{C}_{J-1} \, M_J \, \mathbb{E} \begin{pmatrix} v_{nF-1}(z_F) \\ v'_{nF-1}(z_F) \end{pmatrix} \qquad (146)$$

where the final product of all the propagation and matching matrices is defined as the 2x2 matrix

$$\mathbb{F} \equiv \mathbb{C}_1 \, M_2 \, \mathbb{C}_2 \, M_3 \, \mathbb{C}_3 \ldots M_{J-1} \, \mathbb{C}_{J-1} \, M_J \, \mathbb{E}. \qquad (147)$$

The pressure-release boundary condition of the surface $(j=1)$ gives $u_{n1}(z_1 = 0) = 0$ and the derivative of the eigenfunction at the surface will be arbitrarily set to unity since the normalization condition will take care of its proper evaluation. This gives

$$\begin{pmatrix} 0 \\ 1 \end{pmatrix} = F \begin{pmatrix} v_{nF-1}(z_F) \\ v'_{nF-1}(z_F) \end{pmatrix} \tag{148}$$

where inverting F gives

$$v_{nF-1}(z_F) = (F_{22} - F_{12}(F_{21}/F_{11}))^{-1} \tag{149a}$$

and

$$v'_{nF-1}(z_F) = (F_{21} - F_{11}(F_{22}/F_{12}))^{-1}. \tag{149b}$$

A final substitution of the shear eigenfunctions at the rigid bottom interface into Equation (141) gives the two necessary values to be substituted into the chosen characteristic equation, Equation (143c). The trial value Ξ_n is the square of an eigenvalue k_n when the complex characteristic equation (or determinant) is null, i.e.,

$$W(k_n) \equiv 2\, u'_{nJ}(z_J) + (2\, k_n^2 - \kappa_J^2)\, v_{nJ}(z_J) = 0. \tag{150}$$

Note that the objective is to calculate only $u'_{nJ}(z_J)$ and $v_{nJ}(z_J)$. Therefore, there is no need to calculate the eigenfunctions at the other interfaces to find the eigenvalues of the problem. This same method of matrix multiplication is also used to evaluate the eigenfunctions at all the interfaces for the normalization calculation described in the next chapter.

CASE B. SEMI-INFINITE BASEMENT MODEL

This model is used for the trapped modes and the radiating modes undiscriminatingly. The trapped modes have the property that they are exponentially decreasing with depth in an isovelocity layer and the radiating modes represent out-going propagating waves that oscillate towards infinity without reflections but with absorption which causes its damping. Both, compressional and shear, eigenfunctions can be trapped or radiating. Therefore, it is no longer appropriate to refer to a mode as simply trapped or radiating. In fact, there are four mode classifications. There is the most

46

common mode where the compressional eigenfunction is trapped and the shear eigenfunction is radiating. This type of mode will be labeled a "T-R mode," where the first letter always refers to the compressional function. The compressional eigenfunction of the T-R mode in the semi-infinite layer is described by the exponential function

$$u_{nF-1}(z) = a_{nF-1} \exp(-\eta_{nF-1} z) \tag{151a}$$

and

$$u'_{nF-1}(z) = -\eta_{nF-1} \, u_{nF-1}(z) \tag{151b}$$

where $\eta_{nF-1}^2 = k_n^2 - k_{F-1}^2$. The shear eigenfunction is radiating without reflections, i.e.,

$$v_{nF-1}(z) = c_{nF-1} \, \exp(i\gamma_{nF-1} z) \tag{151c}$$

and

$$v'_{nF-1}(z) = i\gamma_{nF-1} \, v_{nF-1}(z). \tag{151d}$$

Now the eigenfunctions at the top of the basement layer are given by

$$
\begin{pmatrix}
u_{nF-1}(z_{F-1}) \\
u'_{nF-1}(z_{F-1}) \\
v_{nF-1}(z_{F-1}) \\
v'_{nF-1}(z_{F-1})
\end{pmatrix}
=
\begin{pmatrix}
1 & 0 \\
-\eta_{nF-1} & 0 \\
0 & 1 \\
0 & i\gamma_{nF-1}
\end{pmatrix}
\begin{pmatrix}
u_{nF-1}(z_{F-1}) \\
v_{nF-1}(z_{F-1})
\end{pmatrix}
\tag{152}
$$

which gives the values at the top of the basement layer. Lets define the special 4x2 propagating matrix in Equation (152) as $\mathbb{C}_{F-1}$ and only two of its elements must be changed if the mode becomes a T-T, R-T, or R-R mode. To obtain the values at the bottom of the F-2 layer, we multiply by the matching matrix at this interface which gives

$$
\begin{pmatrix}
u_{nF-2}(z_{F-1}) \\
u'_{nF-2}(z_{F-1}) \\
v_{nF-2}(z_{F-1}) \\
v'_{nF-2}(z_{F-1})
\end{pmatrix}
= \mathbb{M}_{F-1} \, \mathbb{C}_{F-1}
\begin{pmatrix}
u_{nF-1}(z_{F-1}) \\
v_{nF-1}(z_{F-1})
\end{pmatrix}
\tag{153}
$$

47

which corresponds to Equation (140) in the previous matrix multiplication method. By the same matching and propagating algorithm the values at the surface of the ocean wave guide are reached with the relationship

$$\begin{pmatrix} 0 \\ 1 \end{pmatrix} = \mathbb{F} \begin{pmatrix} u_{nF-1}(z_{F-1}) \\ v_{nF-1}(z_{F-1}) \end{pmatrix} \tag{154}$$

where the 2x2 matrix

$$\mathbb{F} = \mathbb{C}_1 \, \mathbb{M}_2 \, \mathbb{C}_2 \cdots \mathbb{M}_J \, \mathbb{C}_J \cdots \mathbb{M}_{F-1} \, \mathbb{C}_{F-1} \tag{155}$$

is inverted to obtain $u_{nF-1}(z_{F-1})$ and $v_{nF-1}(z_{F-1})$. After calculating their derivatives using Equations (151b) and (151d), the solution is propagated up to the top of the Jth layer to obtain $u'_{nJ}(z_J)$ and $v_{nJ}(z_J)$ which are needed to calculate the characteristic equation, Equation (150). This method requires one loop of matrix multiplications in the solid to obtain the matrix $\mathbb{E}$ in Equation (142), which is saved for later use, but is also used to keep multiplying matrices in the liquid layers.

After evaluating the eigenvalue, the eigenfunction may be calculated by down-layer multiplication of propagation and matching matrices. For this purpose, the matrices are slightly different from the up-layer ones. The elements of the matching matrix in Equation (125) for down-layer matching of the eigenfunctions are given by

$$M^{\downarrow}_{11} = M^{\downarrow}_{33} = Q_{j+1} + T_j / R_{j+1}, \tag{156a}$$

$$M^{\downarrow}_{14} = Q_{j+1} - Q_j / R_{j+1}, \tag{156b}$$

$$M^{\downarrow}_{22} = M^{\downarrow}_{44} = T_{j+1} + Q_{j+1} / S_{j+1}, \tag{156c}$$

$$M^{\downarrow}_{41} = T_{j+1} - T_j / R_{j+1}, \tag{156d}$$

$$M_{23}^{\downarrow} = M_{41}^{\downarrow} \, k_n^2, \tag{156e}$$

and

$$M_{32}^{\downarrow} = 2 \, (1 - 1 \, / \, S_{j+1}) \, / \, \kappa_{j+1}^2. \tag{156f}$$

The arrows have been include to emphasize the down-layer propagation and matching matrices and to distinguish them from the up-layer ones. The compressional elements of the down-layer propagating matrix in Equation (132) are given by

$$C_{11}^{\downarrow} = \pi \, \Big[\, Ai[\zeta_{nj}(z_{j+1})] \, Bi'[\zeta_{nj}(z_j)] \, - \, Ai'[\zeta_{nj}(z_j)] \, Bi[\zeta_{nj}(z_{j+1})] \, \Big], \tag{157a}$$

$$C_{12}^{\downarrow} = \pi \, \Big[\, Ai(\zeta_{nj}(z_{j+1})) \, Bi(\zeta_{nj}(z_j)) \, - \, Ai(\zeta_{nj}(z_j)) \, Bi(\zeta_{nj}(z_{j+1})) \, \Big] / S_j^{1/3}, \tag{157b}$$

$$C_{21}^{\downarrow} = \pi \, \Big[\, Ai'(\zeta_{nj}(z_j)) \, Bi'(\zeta_{nj}(z_{j+1})) \, - \, Ai'(\zeta_{nj}(z_{j+1})) \, Bi'(\zeta_{nj}(z_j)) \, \Big] S_j^{1/3}, \tag{157c}$$

and

$$C_{22}^{\downarrow} = \pi \, \Big[\, Ai[\zeta_{nj}(z_j)] \, Bi'[\zeta_{nj}(z_{j+1})] \, - \, Ai'[\zeta_{nj}(z_{j+1})] \, Bi[\zeta_{nj}(z_j)] \, \Big]. \tag{157d}$$

The shear elements of the down-layer propagating matrix are given by

$$C_{33}^{\downarrow} = C_{44}^{\downarrow} = \cos(\gamma_{nj} D_j) \tag{158a}$$

$$C_{34}^{\downarrow} = \gamma_{nj}^{-1} \, \sin(\gamma_{nj} D_j) \tag{158b}$$

and

$$C_{43}^{\downarrow} = -\gamma_{nj} \, \sin(\gamma_{nj} D_j). \tag{158c}$$

However, to obtain the eigenfunctions, the zeros of the complex characteristic equation, Equation (150), must be found. The most optimum method for finding the complex zeros may never be known[46] since many

49

challenging environmental conditions can be encountered. Examples are secondary sound channels and surface ducts which cause degenerate eigenvalues with irregular spacing and some of these eigenvalues may be too close to each other for the limited precision of a computer. Ellis[60] has tackled a similar problem with a two-ended shooting technique, but the model incorporates the effects of shear wave and the attenuation coefficients as an approximation for small values, he does not take into account the radiating modes, and does not search for the eigenvalues in the complex plane. However, a simple algorithm may be obtained after analyzing the behavior of Equation (150) for a simplistic ocean environment and it may be eventually improved as we encounter more difficult situations.

The complex determinant in Equation (150) was calculated as a function of the complex trail wave number for the very simple case of a water column over a semi-infinite bottom layer. To start with a very simple case, the bottom is a fluid layer with the acoustic properties in the second row of Table 1. These fluid properties are obtained from Jensen,[17] the properties of clay-silt, sand, and basalt are taken from the paper by Werby and Tango,[61] and the parameters for chalk are given by Ellis.[11] The first case is the fluid bottom with a water column 200.0 meters deep and a constant sound speed of 1500.0 m/s. The bottom is fluid-like because of the very small shear speed (1.0 m/s) and the relatively large shear attenuation coefficient to rapidly damp-out the remaining shear contribution. The frequency of the sound is 25.0 Hz and all other bottom properties are given in Table 1.

The contour plot of the complex determinant is displayed in Figure 6. The dash curves represent the contour where the real part of the determinant is zero, and the solid curves represent the contour where the imaginary part of the determinant is zero. Since both components of Equation (150) must be zero simultaneously, then the complex eigenvalues are given by the points where both curves intersect. Note that these curves are perpendicular at the point of intersection, therefore Equation (150) is an analytic equation that satisfies Cauchy-Riemann relations. This simplifies the Newton-Raphson method for converging into the complex zeros. The real part of the determinant along the real axis is plotted in Figure 7 where the number of eigenvalues is equal to the number of zeros of this curve. The maximum trail wave number is given by the minimum speed in the water column and a general behavior of this curve

is that it tends to infinity as the wave number approaches zero. A search for the change in the sign of this curve will be used to obtain an initial estimate of the eigenvalue. Nagl[41] made a detailed study of the behavior of the purely real eigenvalues along the real axis and derived the useful approximation

$$\Delta k(n) \cong (n \ \pi \ c_{min})/(2 \ f \ z_J^2) \qquad (159)$$

which gives the approximate spacing of the eigenvalues as a function of the mode number n, the frequency f, the depth of the ocean floor, and the minimum sound speed in the water column. This equation is used to establish the step size in the search for the first couple of eigenvalues. The spacing between the previous two eigenvalues is later used to establish the step size for the next eigenvalues.

After these zeros are found, we vary the imaginary part of the trail wave number in order to follow the dash curves in Figure 6 until a change in sign of the imaginary part of the determinant is detected. Newton-Raphson[46] method was tried to pin-down the complex eigenvalues in double precision accuracy but there where times when it converged to unrealistic values. This method was also used by Otsubo[62] for relatively simple ocean environments without the effects of shear waves but we have discarded it as "not uniformly convergent." A more uniformly convergent method is described by Morris[48] where, instead of searching for the complex zeros of Equation (150), we search for the local minima of the magnitude of the determinant. These minima are located exactly where the complex eigenvalues are, the method uniformly converges to the local minima, but the convergence is slightly slower than the Newton-Raphson method. Since the uniform convergence is more important, this is the method used in this model.

A plot of the eigenvalues in the complex k-plane is given in Figure 8 where the three trapped modes have eigenvalues with negligible imaginary parts, and the four radiating modes have eigenvalues with real parts smaller than 0.09 1/m. Note that the radiating eigenvalues have such a large imaginary part that they get rapidly attenuated as they propagate in range therefore contributing only to the intensity near the source.

If a rigid false boundary is placed at a depth of 1200.0 meters,[53] the

radiating spectrum becomes the one displayed in Figure 9, which agrees with Miller's perturbative approximation. The real part of the minima corresponds to the four radiating eigenvalues in Figure 8, which means that the rigid false bottom method is trying to give preference to the true radiating eigenvalues over the "pseudo-eigenvalues" by giving the latter a larger imaginary part.

The trapped and radiating eigenvalues are not unique in the complex wave number spectrum. Surface waves may also be incorporated in this ocean model. The surface wave produced at a solid-vacuum interface is called a Rayleigh wave. In the case of a liquid-solid interface the surface wave is called a Generalized Rayleigh wave, while the solid-solid surface wave is called a Stoneley wave. These waves satisfy the wave equation and the boundary conditions but they decay exponentially in both directions very rapidly. Therefore surface waves are not expected to be of extremely high importance when the receiver is greater than a wavelength away from interface, even though they may be added in these transmission loss calculations without complications.[63,64]

The spherical waves diverging from the source may be expressed as the infinite summation of plane waves. Each plane wave hits the liquid-solid boundary and each solid-solid interface of the wave guide at a different angle of incidence. Some of them will have an angle of incidence greater or equal to the compressional critical angle and/or the shear critical angle of an elastic layer. Under this condition, total internal reflection occurs and the wave propagates parallel to the interface. This wave is also called a surface wave since its amplitude decays exponentially with the normal distance from the interface along which the propagation occurs.

Lateral waves propagate at the solid side of the liquid-solid interface and they are automatically incorporated in the model when the trapped and radiating modes are used. When a spherical wave from a nearby source hits the liquid-solid interface, two lateral waves are created which will propagate in the elastic layer and parallel to the interface. One is caused by the shear critical angle of incidence and the other is caused by the compressional one.[65] As they propagate, they reradiate back into the liquid layer causing the Schmidt head wave.

CHAPTER 7

THE NORMALIZATION COEFFICIENT

The depth functions are complete and orthogonal. However, they are not necessarily normalized since the wave equation is satisfied regardless of the constant in front of the solution. Remember that the derivative of the eigenfunction at the surface has been set to unity under the condition that the normalization constant would take care of this last unknown. For the transmission loss calculation in the next chapter, the summation of normalized eigenfunctions is needed to obtain the proper contribution of each mode.

The normalization constant for each mode is given by

$$N_n = \sum_{j=1}^{F-1} N_{nj} \tag{160a}$$

where N_{nj} is the contribution of the jth layer to the nth mode, i.e.,

$$N_{nj} = \rho_j \int_{z_j}^{z_{j+1}} u_{nj}(z)\, u_{nj}(z)\, dz. \tag{160b}$$

The normalization coefficient is in general a complex number, and the eigenfunctions at all the interfaces are known after the eigenvalues are found.

In this ocean model, the water layers have variable sound speed and negligible attenuation coefficient compared to the absorption of the bottom layers. However, these elastic layers of the bottom have constant acoustic properties. Therefore, the normalization calculation for both types of layers is different.

The water layers are defined to be the ones where $1 \leq j < J$. Gordon's formulas[55] provide the analytical integration of a linear combination of Airy

53

functions. The formulas to use are

$$\int A[a(z+b)] \, B[a(z+b)] \, dz = (z+b)AB - A'B'/a \tag{161a}$$

and

$$\int A[a(z+b_1)] \, B[a(z+b_2)] \, dz = \frac{A'B - AB'}{a^2(b_1 - b_2)} \tag{161b}$$

where

$$A[a(z+b_1)] \equiv a_1 Ai[a(z+b_1)] + b_1 Bi[a(z+b_1)] \tag{162a}$$

and

$$B[a(z+b_2)] \equiv a_2 Ai[a(z+b_2)] + b_2 Bi[a(z+b_2)] \tag{162b}$$

represent any linear combination of Airy functions.

Equation (161a) relates to Equation (160b) where $A = B$. In this case,

$$N_{nj} = \rho_j \left[(z + \mathscr{b}_{nj}) \, u_{nj}^2(\zeta_{nj}) + u_{nj}'^2(\zeta_{nj})/S_j^{1/3} \right]_{z_j}^{z_{j+1}} \tag{163}$$

where

$$\mathscr{b}_{nj} \equiv (k_j^2 - k_n^2) / S_j - z_j . \tag{164}$$

Note that, even if the attenuation coefficient of the water column is neglected, the argument of the Airy function is complex because of the complex eigenvalue. Therefore, the absorption of the bottom layers are affecting the propagation of sound in the water column

The calculation of the normalization contribution in the elastic layers is simplified by the assumption of sediments with constant acoustic properties, but a distinction must be made for the case where the function decays exponentially with depth (trapped mode) or if it oscillates (radiating mode).

In the case of a trapped mode, the compressional eigenfunction in the jth layer is given by

$$u_{nj}(z) = u_{nj}(z_j) \exp\left[-\eta_{nj}(z - z_j)\right] \tag{165}$$

for $z_j \leq z \leq z_{j+1}$ and where $\eta_{nj}^2 = k_n^2 - k_j^2$. Substituted into Equation (160b) gives the solution

$$N_{nj} = \rho_j \, u_{nj}^2(z_j) \left\{ 1 - \exp\left[-2 \, D_j \, \eta_{nj}\right] \right\} / [2 \, \eta_{nj}] \qquad (166)$$

where $D_j = z_{j+1} - z_j$ is the thickness of the elastic layer.

The compressional eigenfunction to use for the oscillatory depth function in the jth layer is

$$u_{nj}(z) = u_{nj}(z_j) \, \cos[\eta_{nj}(z-z_j)] + u'_{nj}(z_j) \, \eta_{nj}^{-1} \, \sin[\eta_{nj}(z-z_j)] \qquad (167)$$

and the Equation (160b) becomes

$$N_{nj} = \rho_j \left(u_{nj}^2 + u'^2_{nj} \, \eta_{nj}^{-2} \right) \left[\frac{1}{2} D_j + \frac{\sin(2 \, D_j \, \eta_{nj})}{4 \, \eta_{nj}} \right] + \rho_j \, u_{nj} \, u'_{nj} \left(\frac{\sin(D_j \, \eta_{nj})}{\eta_{nj}} \right)^2$$

$$(168)$$

where the argument of the eigenfunction has been omitted for simplicity and where $J \leq j < F$.

Finally, the normalized eigenfunctions and their derivatives are given by

$$\hat{u}_{nj}(z) \equiv u_{nj}(z) / N_n^{1/2}, \qquad (169a)$$

$$\hat{u}'_{nj}(z) \equiv u'_{nj}(z) / N_n^{1/2}, \qquad (169b)$$

$$\hat{v}_{nj}(z) \equiv v_{nj}(z) / N_n^{1/2}, \qquad (169c)$$

and

$$\hat{v}'_{nj}(z) \equiv v'_{nj}(z) / N_n^{1/2}. \qquad (169d)$$

After all the eigenvalues and normalized eigenfunctions are found, it is next to calculate the transmission loss of sound in this ocean wave guide.

CHAPTER 8

THE TRANSMISSION LOSS

Any massive object that vibrates radiates acoustic energy. *Power* is the time rate at which energy is radiated and *intensity* is defined as the rate of energy flow through a unit area. The intensity is a vector quantity which also gives the direction of the energy flow. However, the fluctuations of the intensity, the pressure, and the power are of order of magnitudes and this presents problems when plotting them. Therefore, in acoustics, the intensity is converted into decibels in order to reduce the high fluctuations. The power of background noise is about 30μWatts with a maximum sound pressure of 3000μPascals which converted into decibel units gives a sound pressure level of about 40dB. However, the power of very loud music may be 30 Watts with a sound pressure of 3 Pascals which corresponds to a sound pressure level near 100dB.

The *transmission loss* is defined as

$$TL = - 10 \log\left(\frac{I(r,z)}{I_0}\right) \tag{170}$$

where, in the water column, $I(r,z)$ is the magnitude of the acoustic intensity in Equation (33) and I_0 is the reference intensity at one meter from the source in the water column. Since spherical spreading of the waves occurs at one meter from the source, the reference intensity is equal to the square of the time-averaged *rms* pressure at one meter from the source divided by the acoustic impedance at this same distance. The reference pressure is given by Equation (28). Substitution of the scalar potential into Equation (28) gives

$$p(r,z) = \frac{1}{4} \omega \rho(z_0) \rho(z) \sum_{n=1}^{N} \hat{u}_n(z_0) \hat{u}_n(z) H_0^{(1)}(k_n r) \tag{171}$$

and this expression substituted into the transmission loss expression gives

$$TL_c(r,z) = 20 \log \left| -i\pi\rho(z) \sum_{n=1}^{N} \hat{u}_n(z_0) \hat{u}_n(z) H_0^{(1)}(k_n r) \right| \qquad (172)$$

which is called the *coherent* transmission loss because the phase factor of each mode has been taken into account in the summation, and the absolute value is taken after the summation is completed. The layer subscript j has been erased from the variables to minimize the complexity of the equations. Note that the transmission loss is also a function of the depth of the source z_0 and the fact that the acoustic intensity is proportional to the pressure squared has been used. This coherent transmission loss is highly variable in space due to phase-dependent interference effects among the eigenfunctions and a smoother function is more appropriate for sonar predictions.

The detailed interference effects may be averaged-out to yield smooth transmission loss curves by summing the individual modal energies. The result is called the *incoherent* transmission loss. The resulting incoherent transmission loss in the water column is

$$TL_i(r,z) = 10 \log \left(\pi^2 \rho^2(z) \sum_{n=1}^{N} \left| \hat{u}_n(z_0) \hat{u}_n(z) H_0^{(1)}(k_n r) \right|^2 \right) \qquad (173)$$

where the logarithm is of base 10, the transmission loss is always purely real, and its dimension is in decibels.

In the elastic layers, the intensity at the point of observation is now given by the expression

$$I(r,z) = \left| \overleftrightarrow{P} \cdot \vec{v} \right| \qquad (174)$$

where $\overleftrightarrow{P}$ is the stress matrix in Equation (111) and $\vec{v}$ is the particle velocity in Equations (55), (60a), and (60b) where the potentials are given in Equations (86) and (101). With these equations, the vector intensity is written as

$$\vec{I} = \hat{P} \cdot \vec{v} = I_r \hat{r} + I_z \hat{z} \tag{175}$$

where

$$I_r = \left\{ v_r \left[(\lambda+2\mu) \frac{\partial v_r}{\partial r} + \lambda \left(\frac{v_r}{r} + \frac{\partial v_z}{\partial z} \right) \right] + v_z \, \mu \left(\frac{\partial v_r}{\partial z} + \frac{\partial v_z}{\partial r} \right) \right\} /i\omega \tag{176a}$$

and

$$I_z = \left\{ v_z \left[(\lambda+2\mu) \frac{\partial v_z}{\partial z} + \lambda \left(\frac{v_r}{r} + \frac{\partial v_r}{\partial r} \right) \right] + v_r \, \mu \left(\frac{\partial v_r}{\partial z} + \frac{\partial v_z}{\partial r} \right) \right\} /i\omega. \tag{176b}$$

Direct substitution of the scalar potentials in Equations (86) and (101) into the particle velocity components in Equations (60a) and (60b) gives

$$v_z(r,z) = \sum_{n=1}^{N} \left(v_z \right)_n \tag{177}$$

where the contribution from the nth mode is given by

$$\left(v_z \right)_n = (i/4) \, \rho(z_o) \, \hat{u}_n(z_o) \left[\hat{u}'_n(z) + k_n^2 \, \hat{v}_n(z) \right] H_o^{(1)}(k_n r) \tag{178}$$

and

$$v_r(r,z) = \sum_{n=1}^{N} \left(v_r \right)_n \tag{179}$$

where

$$\left(v_r \right)_n = (i/4) \, \rho(z_o) \, \hat{u}_n(z_o) \left[\hat{u}_n(z) + \hat{v}'_n(z) \right] k_n \, H_o^{(1)\prime}(k_n r) \tag{180}$$

and the prime over the Hankel function stands for the derivative with respect to the argument.

By the same token, the derivatives of the components of the particle velocity are given by the summation of the modal contributions given by

58

$$(\partial v_z/\partial r)_n = (i/4)\ \rho(z_o)\ \hat{u}_n(z_o)\ [\hat{u}_n'(z) + k_n^2\ \hat{v}_n(z)]\ k_n\ H_o^{(1)'}(k_n r)$$

$$(181a)$$

$$(\partial v_r/\partial r)_n = (i/4)\ \rho(z_o)\ \hat{u}_n(z_o)\ [\hat{u}_n(z) + \hat{v}_n'(z)]\ k_n^2\ H_o^{(1)''}(k_n r)$$

$$(181b)$$

$$(\partial v_z/\partial z)_n = (i/4)\ \rho(z_o)\ \hat{u}_n(z_o)\ \{k_n^2[\hat{u}_n(z) + \hat{v}_n'(z)] - k^2(z)\ \hat{u}_n(z)\}\ H_o^{(1)}(k_n r)$$

$$(181c)$$

and

$$(\partial v_r/\partial z)_n = (i/4)\ \rho(z_o)\ \hat{u}_n(z_o)\ [\hat{u}_n'(z) + k_n^2\ \hat{v}_n(z) - \kappa^2(z)\ \hat{v}_n(z)]\ k_n\ H_o^{(1)'}(k_n r)$$

$$(181d)$$

where $H_o^{(1)''}(x) = -H_o^{(1)}(x) - H_o^{(1)'}(x)\ /\ x$. After calculating the particle velocity and their derivatives, these are substituted in the intensity and this one in the transmission loss equation

$$TL_c(r,z) = 5\ \log\left|\ I_r^2 + I_z^2\ \right|$$

$$(182)$$

to obtain the coherent transmission loss in the elastic bottom layers with unit reference intensity.

For the incoherent transmission loss in the solid layers, the components of the intensity are calculated for each mode, i.e.,

$$(I_r)_n = \left\{ (v_r)_n \left[(\lambda+2\mu) \left(\frac{\partial v_r}{\partial r}\right)_n + \lambda \left[\frac{(v_r)_n}{r} + \left(\frac{\partial v_z}{\partial z}\right)_n \right] \right] + \right.$$

$$\left. (v_z)_n\ \mu \left[\left(\frac{\partial v_r}{\partial z}\right)_n + \left(\frac{\partial v_z}{\partial r}\right)_n \right] \right\}\ /\ i\omega$$

$$(183a)$$

and

$$(I_z)_n = \left\{ (v_z)_n \left[(\lambda+2\mu) \left(\frac{\partial v_z}{\partial z}\right)_n + \lambda \left[\frac{(v_r)_n}{r} + \left(\frac{\partial v_r}{\partial r}\right)_n \right] \right] + \right.$$
$$\left. (v_r)_n \; \mu \left[\left(\frac{\partial v_r}{\partial z}\right)_n + \left(\frac{\partial v_z}{\partial r}\right)_n \right] \right\} \; / \; i\omega$$

(183b)

and they are added using

$$I_r = \sum_{n=1}^{N} (I_r)_n \tag{184a}$$

and

$$I_z = \sum_{n=1}^{N} (I_z)_n \tag{184b}$$

to substitute into Equations (182), where the subscript in the transmission loss is replaced by the incoherent one.

Use caution when predicting the propagation of sound using any incoherent transmission loss expression since this is just an approximation to obtain a smooth curve. The coherent and incoherent transmission loss curve should be displayed together to be aware of the variability of the result.

As an example, the transmission loss (see Figure 10) is calculated using the seven eigenvalues in Figure 8. The solid curve represents the coherent transmission loss and the dash curve is the incoherent calculation. The depth of the source and the receiver is 112.0 meters. The high oscillations of the coherent curve is caused by the constructive and destructive interference of the trapped modes. The radiating modes hardly contribute to the transmission loss calculations in the water column because of the large imaginary part of their respective eigenvalues.

As usual, if the acoustic properties used are inaccurate, then the calculated transmission loss will be erroneous.

Hamilton has been actively involved in the determination of the geo-acoustic properties of the ocean floor by the use of more easily measurable quantities. His work on the determination of the compressional sound speed in the elastic bottom is presented in References 66 and 67 while some results of the shear wave velocity are given in Reference 68. The shear and compressional

attenuation coefficients are given in References 69 and 70 and an informative geo-acoustic compendium is available in Reference 71. Laboratory measurements of the shear speed[72] and the shear attenuation coefficient[73] have been made as functions of depth and frequency, but there are concerns about the effectiveness of a laboratory to mimic the conditions that the sediment encounters under the unusual pressure and temperature of an ocean column. An accurate non-destructive method must be created for the proper evaluation of these acoustic properties. Even though there are disagreements about most geo-acoustic properties, a couple of inequalities have been created based on experimental observations.[28] The ratio of shear to compressional attenuation coefficients should satisfy

$$b_j/c_j \leq \sqrt{0.75} \tag{185a}$$

and the ratio of shear to compressional attenuation coefficients should satisfy

$$\beta_j/\alpha_j \leq 0.75 \, (c_j/b_j)^2 \tag{185b}$$

for each elastic layer from $j = J, \ldots, F-1$.

CHAPTER 9

COMPARISON WITH SIMPLE RANGE-INDEPENDENT MODELS

A few very simple range-independent benchmark ocean models will be considered to compare our calculations.

1. The first model is a one-layer water wave guide with constant acoustic properties, a pressure-release surface, and a rigid bottom. This model resembles the infinite well in quantum mechanics with the exception that the boundary condition at the bottom is $u_n'(z=D) = 0$. The soft surface is described mathematically by $u_n(z=0) = 0$ and the eigenfunction that satisfies the wave equation and both boundary conditions is given by

$$u_n(z) = a_n \sin(\eta_n z), \qquad n = 1, 2, 3, \ldots, N \qquad (186)$$

where

$$\eta_n = \left(\omega^2/c^2 - k_n^2 \right)^{1/2} = (n - 1/2)\pi/D \qquad (187)$$

which provides the eigenvalues

$$k_n^2 = \omega^2/c^2 - (n - 1/2)^2\pi^2/D^2 \qquad (188)$$

without the necessity of a characteristic equation to search for the zeros. Note that the fundamental mode is given by n=1 and as n increases, the eigenvalue decreases towards zero until a limit is reached when k_n converts from purely real (propagating mode) to purely imaginary. The maximum number of modes N is obtained by setting $k_N=0$ giving

$$N = \frac{D\omega}{\pi c} + \frac{1}{2}. \qquad (189)$$

The normalization equation provides the amplitude of the eigenfunctions. The resulting amplitude is

$$a_n^2 = 2/(\rho D) \qquad (190)$$

where ρ is the density of the water and the subscript n is not necessary because the normalization coefficient is constant for all the modes. Finally, substitution of the normalized eigenfunctions in the equation for the coherent transmission loss gives

$$TL(r,z) = 20 \log\left|-2\pi i/D \sum_{n=1}^{N} \sin\left[(n - 1/2)\pi z_0/D\right] \sin\left[(n - 1/2)\pi z/D\right] H_0^{(1)}(k_n r)\right| \qquad (191)$$

where the density of the water has been canceled out from the transmission loss calculation providing no contribution. The same result would be obtained if the orthonormalization condition has no weighting function. The density would contribute only if a finite impedance mismatch exists in the wave guide. Note also that this model allows the introduction of the attenuation coefficient as the imaginary part of the sound speed. This provides complex eigenvalues but the eigenfunctions are still purely real.

If the liquid layer is 200.0 meters deep and has a sound speed of 1500.0 m/s then the 25.0 hz source mentioned in the previous sections would excite seven modes with the eigenvalues given in the second column of Table 2.

2. The second model is similar to the first one, but the bottom boundary is a pressure-release interface. In this case, the eigenfunction is still given by Equation (186), but with

$$\eta_n^2 = (n\ \pi) / D , \quad n = 1, 2, 3, \ldots, N \qquad (192)$$

where

$$N = (\omega D) / (\pi c) \tag{193}$$

and the maximum amplitude of the eigenfunction is still given by Equation (190). The eigenvalues are now given by

$$k_n^2 = \omega^2/c^2 - n^2\pi^2/D^2 \tag{194}$$

and the final transmission loss equation is

$$TL(r,z) = 20 \log\left| -2\pi i/D \sum_{n=1}^{N} \sin[(n\pi z_0)/D] \sin[(n\pi z)/D] H_0^{(1)}(k_n r) \right|. \tag{195}$$

The six resulting eigenvalues for the case of a 200.0 meters deep water column with a sound speed of 1500.0 m/s, a soft bottom, and a 25.0 hertz continuous wave are given in the third column of Table 2. Note that the soft-bottom eigenvalues are practically located half-way between the locations of the rigid-bottom eigenvalues and it is expected that the true eigenvalues for a wave guide with penetrable bottom be located between these two limiting cases.

3. Another way to compare the calculated eigenvalues is to use the perturbation method for small attenuation coefficients. If the elastic media has a negligible shear contribution and the compressional attenuation coefficient in each layer is very small, then both methods must give nearly the same answer.

Consider the complex eigenequation,

$$\frac{d^2}{dz^2} u_n(z) + [\hat{k}^2(z) - \hat{k}_n^2] u_n(z) = 0 \tag{196}$$

where we redefine the wave number as $\hat{k}(z) = k(z) + i\epsilon\alpha(z)$, ϵ is used here to keep track of the effects of every term in the resulting approximate complex eigenequation and it will be set to unity at the end of the calculations, $\alpha(z)$ is the attenuation coefficient in nepers/meter, and $k(z) = \omega/c(z)$. The complex wave number in Equation (196) makes the eigenvalues and eigenfunctions complex. If $\alpha(z) << k(z)$, then we can use the perturbation method to obtain a

64

more accurate transmission loss. In this case we will write

$$u_n(z) \longrightarrow u_n^{(0)} + \varepsilon\, u_n^{(1)} + \varepsilon^2 u_n^{(2)} \tag{197a}$$

and

$$k_n^2 \longrightarrow \lambda_n^{(0)} + \varepsilon\, \lambda_n^{(1)} + \varepsilon^2 \lambda_n^{(2)} \tag{197b}$$

which substituted in the complex eigenequation gives,

$$\left[\frac{d^2}{dz^2} + k^2(z) + 2i\varepsilon k(z)\alpha(z) - \varepsilon^2\alpha^2(z) - \lambda_n^{(0)} - \varepsilon\lambda_n^{(1)} - \varepsilon^2\lambda_n^{(2)}\right]\left(u_n^{(0)} + \varepsilon\, u_n^{(1)} + \varepsilon^2 u_n^{(2)}\right) \approx 0 \tag{198}$$

which is an approximation to the complex eigenequation Equation (196) due to the expansions Equations (197).

Combining the ε^0 terms of this equation gives the 0th order solution to the problem, or

$$\frac{d^2}{dz^2} u_n^{(0)} + [k^2(z) - \lambda_n^{(0)}]\, u_n^{(0)} = 0 \tag{199}$$

which is the unperturbed eigenequation that has been solved for the purely real eigenvalues $\lambda_n^{(0)} \equiv k_n^2$ and eigenfunctions $u_n^{(0)} \equiv u_n$. This unperturbed eigenequation corresponds to Equation (69).

Combining the terms with ε^1, which corresponds to the first order perturbation terms, gives

$$\frac{d^2}{dz^2} u_n^{(1)} + [2ik(z)\alpha(z) - \lambda_n^{(1)}]\, u_n^{(0)} + [k^2(z) - \lambda_n^{(0)}]\, u_n^{(1)} = 0 \tag{200}$$

where the unperturbed eigenfunctions are normalized by

$$\int_0^{z_b} \rho(z)\, u_n^{(0)}(z)\, u_m^{(0)}(z)\, dz = \delta_{nm} \tag{201}$$

where z_b is the depth of the resilient bottom of the basement.

Multiplying Equation (200) by $\rho u_n^{(0)}$ and integrating yields

$$\int_0^{z_b} \rho u_n^{(0)} \frac{d^2 u_n^{(1)}}{dz^2} dz + \int_0^{z_b} \rho u_n^{(0)} [2ik(z)\alpha(z) - \lambda_n^{(1)}] u_n^{(0)} dz + \int_0^{z_b} \rho u_n^{(0)} [k^2(z) - \lambda_n^{(0)}] u_n^{(1)} dz = 0$$

(202)

where using the orthonormality condition of the unperturbed eigenfunctions in the second term of this equation, integrating by parts twice the first term, and using the boundary conditions at every interface to cancel out the surface contributions gives

$$\int_0^{z_b} \rho u_n^{(1)} \frac{d^2 u_n^{(0)}}{dz^2} dz + 2i \int_0^{z_b} \rho u_n^{(0)} k(z)\alpha(z) u_n^{(0)} dz + \int_0^{z_b} \rho u_n^{(0)} [k^2(z) - \lambda_n^{(0)}] u_n^{(1)} dz = \lambda_n^{(1)}$$

(203)

and with the help of Equation (199) the first and second integrals cancel out giving us the expression

$$\lambda_n^{(1)} = 2i \int_0^{z_b} \rho\, k(z)\, \alpha(z)\, |u_n^{(0)}|^2 dz$$

(204)

which is the first order perturbation term for the eigenvalue and its values are purely imaginary.

Now we write the perturbed part of the eigenfunction under the basis of the unperturbed part since this is an orthonormal basis, i.e.,

$$u_n^{(1)} = \sum_m A_{nm}\, u_m^{(0)}$$

(205)

and substitute in Equation (200) to obtain

$$\sum_m A_{nm} \left[\frac{d^2 u_m^{(0)}}{dz^2} + (k^2(z) - \lambda_n^{(0)}) u_n^{(0)} \right] + [2ik(z)\alpha(z) - \lambda_n^{(1)}] u_n^{(0)} = 0$$

(206)

then multiply by $\rho u_l^{(0)}$ and integrate as done before. Integration by parts twice cancels a few terms, and the orthonormality condition yields

66

$$A_{nl} = \frac{2i}{\lambda_n^{(0)} - \lambda_l^{(0)}} \int_0^{z_b} \rho \, k(z)\alpha(z) \, u_n^{(0)} u_l^{(0)} dz \qquad (207)$$

which is in terms of the unperturbed eigenfunctions and eigenvalues, is directly proportional to the absorption coefficient, and is a purely imaginary term.

In the cases of trapped modes, where the imaginary part of the eigenvalues is extremely small, we can rely on the rapid convergence of the perturbation method and forget about a second order perturbation term. When radiating modes are taken into account, we must consider calculating the second order perturbation term.

The ϵ^2 terms of Equation (200) into a second order equation gives

$$\frac{d^2}{dz^2} u_n^{(2)} + [k^2(z) - \lambda_n^{(0)}]u_n^{(2)} + [2ik(z)\alpha(z) - \lambda_n^{(0)}]u_n^{(1)} = [\alpha^2(z) + \lambda_n^{(2)}]u_n^{(0)}$$

$$(208)$$

which multiplied by $\rho u_n^{(0)}$ and integrated as done with the first order eigenvalue leads us to the equation

$$\lambda_n^{(2)} = 2i\int_0^{z_b}\rho k(z)\alpha(z)u_n^{(0)}u_n^{(1)}dz - \lambda_n^{(1)}\int_0^{z_b}\rho u_n^{(0)}u_n^{(1)}dz - \int_0^{z_b}\rho\alpha^2(z)|u_n^{(0)}|^2 dz$$

$$(209)$$

where substituting Equation (205) and the orthonormality condition of the unperturbed eigenfunctions gives

$$\lambda_n^{(2)} = 2i\sum_m A_{nm}\int_0^{z_b}\rho k(z)\alpha(z)u_n^{(0)}u_m^{(0)}dz - \int_0^{z_b}\rho\alpha^2(z)|u_n^{(0)}|^2 dz \qquad (210)$$

or with Equation (207) we get the simpler form

$$\lambda_n^{(2)} = \sum_m A_{nm}^2 (\lambda_n^{(0)} - \lambda_m^{(0)}) - \int_0^{z_b}\rho\alpha^2(z)|u_n^{(0)}|^2 dz \qquad (211)$$

which is purely real and a much smaller term since it is proportional to α^2.

If we write

$$u_n^{(2)} = \sum_m B_{nm} u_m^{(0)} \qquad (212)$$

then Equation (208) becomes

$$\sum_m B_{nm} \frac{d^2}{dz^2} u_m^{(0)} + \sum_m B_{nm} [k^2 - \lambda_n^{(0)}] u_m^{(0)} + \sum_m A_{nm} [2ik\alpha - \lambda_n^{(1)}] u_m^{(0)} = [\alpha^2 - \lambda_n^{(2)}] u_n^{(0)}$$

$$(213)$$

which multiplied by $\rho u_1^{(0)}$ and integrated using integration by parts and the orthonormality condition reduces the equation to

$$(\lambda_1^{(0)} - \lambda_n^{(0)}) B_{nl} = \lambda_n^{(1)} A_{nl} - \sum_m A_{nm} A_{lm}, \quad 1 \neq n \qquad (214)$$

which makes B_{nl} purely real and directly proportional to α^2.

We have already assumed layers of constant density in order to simplify the elastic wave equation. Therefore, we may define an element of a G-matrix as

$$G_{nm} \equiv 2i \sum_{j=1}^{J+1} \rho_j \int_{z_j}^{z_{j+1}} k_j(z) \, \alpha_j(z) \, u_{nj}^{(0)}(z) \, u_{mj}^{(0)}(z) \, dz = G_{mn} \qquad (215a)$$

and that of an H-vector as

$$H_n \equiv \sum_{j=1}^{J+1} \rho_j \int_{z_j}^{z_{j+1}} \alpha_j^2(z) |u_{nj}^{(0)}|^2 dz. \qquad (215b)$$

Note that all elements of the G-matrix are purely imaginary and symmetric, while those of the H-vector are purely real. These integrals must be evaluated in order to calculate the perturbed parts of the eigenvalues and eigenfunctions.

Now the first order perturbation term of the eigenvalue, Equation (204), becomes

$$\lambda_n^{(1)} = G_{nn} \qquad (216)$$

which tells us that the diagonal components of the G-matrix are the first-order perturbation term of the eigenvalues. The second order term, Equation (209), simplifies to

$$\lambda_n^{(2)} = \sum_{l \neq n} \frac{G_{nl}^2}{\lambda_n^{(0)} - \lambda_l^{(0)}} - H_n \tag{217}$$

which substituted into

$$k_n^2 \simeq \lambda_n^{(0)} + \lambda_n^{(1)} + \lambda_n^{(2)} \tag{218}$$

gives the perturbed eigenvalues of the problem. Since $\lambda_n^{(1)}$ is the only contributor to the imaginary part of the eigenvalue, we may define

$$\mathcal{R}_n^2 = \lambda_n^{(0)} + \lambda_n^{(2)} \tag{219}$$

as the real part of the eigenvalue. Then to obtain k_n from Equation (218) we expand its square root as follows:

$$k_n \simeq \mathcal{R}_n \left(1 + \frac{\lambda_n^{(1)}}{\mathcal{R}_n^2} \right)^{1/2} \cong \mathcal{R}_n \left(1 + \frac{\lambda_n^{(1)}}{2 \mathcal{R}_n^2} \right) = \mathcal{R}_n + \frac{\lambda_n^{(1)}}{2 \mathcal{R}_n} \tag{220}$$

where we have assumed that $\mathcal{R}_n^2 \gg \lambda_n^{(1)}$. Now the imaginary part of the eigenvalue will be defined as

$$\mathcal{I}_n \simeq \frac{\lambda_n^{(1)}}{2 \mathcal{R}_n} \tag{221}$$

which is the same expression in Equation (474) of Reference 53 where only first order perturbation has been used. By the same token, the real part is given from Equation (219)

$$\mathcal{R}_n \simeq \sqrt{\lambda}_n^{(0)} + \frac{\lambda_n^{(2)}}{2\sqrt{\lambda}_n^{(0)}} \tag{222}$$

where it is assumed that $\lambda_n^{(2)} \ll \lambda_n^{(0)}$ and the same power expansion has been used. Equation (221) is a crude approximation made by many underwater acousticians and it can be avoided by taking the complex square root of Equation (218).

As the first order correction of the eigenfunction, Equation (207) simply becomes

$$A_{n1} = \frac{G_{n1}}{\lambda_n^{(0)} - \lambda_1^{(0)}}, \quad n \neq 1 \tag{223}$$

and for the second order correction, Equation (214), we get

$$B_{n1} = \frac{-G_{nn} G_{n1}}{(\lambda_n^{(0)} - \lambda_1^{(0)})^2} + \sum_{m \neq n} \frac{G_{nm} G_{m1}}{(\lambda_n^{(0)} - \lambda_m^{(0)})(\lambda_n^{(0)} - \lambda_1^{(0)})}, \quad n \neq 1 \tag{224}$$

which substituted into the equation

$$u_n(z) = u_n^{(0)} + \sum_{1 \neq n} [A_{n1} + B_{n1}] u_1^{(0)} \tag{225}$$

gives a better estimate of the eigenfunction.

It is left to properly evaluate the G-matrix and the H-vector in Equations (215). They can be obtained by numerical integration or by the approximate method developed in Reference 53. Since we are interested here in the simple case of a semi-infinite fluid-type bottom Equations (215) become trivial integrations of exponential functions. The resulting trapped eigenvalues are given in the fourth column of Table 2. Note that the second order perturbation term was not enough to make the real part of the eigenvalue closer to the exact one. Therefore, the attenuation coefficient chosen by Miller[42,43] is too high for the perturbation method to produce accurate results for the trapped eigenvalues, and it is presumably worst for the

radiating ones.

4.   The next model is a layer of water over a semi-infinite elastic layer which was used by Ellis[11] to model the propagation of underwater explosives over an ocean floor made of chalk. Both layers have constant acoustic properties. Since the surface of the water is pressure-release, the eigenfunction is given by

$$u_{n1}(z) = a_1 \sin(\eta_{n1} z) \tag{226}$$

where $\eta_{n1}^2 = k_1^2 - k_n^2$ and where $z_1 = 0 \leq z < z_2$. The compressional and shear eigenfunctions in the semi-infinite layer radiated without reflecting back, therefore the compressional mode is given by

$$u_{n2}(z) = a_2 \exp(i\eta_{n2} z) \tag{227}$$

where $\eta_{n2}^2 = k_2^2 - k_n^2$ and the shear mode is

$$v_n(z) = b \exp(i\gamma_n z) \tag{228}$$

where $\gamma_n^2 = \kappa^2 - k_n^2$. The three unknown constants, a_1, a_2, and b, are determined by the three liquid-solid boundary conditions in Equations (113), (115), and (116). Direct substitution of the given eigenfunctions in the three boundary conditions provides two equations with the three unknowns, i.e.,

$$a_1 \eta_{n1} \cos(\eta_{n1} z_2) = a_2 i \eta_{n2} \exp(i\eta_{n2} z_2) + k_n^2 b \exp(i\gamma_{n2} z) \tag{229a}$$

and

$$\rho_1 \kappa^2 a_1 \sin(\eta_{n1} z_2) = \rho_2 (\kappa^2 - 2k_n^2) a_2 \exp(i\eta_{n2} z_2) - 2\rho_2 k_n^2 b \, i\gamma_{n2} \exp(i\gamma_{n2} z_2)$$

$$\tag{229b}$$

and a third equation with two of the unknowns, i.e.,

$$2 a_2 i \eta_{n2} \exp(i\eta_{n2} z_2) + (2k_n^2 - \kappa^2) b \exp(i\gamma_{n2} z_2) = 0. \tag{229c}$$

If this third equation is solved for one of the unknowns to be substituted into the other two equations, we obtain two equations with two unknowns. The two equations are divided to eliminate the remaining unknowns, and to form the characteristic equation

$$W(k_n) \equiv \eta_{n2} \, \kappa^4 \, \tan(\eta_{n1} z_2) + i \, \rho_2/\rho_1 \left[(2k_n^2 - \kappa^2)^2 + 4 \, \gamma_{n2} \, \eta_{n2} \, k_n^2 \right] = 0$$

(230)

which is a complex equation even if the attenuation coefficients are not included in the model. The transmission loss is calculated using the same equations derived in the previous section.

Substitution of the parameters in the "Fluid bottom" case, shown in Table 1, into this simple model gives the three eigenvalues displayed in the last column of Table 2. These eigenvalues agree with double precision accuracy with the ones obtained using our multilayered model, hence the figures in the last column of Table 2 represent the solutions from both methods. Double precision accuracy was also found between the resulting eigenvalues from this simple model and our multilayer model when the bottom is a semi-infinite layer of Clay-silt, Sand, Basalt, or Chalk (see Table 1).

Note that these eigenvalues are located between the rigid-bottom and soft-bottom eigenvalues. Hence, these two simple cases may be used to establish limits to the eigenvalues searched.

With the use of these simple models, the range-independent multilayer model has been compared in the limit when the number of layers is a minimum (with or without shear waves). Therefore, some transmission loss results will be made for the various bottom types given in Table 1.

The first case to consider is a water column 200.0 meters deep over the semi-infinite sand ocean floor with the acoustic properties in Table 1. A total of seven eigenvalues were found (see Figure 11) for a 25.0 Hz source. The real part of the normalized fundamental mode is shown in Figure 12 where the solid curve represents the compressional eigenfunction and the dotted curve is the shear contribution. The imaginary part of this fundamental mode is displayed in Figure 13 where the discontinuity at the liquid-solid interface is caused by the impedance mismatch and the presence of the shear contribution. The first three eigenfunctions are T-R modes because the compressional sound speed in the basement layer is greater than the sound

speed in the water column (1500.0 m/s) and the shear sound speed is smaller
than the water sound speed. The fourth and higher depth functions are R-R
modes. The real part of the fourth mode is given in Figure 14 where the
compressional eigenfunction starts to oscillate into the bottom. The imaginary
part of this mode is plotted in Figure 15. Note that the first and fourth mode
are damped out when they reach the depth of 600.0 meters. At this depth the
higher order radiating modes take over in the transmission loss calculation.

For best visualization of the propagation of sound in range and depth, the
three-dimensional plots and the contour plots have been proven to be useful
tools. The advantage of the three dimensional plots is that every calculated
point is plotted. However, the disadvantage is that it is more difficult to
visually extrapolate the numerical values of any point. The advantage of the
contour plot is that it is a two-dimensional plot and numerical values can be
roughly extrapolated visually, but not all the calculated values are used to
obtain the contours and there is less information in this type of graphical
display. For the various tastes of the readers, both plots will be displayed.

The three-dimensional transmission loss plot versus range (in kilometers)
and depth (in meters) is given in Figure 16 for the same case of the
semi-infinite sand basement and a 25.0 hertz source located 100.0 meters deep.
The transmission loss at the liquid-solid interface has been intentionally
omitted from the plot to mark the location of the water depth. Note the
oscillatory behavior of the transmission loss surface at short ranges which is
caused by the interference of the seven normal modes of this wave guide.
However, the high imaginary component of the excited eigenvalues (see Figure
11) causes all the modes, except the fundamental mode, to completely damp out
at ranges beyond 10.0 kilometers. The contour plot for the results in Figure
16 is displayed in Figure 17. The legend at the bottom of the contour plot
relates the curve type to the contour transmission loss value in decibels.

The next case to consider is the 200.0 meters deep water column over a
semi-infinite clay-silt ocean floor with the acoustic properties in Table 1. A
total of seven eigenvalues were found (see Figure 18) for the 25.0 Hz source.
The real (imaginary) part of the calculated fundamental mode is plotted in
Figure 19 (see Figure 20 also). A very interesting observation made is that
all the modes are R-R modes which radiate into the bottom. This is because the
compressional speed in the solid basement is almost equal to the water sound

speed. Also, there is hardly any contribution from the shear waves because of the relatively low shear speed of the clay-silt ocean floor. Since the excited modes display the same oscillatory behavior, they are not illustrated. The three-dimensional transmission loss plot in Figure 21 exhibit a faster decay of the contribution from the excited modes, compared to the sand bottom case in Figure 16, despite the lower attenuation coefficients. At ranges greater than 5.0 kilometers the fundamental mode becomes the only contributor to the transmission loss. This rapid decay of the higher modes is caused by the very low compressional sound speed of the clay-silt basement. Only R-R modes are excited by the source and these radiating modes are strongly affected by the acoustic absorption of the bottom. The trapped modes in the sand bottom case are evanescent in the bottom and are much less affected by the high attenuation of sand. Comparison of the contour plot for clay-silt bottom (see Figure 22) with the one for sand bottom (see Figure 17) shows that the fundamental mode propagates further in the water column if the bottom is made of sand. The same conclusion can be obtained by comparison of Figures 16 and 21, but it is easier to visualize with the contour plot.

It is almost impossible to find a water column directly over basalt. However, the case will be considered only for its interesting acoustic features. Note, from Table 1, that basalt has lower attenuation coefficients relative to those of sand or clay-silt and that both sound speeds are much higher than the water sound speed. The eight complex eigenvalues found are plotted in Figure 23. The first five modes are T-T modes because of the high sound speeds of basalt. Figure 24 displays the real part of the normalized fundamental depth function and Figure 25 is the fifth normal mode.* As the mode number increases, the effects of bottom absorption increases and the imaginary part of the eigenvalue in Figure 23 increases. The sixth mode (see Figure 26) is the first R-T mode and absorptive effect to the oscillatory compressional mode is different from the effect to the exponential one, hence the irregular pattern displayed in Figure 23. The seventh eigenvalue corresponds to the second R-T mode (see Figure 27), and the last eigenvalue represents the only

---

*To minimize the number of figures displayed for this case, the imaginary part of the eigenfunctions are omitted.

R-R mode (see Figure 28) of the set.

The three-dimensional plot of the coherent transmission loss for this case is given in Figure 29. All the modes contribute to the transmission loss for ranges smaller than 5.0 kilometers. In the case of larger ranges, only the first four normal modes are needed. The second, third, and fourth modes are not damped out at 10.0 kilometers because they are T-T modes that propagate mostly in the water column and experience a negligible effect from the absorption of the bottom. The fifth mode is also a T-T mode, but the imaginary component of its eigenvalue (see Figure 23) is much higher, causing the mode to dampen out rapidly.

The contour plot for this same data is provided in Figure 30 where the discontinuity in the transmission loss at the liquid-solid interface is a result of the impedance mismatch of the boundary. The highly oscillatory behavior of the transmission loss makes the contour plot somewhat complicated to interpret. In this case, the three-dimensional plot may be more useful. However, the contour plot does show the bundle of acoustic energy that scatters the bottom several times at the critical angle of incidence. There are 17 surface and bottom bounces for ranges between 3.83 kilometers and 14.85 kilometers. This corresponds to a critical angle of incidence of about 72.8 degrees relative to the vertical axis. This plot provides a relationship between the normal mode theory and the ray theory.

CHAPTER 10

ADIABATIC NORMAL-MODE THEORY WITH SHEAR WAVES

After verifying that the range-independent normal mode calculations agree with the calculation obtained with simple benchmark models, the next step is to include range dependence with the shear effects of the elastic bottom sediments.

The range-dependent Helmholtz equation in the water layers of the ocean wave guide is given as,

$$\nabla^2 \varphi(r,z) + k^2(r,z)\ \varphi(r,z) = \frac{-1}{2\pi r}\ \delta(r)\ \delta(z-z_0) \qquad (231)$$

where now k^2 displays the range-dependence of the acoustic properties of the ocean. The range-dependence of the boundaries are displayed in the boundary conditions themselves.

The range-independent solution was found to be given by,

$$\varphi(r,z) = \frac{i}{4}\ \rho(z_0) \sum_{n=1}^{N} u_n(z_0)\ u_n(z)\ H_0^{(1)}(k_n r). \qquad (232)$$

However, in the range-dependent case, the eigenfunctions and eigenvalues vary with range, therefore the solution may be written using the quasi- separation of variables as,

$$\varphi(r,z) \equiv \sum_{n=1}^{N} f_n(r)\ u_n(r,z) \qquad (233)$$

where $u_n(r,z)$ are taken as the basis depth functions that satisfy the equation

$$\frac{\partial^2}{\partial z^2} u_n(r,z) + \left[k^2(r,z) - k_n^2(r)\right] u_n(r,z) = 0 \tag{234}$$

and the orthonormality condition

$$\int_0^{Z_F} \rho(z)\, u_n(r,z)\, u_m(r,z)\, dz = \delta_{nm}. \tag{235}$$

Direct substitution of Equation (232) into Equation (231) gives,

$$\sum_{n=1}^{N} \left\{ \nabla_r^2\left[f_n(r)\, u_n(r,z)\right] + f_n(r)\left[\partial^2/\partial z^2 + k^2(r,z)\right]u_n(r,z) \right\} = \frac{-1}{2\pi r}\,\delta(r)\,\delta(z-z_0) \tag{236}$$

where

$$\nabla_r^2 \equiv \frac{1}{r}\,\frac{\partial}{\partial r}\left(r\,\frac{\partial}{\partial r}\right) \tag{237}$$

and we may substitute

$$\nabla_r^2\left[f_n(r)\, u_n(r,z)\right] = u_n \nabla_r^2 f_n + 2\,\vec{\nabla}_r f_n \cdot \vec{\nabla}_r u_n + f_n \nabla_r^2 u_n \tag{238}$$

to obtain

$$\sum_{n=1}^{N} \left\{ \left[(\nabla_r^2 + k_n^2)f_n\right]u_n + 2\,\vec{\nabla}_r f_n \cdot \vec{\nabla}_r u_n + f_n \nabla_r^2 u_n \right\} = \frac{-1}{2\pi r}\,\delta(r)\,\delta(z-z_0) \tag{239}$$

which multiplied both sides by $\rho(z)\, u_m(0,z)$ and integrated throughout depth gives the inhomogeneous range equation

$$\left[\frac{1}{r}\,\frac{\partial}{\partial r}\left(r\,\frac{\partial}{\partial r}\right) + k_n^2(r)\right]f_n(r) = \frac{-1}{2\pi r}\,\delta(r)\,\rho(z_0)\, u_n(0,z_0) - \tag{240}$$

$$2\sum_{m=1}^{N} f_m'(r)U_{nm}(r) - \sum_{m=1}^{N} f_m(r)W_{nm}(r)$$

where

$$U_{nm}(r) \equiv \int_0^{Z_F} \rho(z) \, u_m(r,z) \, \frac{\partial}{\partial r} \, u_n(r,z) \, dz \qquad (241a)$$

and

$$W_{nm}(r) \equiv \int_0^{Z_F} \rho(z) \, u_m(r,z) \, \frac{1}{r} \frac{\partial}{\partial r} \left(r \frac{\partial}{\partial r} \right) u_n(r,z) \, dz \qquad (241b)$$

are the elements of the coupling matrices that will take care of the exchange of energy of the normal modes in the range-dependent environment. The prime stands for the derivative with respect to the argument.

In the case where the acoustic properties and the boundaries of the ocean wave guide slowly vary with range, the coupling integrals are negligible and the adiabatic approximation is feasible. The adiabatic range equation is

$$\left[\frac{1}{r} \frac{\partial}{\partial r} \left(r \frac{\partial}{\partial r} \right) + k_n^2(r) \right] f_n(r) = \frac{-1}{2\pi r} \, \delta(r) \, \rho(z_0) \, u_n(0,z_0) \qquad (242)$$

where the range-dependent waveguide will be divided into M number of range-independent segments. The procedure is to calculate a fixed number of trapped and radiating modes for each range-independent segment. The resulting set of eigenfunctions provides the function $u_n(r,z)$. The unknown function, $f_n(r)$, is obtained from the range equation and the range boundary conditions.

Range segment #1 is defined as the one where the source is located. The homogeneous solution for the first range segment is

$${}^1f_n(r) \equiv {}^1\alpha_n \, H_0^{(1)}({}^1k_n r) + {}^1\beta_n \, H_0^{(2)}({}^1k_n r) \qquad (243)$$

where the left-side superscripts is the range segment number, and the unknown constants are to be determined with the range boundary conditions.

In the limit as ${}^1k_n r \to 0$ the asymptotic forms of the Hankel functions

$$H_0^{(1)}({}^1k_n r) = - H_0^{(2)}({}^1k_n r) \to 2i/\pi \, \log_e({}^1k_n r) \qquad (244)$$

gives

$${}^1f_n(r) \to 2i/\pi \, ({}^1\alpha_n - {}^1\beta_n) \, \log_e({}^1k_n r). \qquad (245)$$

The particular solution is obtained by integrating the inhomogeneous range

78

equation over a small cylinder of radius a containing the source, i.e.,

$$\int_0^a {}^1f_n''(r)\ dr\ +\int_0^a \frac{1}{r}\ {}^1f_n'(r)\ dr\ +\int_0^a {}^1k_n^2(r)\ {}^1f_n(r)\ dr\ = \tag{246}$$

$$-\rho(z_0)\ u_n(0,z_0)/(2\pi)\int_0^a \frac{\delta(r)}{r}\ dr.$$

Integrating by parts gives,

$${}^1f_n'(r)\Big|_0^a +\ {}^1f_n(r)/r\Big|_0^a +\int_0^a \left(r^{-2}+\ {}^1k_n^2(r)\ \right)\ {}^1f_n(r)\ dr\ = \tag{247}$$

$$-\rho(z_0)\ u_n(0,z_0)/(2\pi)\int_0^a \frac{\delta(r)}{r}\ dr$$

which in the limit as $a \rightarrow 0$, only the slope at $r = 0$ and the integral over the delta function remains, i.e.,

$$d\ {}^1f_n(r)/dr \rightarrow -\ \rho(z_0)\ u_n(0,z_0)\ /\ (2\pi r) \tag{248}$$

which yields

$${}^1f_n(r) \rightarrow \frac{-1}{2\pi}\ \rho(z_0)\ u_n(0,z_0)\ \log_e({}^1k_n r). \tag{249}$$

Equating the two solutions provides the relationship

$${}^1\alpha_n -\ {}^1\beta_n = \frac{i}{4}\ \rho(z_0)\ u_n(0,z_0) \tag{250}$$

where the right-hand-side term is the constant in the range-independent solution and this equation will be used as the relationship between both unknowns in the first range segment.

The range segments labeled 2 to M-1 are characterized by the homogeneous range equation, therefore the solutions are,

$${}^mf_n(r) = {}^m\alpha_n\ H_0^{(1)}({}^mk_n r)\ +\ {}^m\beta_n\ H_0^{(2)}({}^mk_n r) \tag{251}$$

where $2 \leq m < M$.

The last range segment is assumed semi-infinite and with no source present, therefore only the divergent solution of the homogeneous range equation satisfies causality. The solution for the Mth range-independent segment is

$$^{M}f_{n}(r) = {}^{M}\alpha_{n} H_{0}^{(1)}({}^{M}k_{n}r). \tag{252}$$

The unknowns are determined by the radial boundary conditions. These are:

1. Continuity of the normal particle velocity

$$\frac{\partial}{\partial r} \sum_{n=1}^{N} {}^{m}f_{n}(r) \, u_{n}(r,z)\bigg|_{r=r_{m}} = \frac{\partial}{\partial r} \sum_{n=1}^{N} {}^{m+1}f_{n}(r) \, u_{n}(r,z)\bigg|_{r=r_{m}} \tag{253a}$$

2. Continuity of the pressure

$$\rho \sum_{n=1}^{N} {}^{m}f_{n}(r) \, u_{n}(r,z)\bigg|_{r=r_{m}} = \rho \sum_{n=1}^{N} {}^{m+1}f_{n}(r) \, u_{n}(r,z)\bigg|_{r=r_{m}} \tag{253b}$$

Since the eigenfunctions already satisfy the boundary conditions at every range and depth, in a slowly varying range-dependent environment, the conditions to satisfy for each mode are

$$^{m}f_{n}(r) = \text{continuous} \tag{254a}$$

and

$$^{m}f'_{n}(r) = \text{continuous} \tag{254b}$$

for $1 \leq m < M$.

Application of these radial boundary conditions to the M-1 interface gives

$$^{M-1}\alpha_{n} H_{0}^{(1)}({}^{M-1}k_{n}r_{M-1}) + {}^{M-1}\beta_{n} H_{0}^{(2)}({}^{M-1}k_{n}r_{M-1}) = {}^{M}\alpha_{n} H_{0}^{(1)}({}^{M}k_{n}r_{M-1})$$

$$\tag{255a}$$

and

80

$$^{M-1}k_n \left[^{M-1}\alpha_n \, H_1^{(1)}(^{M-1}k_n r_{M-1}) + {}^{M-1}\beta_n \, H_1^{(2)}(^{M-1}k_n r_{M-1}) \right] = {}^{M}\alpha_n \, {}^{M}k_n \, H_1^{(1)}(^{M}k_n r_{M-1})$$

(255b)

which is rewritten in matrix form as

$$^{M-1}\mathbb{H}_{n,M-1} \, {}^{M-1}\mathbb{A}_n = {}^{M}\mathbb{H}_{n,M-1} \, {}^{M}\mathbb{A}_n$$

(256)

where

$$^{J}\mathbb{H}_{n,i} \equiv \begin{pmatrix} H_0^{(1)}(^{J}k_n r_i) & H_0^{(2)}(^{J}k_n r_i) \\ {}^{J}k_n \, H_1^{(1)}(^{J}k_n r_i) & {}^{J}k_n \, H_1^{(2)}(^{J}k_n r_i) \end{pmatrix}$$

(257)

and

$$^{J}\mathbb{A}_n \equiv \begin{pmatrix} ^{J}\alpha_n \\ {}^{J}\beta_n \end{pmatrix}$$

(258)

for $i, j = 2, 3, 4, \ldots, M$ and where $^{M}\beta_n = 0$. To obtain $^{M-1}\mathbb{A}_n$ in terms of $^{M}\mathbb{A}_n$, we write

$$^{M-1}\mathbb{A}_n = (^{M-1}\mathbb{H}_{n,M-1})^{-1} \, {}^{M}\mathbb{H}_{n,M-1} \, {}^{M}\mathbb{A}_n.$$

(259)

The M-2 boundary has the relationship

$$^{M-2}\mathbb{H}_{n,M-2} \, {}^{M-2}\mathbb{A}_n = {}^{M-1}\mathbb{H}_{n,M-2} \, {}^{M-1}\mathbb{A}_n$$

(260)

and substituting the previous relationship for $^{M-1}\mathbb{A}_n$ gives

$$^{M-2}\mathbb{A}_n = (^{M-2}\mathbb{H}_{n,M-2})^{-1} \, {}^{M-1}\mathbb{H}_{n,M-2} \, (^{M-1}\mathbb{H}_{n,M-1})^{-1} \, {}^{M}\mathbb{H}_{n,M-1} \, {}^{M}\mathbb{A}_n.$$

(261)

By the same token, we can propagate the solution to the first segment with

$$^{1}\mathbb{H}_{n,1} \, {}^{1}\mathbb{A}_n = {}^{2}\mathbb{H}_{n,1} \, {}^{2}\mathbb{A}_n$$

(262)

which gives

$$
{}^{1}\!A_n = \left\{ \prod_{m=1}^{M-1} ({}^{m}\!H_{n,m})^{-1} \, {}^{m+1}\!H_{n,m} \right\} \, {}^{M}\!A_n \tag{263}
$$

where the term in the parenthesis is now defined as the 2x2 matrix X and the coefficients in the first range segment are given by

$$
{}^{1}\!\alpha_n = X_{11} \, {}^{M}\!\alpha_n \tag{264}
$$

and

$$
{}^{1}\!\beta_n = X_{21} \, {}^{M}\!\alpha_n . \tag{265}
$$

Substitution of these relationships into Equation (250) gives

$$
\frac{i}{4} \, \rho(z_0) \, u_n(0,z_0) = (X_{11} - X_{21}) \, {}^{M}\!\alpha_n \tag{266}
$$

which is solved for the unknown at the semi-infinite range segment and this solution can be propagated to obtain the other unknowns.

The potentials for the range-independent solid layers are given by,

$$
\varphi(r,z) = \sum_{n=1}^{N} \left[\frac{i}{4} \, \rho(z_0) \, u_n(z_0) \, H_0^{(1)}(k_n r) \right] u_n(z) \tag{267a}
$$

and

$$
\psi(r,z) = \sum_{n=1}^{N} \left[\frac{i}{4} \, \rho(z_0) \, u_n(z_0) \, H_0^{(1)}(k_n r) \right] v_n(z) \tag{267b}
$$

where the term in the brackets is common to both solutions. With this observation in mind, the range-dependent solutions in the solid layers will be written as

$$
\varphi(r,z) = \sum_{n=1}^{N} f_n(r) \, u_n(r,z) \tag{268a}
$$

and

$$
\psi(r,z) = \sum_{n=1}^{N} f_n(r) \, v_n(r,z) \tag{268b}
$$

82

which must satisfy the four boundary conditions throughout range and depth.

The range function for these potentials is the same as the one given for each range segment in the liquid layers. The unknown constants are evaluated by the four radial boundary conditions. One of them is that the tangential component of the particle velocity must be continuous, i.e.,

$$v_z(r_m,z) = \left(\frac{\partial}{\partial z}\varphi + k_n^2\psi\right)_{r_m} = \text{continuous} \qquad (269)$$

where substitution of φ and ψ gives

$$f_n(r_m)\left[u_n'(r_m,z) + k_n^2 v_n(r_m,z)\right] = \text{continuous.} \qquad (270)$$

However, since the eigenfunctions already satisfy the boundary conditions in Equation (119), then all we have left to satisfy is the continuity of $f_n(r_m)$.

The normal component of the particle velocity is another boundary condition to be satisfied. This is given by

$$v_r(r_m,z) = \frac{\partial}{\partial r}\left[\varphi(r_m,z) + \frac{\partial}{\partial z}\psi(r_m,z)\right] = \text{continuous} \qquad (271)$$

and substitution of φ and ψ gives

$$f_n'(r_m)\left[u_n + v_n'\right]_{r_m} + f_n(r_m)\frac{\partial}{\partial r}\left[u_n + v_n'\right]_{r_m} = \text{continuous} \qquad (272)$$

where, in a slowly varying environment, the change in (u_n+v_n') with respect to range is much smaller than the change of the Hankel functions in $f_n(r)$ with range. Therefore, the only functions to make continuous are $f_n(r)$ and $f_n'(r)$. The same conditions are found from the continuity of P_{rz} and P_{zz}. With this adiabatic approximation, the need to match four boundary conditions explicitly has been avoided and only two equations must be satisfied. The equations to match turn out to be the same as the ones in the liquid layers, therefore the same function $f_n(r)$ can be used for both states of the matter. This property may decrease the computation time by orders of magnitude.

After all the coefficients of the range-dependent waveguide are

determined, the coherent and incoherent transmission loss in the solid layers are obtained by Equations (176) through (184) where the components of the particle velocity are

$$v_z = \sum_{n=1}^{N} f_n(r) \left[u'_n(r,z) + k_n^2 v_n(r,z) \right] \tag{273a}$$

and

$$v_r \simeq \sum_{n=1}^{N} f'_n(r) \left[u_n(r,z) + v'_n(r,z) \right] \tag{273b}$$

where it has been assumed that the change of the eigenfunctions with range is negligible compared to the change in the Hankel functions. The derivatives with respect to range are given by

$$\frac{\partial}{\partial r} v_z \simeq \sum_{n=1}^{N} f'_n(r) \left[u'_n(r,z) + k_n^2 v_n(r,z) \right] \tag{274a}$$

and

$$\frac{\partial}{\partial r} v_r \simeq \sum_{n=1}^{N} f''_n(r) \left[u_n(r,z) + v'_n(r,z) \right] \tag{274b}$$

where the homogeneous range equation gives

$$f''_n(r) = - f'_n(r)/r - k_n^2(r) f_n(r). \tag{275}$$

The derivatives with respect to depth are given by

$$\frac{\partial}{\partial z} v_z = \sum_{n=1}^{N} f_n(r) \left[k_n^2 (u_n + v'_n) - k^2 u_n \right] \tag{276a}$$

and

$$\frac{\partial}{\partial z} v_r \simeq \sum_{n=1}^{N} f'_n(r) \left[u'_n + (k_n^2 - \kappa^2) v_n \right]. \tag{276b}$$

The coherent transmission loss in the range-dependent water column is

84

$$TL_c(r,z) = -20 \log\left[4\pi \frac{\rho(z)}{\rho(z_0)} \left| \sum_{n=1}^{N} f_n(r) u_n(r,z) \right| \right] \tag{277}$$

and the incoherent transmission loss is

$$TL_i(r,z) = -10 \log\left[\left(4\pi \frac{\rho(z)}{\rho(z_0)}\right)^2 \sum_{n=1}^{N} f_n^2(r) u_n^2(r,z) \right] \tag{278}$$

where the range function $f_n(r)$ and the eigenfunctions are complex and the transmission loss is real.

CHAPTER 11

COMPARISON WITH EXPERIMENTAL MEASUREMENTS

The solutions from this range-dependent model can be compared with other range-dependent models with the purpose of validating its results. However, there is no other range-dependent model that can include the effects of shear waves from the ocean bottom. Anyway, if there were an opportunity for the inter-model comparison, their agreement does not rule out the possibility that both models are incorrect. A better way of validating this range-dependent model is to compare its solutions to experimental measurements.

Ellis and Chapman,[11,12] from the Defense Research Establishment Atlantic (DREA), Dartmouth, Canada, have participated in a sea-test at a United Kingdom continental shelf. One of the test areas has a slight range dependence of the ocean floor. The approximate depth of the bottom is 100.0 meters and the composition of the bottom is mostly chalk[*] (see Table 1) with a few meters of sand at the top. They modeled this ocean environment as a range-independent water layer over a semi-infinite chalk basement. Therefore, they neglected the sand sediment and the ubiquitous basalt basement that should be located somewhere under the chalk sediment. This approximation is not valid at frequencies much lower than the optimum frequency of sound propagation, because the penetration capability of its normal modes becomes higher and they may reach the depth of the basalt basement. This simple two-layer model is also not valid at frequencies higher than the optimum frequency because the effects of the depth dependent water column becomes of paramount importance to

---

[*] Note that chalk does not satisfy the second inequality of Equations (185), but it is not unusual for measured attenuation coefficients to be highly erroneous since they are the most difficult ones to obtain. Even though these properties of chalk may by questioned, they will be used for calculating the transmission loss in the range-dependent environment described in References 10 and 11.

the transmission loss calculation. They found the optimum frequency for the environment to be in the vicinity of 300.0 Hz. At much higher frequencies, the effects of the shear waves from the elastic bottom becomes negligible compared to the effects of the depth-dependent water column. Therefore, we will concentrate on the frequencies near and below the optimum frequency.

The source used were explosives that were preset to detonate at a depth of 37.5 ± 1 meters and a hydrophone was located at 71 meters deep. The water depth is about 105 meters at the location of the hydrophone and it has a constant slope with a water depth of 95 meters at a range of 55 kilometers from the hydrophone. This corresponds to a bottom slope of 0.01 degree and it can be considered a range-independent wave guide. A considerable amount of transmission loss measurements have been provided by Chapman for the 1/3 octave band center frequencies of 64, 128, 256, 512, and 1024 Hz as a function of range from 10 to 90 kilometers. It has been found that models with or without shear contribution provide nearly the same transmission loss for frequencies higher than 256 Hz, hence the lower frequencies will be considered here.

Figure 31 is the three-dimensional plot of the range-dependent coherent transmission loss for a frequency of 128 Hz and a source depth of 38 meters. The bottom is a semi-infinite basement of chalk with the properties in Table 1. The water column has a sound speed of 1508 m/s from the surface to a depth of 28 meters, and a constant sound speed of 1494 m/s from a depth of 45 meters to the bottom. The density is a constant 1 gm/cc from the surface to the bottom. The range-dependent wave guide has been divided into 22 range-independent range segments. The first few depth functions are T-R modes similar to the ones for a sandy bottom (see Figures 12 and 13) and all but the fundamental mode have negligible contribution at ranges greater than about 20 kilometers. The contour plot of this down-slope wave guide is shown in Figure 32 where the slight discontinuities in the derivative of the contours are caused by the range segments.

Comparison of the measured and computed transmission loss, for the hydrophone depth of 71 meters, is displayed in Figure 33. The frequency is 128 Hz and the range is extended to 100 kilometers to accommodate the provided measurements. This transmission loss calculation agrees with the one made by Ellis and Chapman with the simple two-layer model[11,12] However, their model is

overestimating the loss at frequencies below 100 Hz.

Figure 34 presents the calculated and measured transmission loss for the frequency of 64 Hz. Note that the excited normal modes are rapidly damped at this lower frequency. If the shear speed of chalk is changed to the fluid-like value in Table 1, the calculated coherent and incoherent transmission loss becomes the one in Figure 35. Now all the normal modes are propagating with much less attenuation, but this fluid-like model is underestimating the loss. Note from these plots the tremendous importance of the shear waves in the transmission loss calculation.

However, there must be a reason for the disagreement between the theoretical and experimental values. Ellis and Chapman speculated that a deep reflector is causing some of the acoustic energy to return to the water column, but their simple model is incapable of including more layers.

Under the assumption that their suggested deep reflector may be the omnipresent basalt basement, a semi-infinite layer has been included in our model with the properties of basalt given in Table 1. The depth of the chalk-basalt interface was taken as a variable in order to fit the calculated transmission loss with the experimental data. This inverse scattering technique provided the best fit for a chalk-basalt interface depth of about 240 meters and the resulting transmission loss is displayed in Figure 36. The disagreement at ranges greater than 60 kilometers may be due to the extremely high transmission loss that makes the signal fall below the noise level of the measured data.

Since the exact location of the sea-test is confidentially kept by the Canadians, there is no way we can verify the true depth of the basalt. However, it has been noticed that this estimated depth is typical for similar ocean environments. Also it has been verified that the semi-infinite layer of basalt hardly changes the transmission loss calculations at 128 Hz (see Figure 33) because the fundamental depth function becomes negligible at 240 meters.

It is true that the wave guide just considered may be taken as range-independent. Therefore, an up-slope range-dependent wave guide will be used to test our model for a steeper bottom slope. A 25.0 Hz source is located at a depth of 112.0 meters in a 200.0 meters deep water column of constant sound speed (1500.0 m/s) over a fluid-like bottom with the properties in Table 1. Three trapped and four radiating modes are detected in this range-independent

wave guide. The source has been placed at a node of the second normal mode to avoid its excitation. The contour plot of the coherent transmission loss is provided in Figure 37 and its three-dimensional display is in Figure 38 where all seven modes have been included in their calculation. Since the Hankel function computation has been performed using the asymptotic approximation, the near field ($r < \lambda = c/f \cong 60$ meters) transmission loss is not correct and is not displayed in the given plots.

To convert this wave guide into a range-dependent one, we will create an up-slope that starts at five kilometers and ends at ten kilometers from the source with a final bottom depth of 150.0 meters deep. Beyond ten kilometers the wave guide remains range independent. The slope has been divided into 50 segments and the third trapped mode becomes a radiating mode in the shallow portion of the wave guide. This slope has an angle of 0.57 degree and only the first three normal modes have been used for this computation because the higher order modes are of no effect to the transmission loss at the region of interest. The results in this range-dependent wave guide are given in Figures 39 and 40. Note that some of the acoustic energy is propagating into the bottom as a consequence of the slope which is converting the third trapped mode into a radiating mode with a higher imaginary component of the eigenvalue. Also note, by comparison of the range-dependent case (see Figure 39) with the range-independent case (see Figure 37), that the transmission loss near the source is almost identical to the one for the range-independent case. Hence, assuring the proper range-dependent transmission loss computations. A similar propagation behavior was detected by Jensen[17] and Miller.[53]

The variation of the real part of the three eigenvalues with range segment number is plotted in Figure 41 where the bottom curve with the highest variation is the third trapped eigenvalue as it becomes a radiating one. The imaginary component of the eigenvalue is displayed in Figure 42 where the imaginary part of the third mode has become so high that its contribution to the transmission loss can be neglected. The real part of the third normal mode at the first range segment with the water depth of 170 meters is given in Figure 43. As the water depth becomes shallower the third normal mode becomes the radiating mode in Figure 44 for the water depth of 160 meters. At 150 meters water depth the mode develops more oscillations into the bottom (see

Figure 45) and its amplitude becomes order of magnitude smaller displaying its negligible contribution. Hence, the precipitated propagation of the interference pattern in Figure 39.

So far, we have performed transmission loss computations for range-dependent wave guides with negligible shear contribution and the water column has been a single layer of constant sound speed and density. An actual sound speed from the Arctic Ocean is provided in Figure 2 with its salinity and temperature profiles. The very low temperature of the environment causes the propagated sound to be much slower than 1500 m/s and the high fluctuations with depth are caused mainly by internal currents typical of the shallow region of this ocean. This microstructure of the sound speed profile is highly important to the propagation of high-frequency sound. For a 25 Hz source, a valid approximation is to consider the 200 meters water column a single layer with surface sound speed of 1435 m/s and a bottom sound speed of 1460 m/s. The sound speed gradient is 0.125 s^{-1} and the bottom is a semi-infinite layer of sand. To consider the case of downslope propagation, the bottom depth increases from 200 meters at five kilometers from the source to 400 meters at 10 km range. The resulting transmission loss in this range-dependent environment, with the bottom slope of -2.29, is provided in Figures 46 and 47. Note, by comparison with Figures 16 and 17, that the gradient causes the sound to interact less with the bottom, therefore causing it to propagate with less loss. Also, as the bottom depth becomes larger, the sound gets trapped in the surface channel caused by the positive gradient. This channeling behavior is also modeled by ray bundles that bend upward and bounce back from the pressure-release surface forming *caustics* at the regions where they contructively interfere. Finally, note the destructive interference that occurs in the bottom at about seven kilometers. As the sound bounces from the ocean floor, some of its energy gets refracted into the bottom. However, at the range-dependent region of the wave guide the angle of reflection is affected by the slope, causing most of the reflected energy to scatter the surface at a shallower angle and become trapped in the water column. The combined effects of sound trapped in the channel and the reflections from the slope contribute to the easy detection of surface ships and submarines from open-ocean receivers.

The plots for the range-dependent wave guides do exhibit sound

penetration into the bottom, but it seems to be more dampen than the one reported by Jensen[17] and the one by Miller[53] A probable explanation is that the mode coupling terms in Equations (240) must be included in the range-dependent transmission loss calculations since the adiabatic approximation breaks down for rapidly varying ocean wave guides.

Another important step for a better ocean model is to include the effects of axial variations. Since the number of radiating modes have been drastically reduced with the approach given in this investigation, the problem of computer memory and storage has been decreased and further computations can be pursued.

This work represents a step closer to the final three-dimensional coupled normal-mode model with shear wave from the ocean floor and the Arctic snow/ice surface layers.

CHAPTER 12

CONCLUSIONS AND RECOMMENDATIONS

A new sound propagation model and its computer code has been developed based on the theory of normal modes. This normal mode model has been expanded to take into account the effects of the elasticity of the ocean floor and the depth dependence of the acoustic properties by dividing the wave guide into horizontal layers with constant density, constant shear speed, and constant attenuation coefficients. However, the water column has layers of linear wave number squared to better simulate the sound speed profile. It has been found that the compressional sound speed in the elastic layers can also have linear wave number squared and the density in the water layers can be a variable and still have a solvable set of wave equations. However, the limited knowledge of the detailed properties of the bottom and the limited applications suggest that these flexibilities can be excluded from the computer code. Since the absorptive properties of the bottom is so high and the attenuation of low-frequency sound in the water is so low, the absorption in the water has been neglected.

The newly developed normal mode model searches for the eigenvalues in the complex wave number plane using the Levenberg-Marquardt algorithm that searches for the minima of the magnitude of the complex determinant. It has been found that the absorptive properties of the semi-infinite bottom causes the radiating wave number spectrum to be inherently discrete, hence the false boundary introduced by Evans has been eliminated and the number of radiating modes has been drastically reduced. The reduced number of modes for the transmission loss calculations allows for the feasibility of calculations at higher frequencies and deeper ocean wave guides.

The transmission loss in the elastic sediments is computed using the magnitude of the acoustic intensity vector. This complex intensity vector is the scalar product of the stress tensor and the particle velocity vector. The

intensity vector can also be used to determine the direction of propagation of the acoustic energy.

Range dependence of the acoustic properties of the ocean wave guide has been taken into account by using a modified version of the adiabatic normal mode theory to include the shear waves. This adiabatic normal mode theory has been developed with the assumption of a slowly varying environment. However, the threshold of maximum variation is not known because of the high degree of complexity of this multilayered model and the large number of acoustic properties that can be varied in range.

The eigenvalues, eigenfunctions, and range-independent transmission loss results have been compared to the benchmark two-layer model, with a semi-infinite elastic bottom, by Ellis and Chapman and the perturbation method for fluid-like bottom by Miller yielding excellent agreement.

The range-dependent coherent transmission loss calculation has been compared to transmission loss measurements by the Defence Research Establishment Atlantic (DREA), Dartmouth, N.S., Canada, at the United Kingdom continental shelf. Very good agreement was obtained at 128 Hz and above with a the model containing a semi-infinite chalk bottom. However, this model overestimates the loss at frequencies below 100 Hz. At these lower frequencies the shear and compressional depth functions extended deeper into the bottom where acoustic properties are unknown, hence the ubiquitous basalt basement has been included at a depth of 240 meters from the ocean surface to provide the agreement at 64 Hz without changing the results at 128 Hz and above. Hence, this multilayered model can also be used for inverse scattering purposes.

The up-slope wedge-like ocean has been modeled for a variable slope to observe the changes in the transmission properties and to test the validity of the adiabatic approximation. Perfect agreement has been found between the range-independent and the range-dependent transmission loss when all the segments had the same acoustic properties and layer thickness. As the slope increased a "tongue," similar to the one observed by Jensen and Miller, was developed. However, increasing inaccuracy of the range-dependent transmission loss with increasing bottom slope is expected due to the need of the coupling terms in the inhomogeneous range equation which involve the range derivative of the eigenfunctions.

The next step to the ultimate transmission loss model is to include these coupling contributions. Also, it is possible to include the azimuthal variations of the ocean using the adiabatic approximation to obtain a three-dimensional transmission loss model for slowly varying environments. Finally, the azimuthal and range coupling contributions can be incorporated in the three-dimensional model to simulate sea-mounts and more complex underwater structures.

Other steps to improve the present computer code are to:

1. Include the effects of the elastic snow/ice layers at the surface of the ocean model to simulate the sound propagation in the Arctic environment. With such a model, it is possible to study the effects of shear waves on ice-mounted receivers.

2. Include layers with linear variation of the density with depth. The variation of density with depth in the water column has been measured and found to be of minimum importance, but its variation in the elastic sediments is often of considerable importance.

3. Include elastic layers with variable compressional sound speed. It has been theoretically proven in this work that the elastic wave equation representing a layer with variable compressional sound speed can be separated into an equation for shear waves and one for the compressional waves.

4. Include absorption effects from the water column. The absorption in the water at low frequencies is negligible. However, its contribution at higher frequencies becomes important and it must be included in the transmission loss calculation.

5. Include the effects from surface and bottom roughness. Very simple equations have been derived by Kuperman and Ingenito[74] with the Kirchhoff approximation. The equations ignore the contributions from the non-specularly reflected acoustic energy and they may be added to the imaginary part of the complex wave numbers after the eigenfunctions are computed.

6. Refine the searching algorithm to "*guarantee*" the uniform convergence to all the complex eigenvalues. The present searching algorithm may not be able to find all the complex eigenvalues for a water column with two or more channels since these create *degenerate* eigenvalues with irregular

94

spacings.

7. Include an option to obtain the transmission loss as a function of frequency and to account for the frequency spectrum of the signal emitted by the source (its signature). The current computer code calculates the transmission loss of continuous wave (CW) acoustic signals and extra computations are required to obtain the transmission loss of pulses and other wave forms.
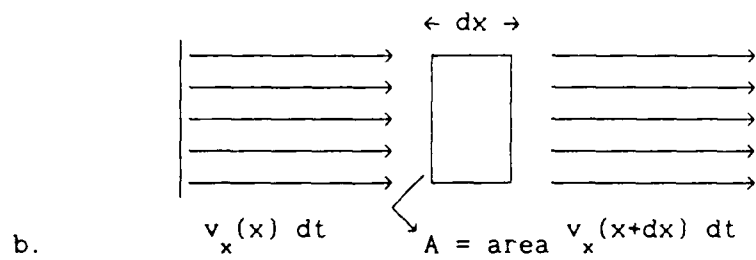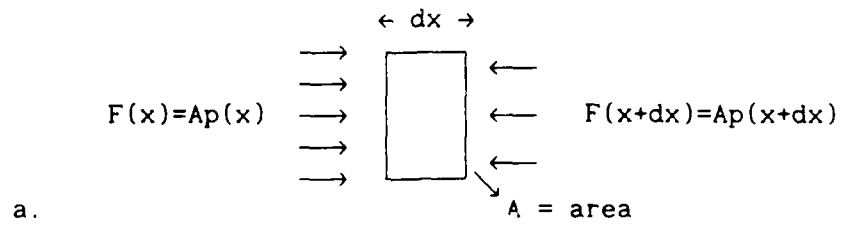
FIGURE 1.   MODELS TO DERIVE THE EULER EQUATION OF MOTION (a) AND THE
            CONTINUITY EQUATION (b)
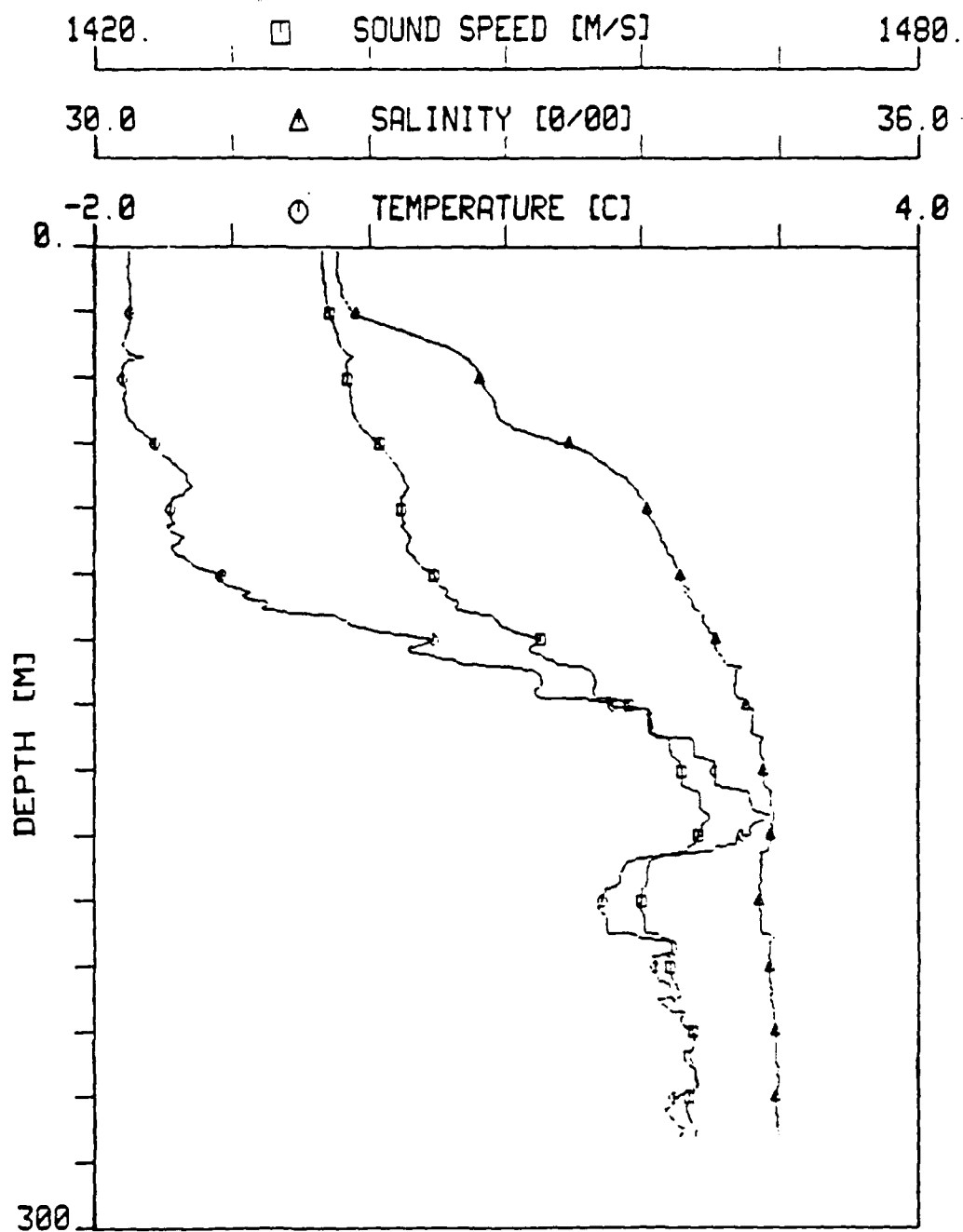
FIGURE 2. SOUND SPEED, SALINITY, AND TEMPERATURE PROFILES TAKEN IN THE EAST
GREENLAND CURRENT (78°N)
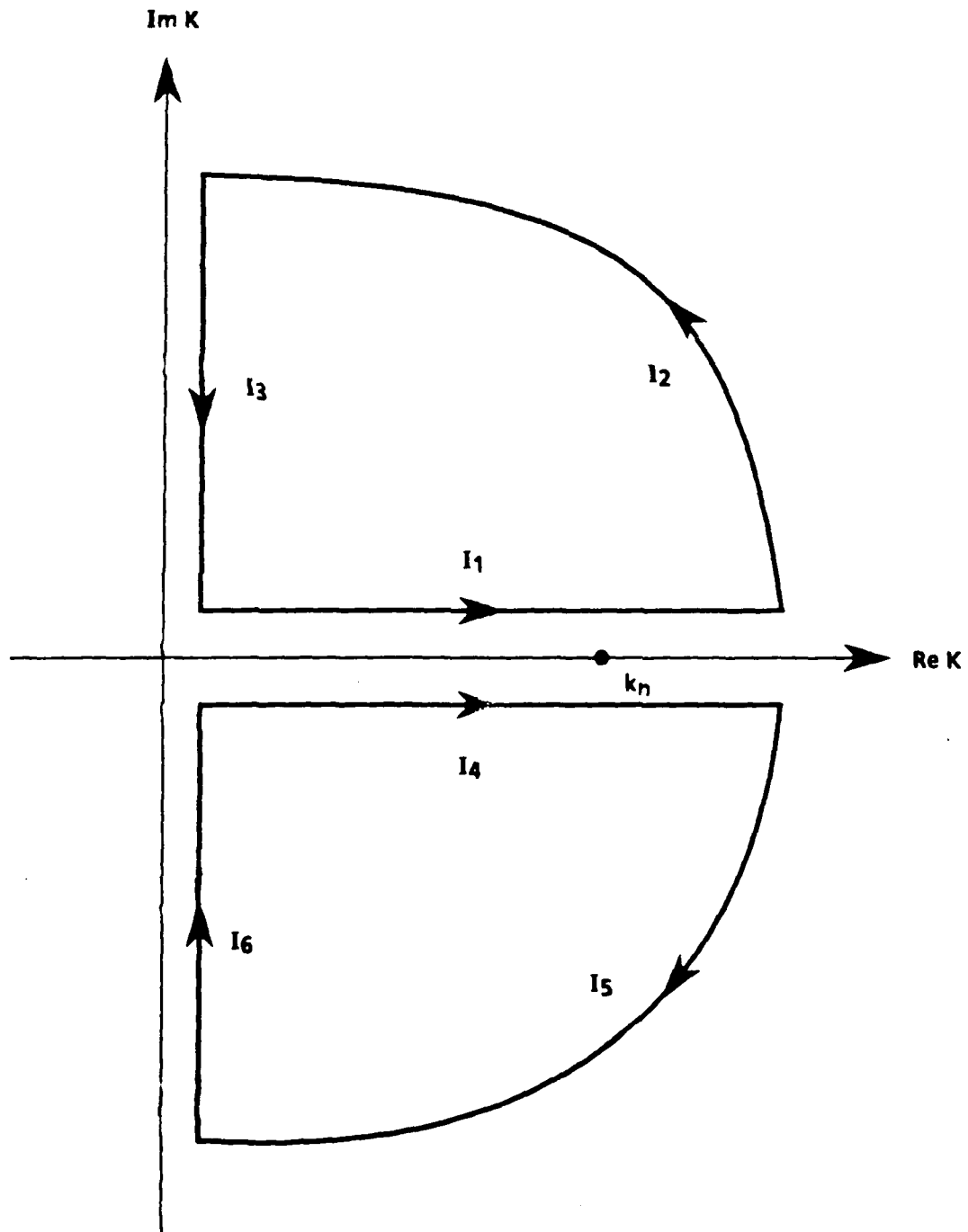
FIGURE 3. THE CONTOUR OF INTEGRATION FOR THE EVALUATION OF THE SCALAR
POTENTIAL USING THE RESIDUES OF THE INTEGRAND
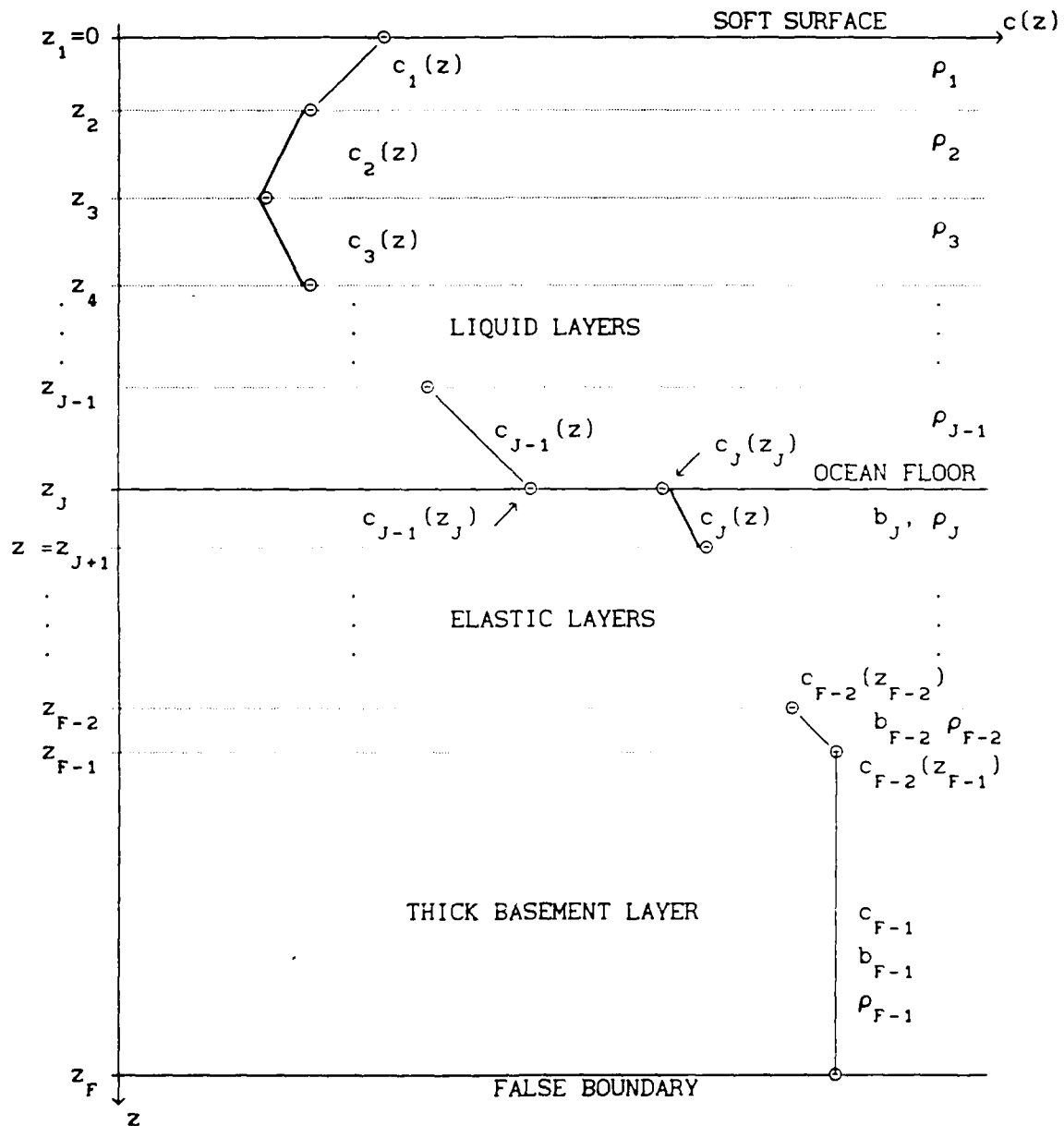
FIGURE 4.   THE FALSE BOUNDARY IN THE HORIZONTALLY STRATIFIED OCEAN MODEL HAS
BEEN ELIMINATED AND THE BASEMENT IS NOW A SEMI-INFINITE ELASTIC
LAYER
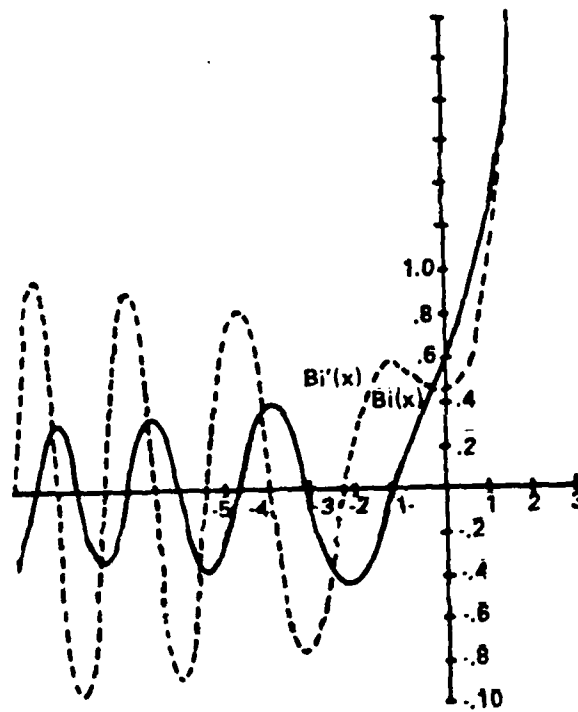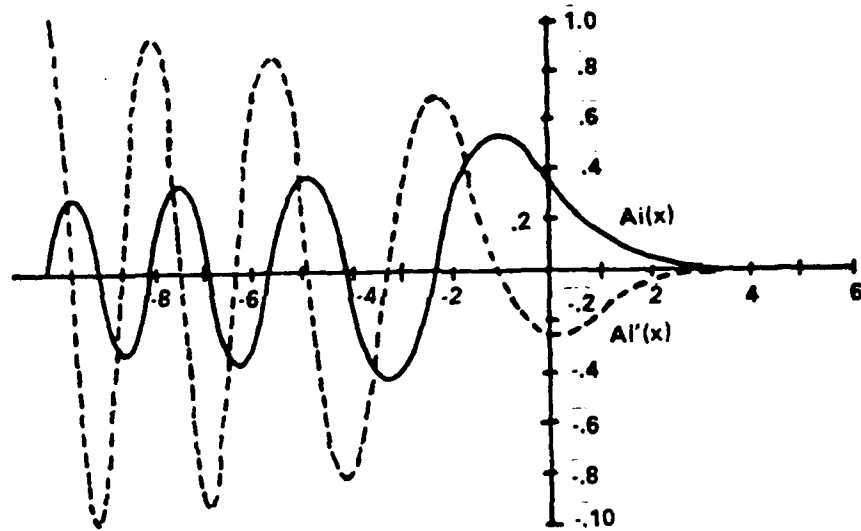
FIGURE 5.   THE AIRY FUNCTIONS AND THEIR DERIVATIVES
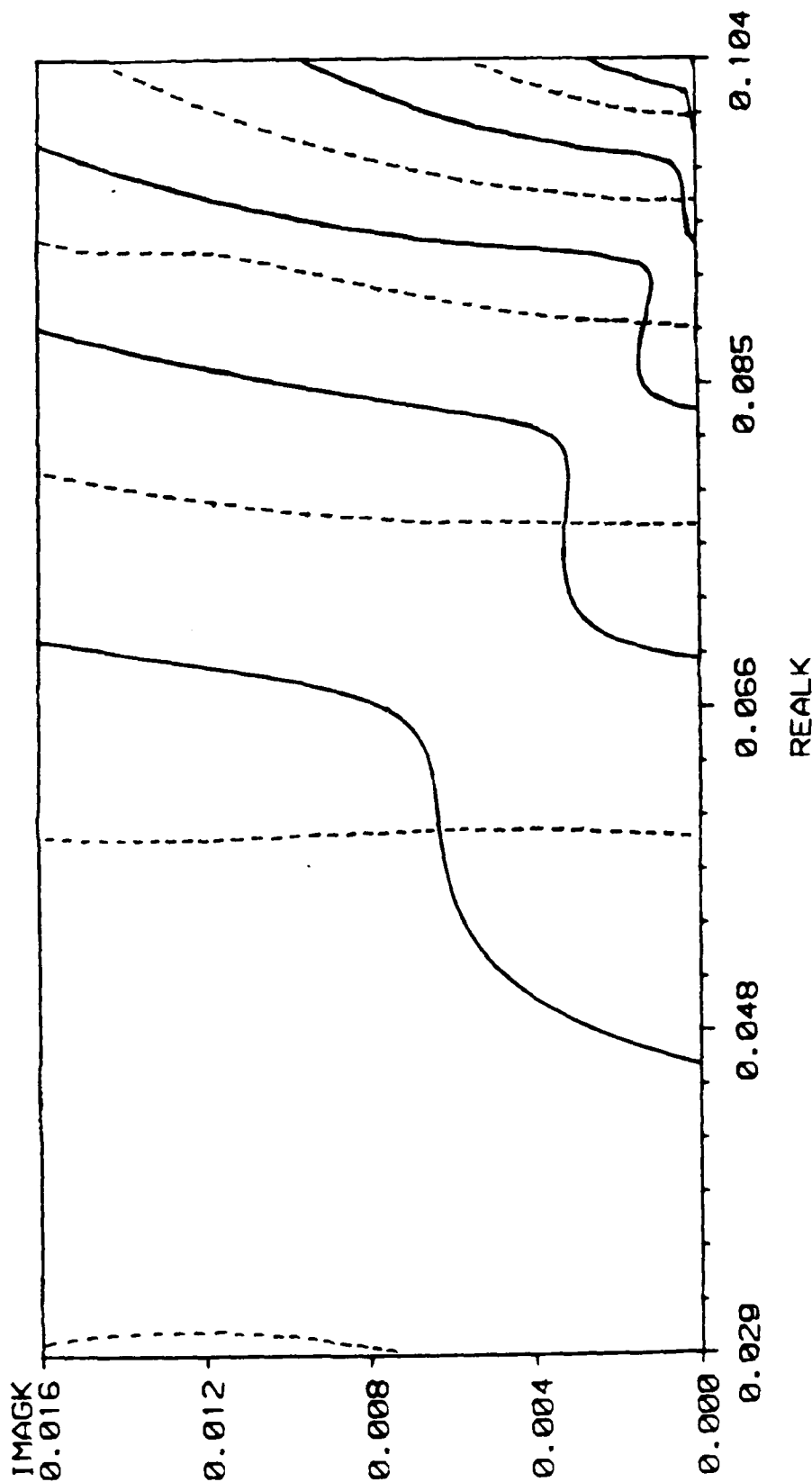
FIGURE 6. CONTOURS WHERE THE REAL AND IMAGINARY PART OF THE COMPLEX CHARACTERISTIC EQUATION ARE ZERO IN THE COMPLEX K-PLANE. THE DASHED CURVE REPRESENTS THE REAL PART AND THE SOLID CURVE IS THE IMAGINARY PART FOR THE FLUID-LIKE BOTTOM AND A 25 HZ SOURCE (THE INTERSECTIONS OF THE CURVES CORRESPOND TO THE LOCATION OF THE COMPLEX EIGENVALUES)
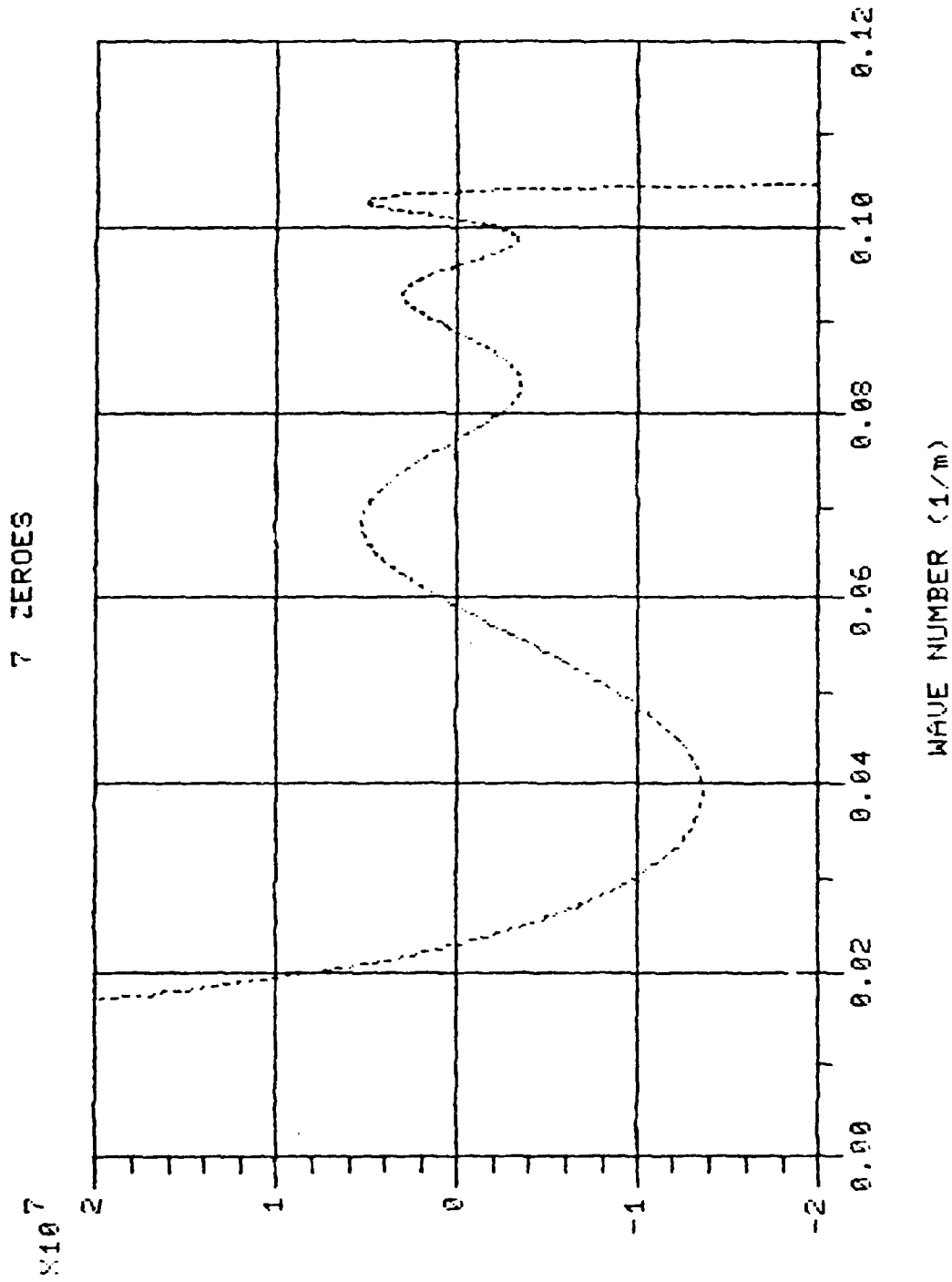
FIGURE 7. THE REAL PART OF THE CHARACTERISTIC EQUATION AS A FUNCTION OF THE
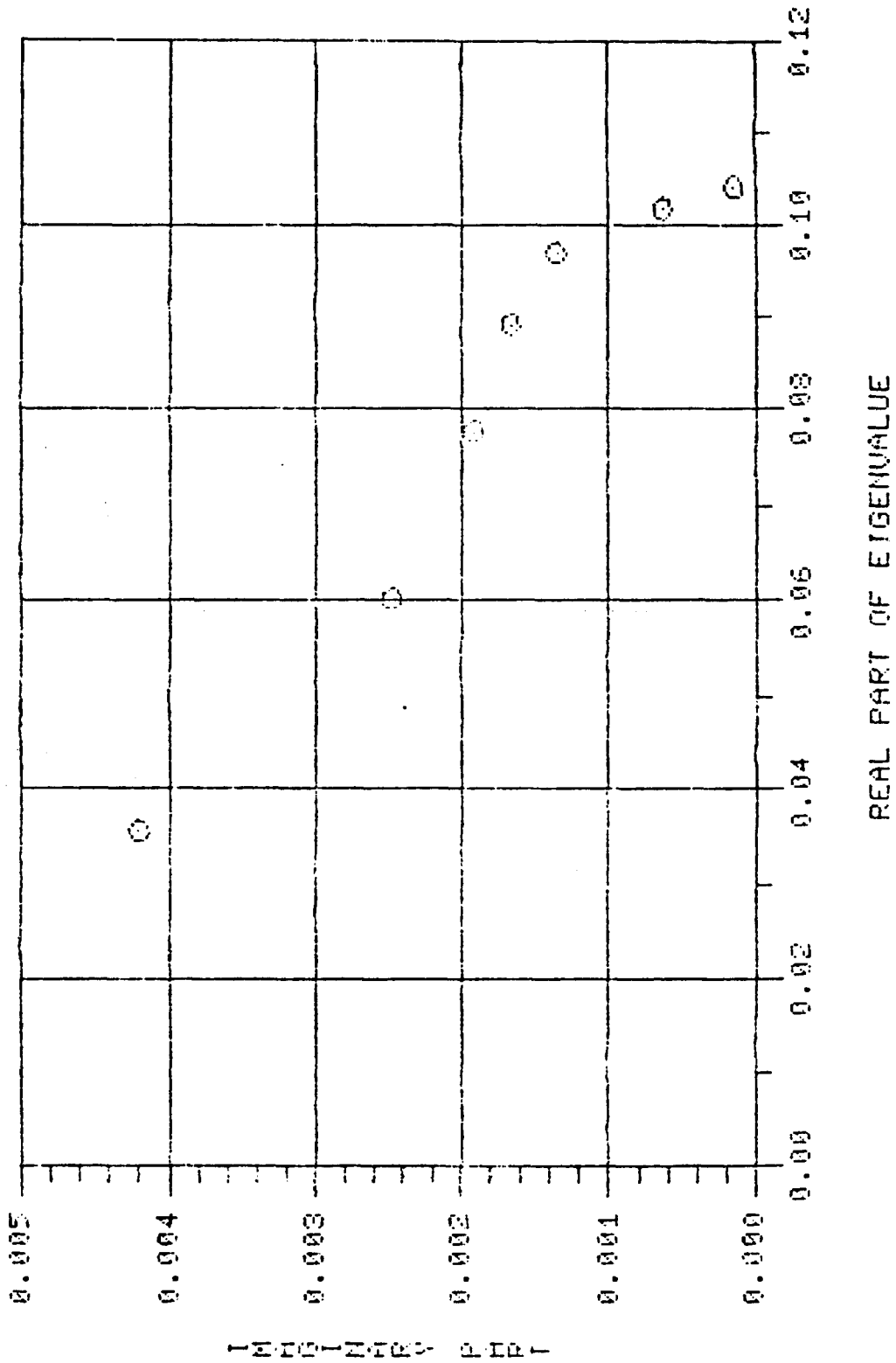REAL PART OF THE WAVE NUMBER
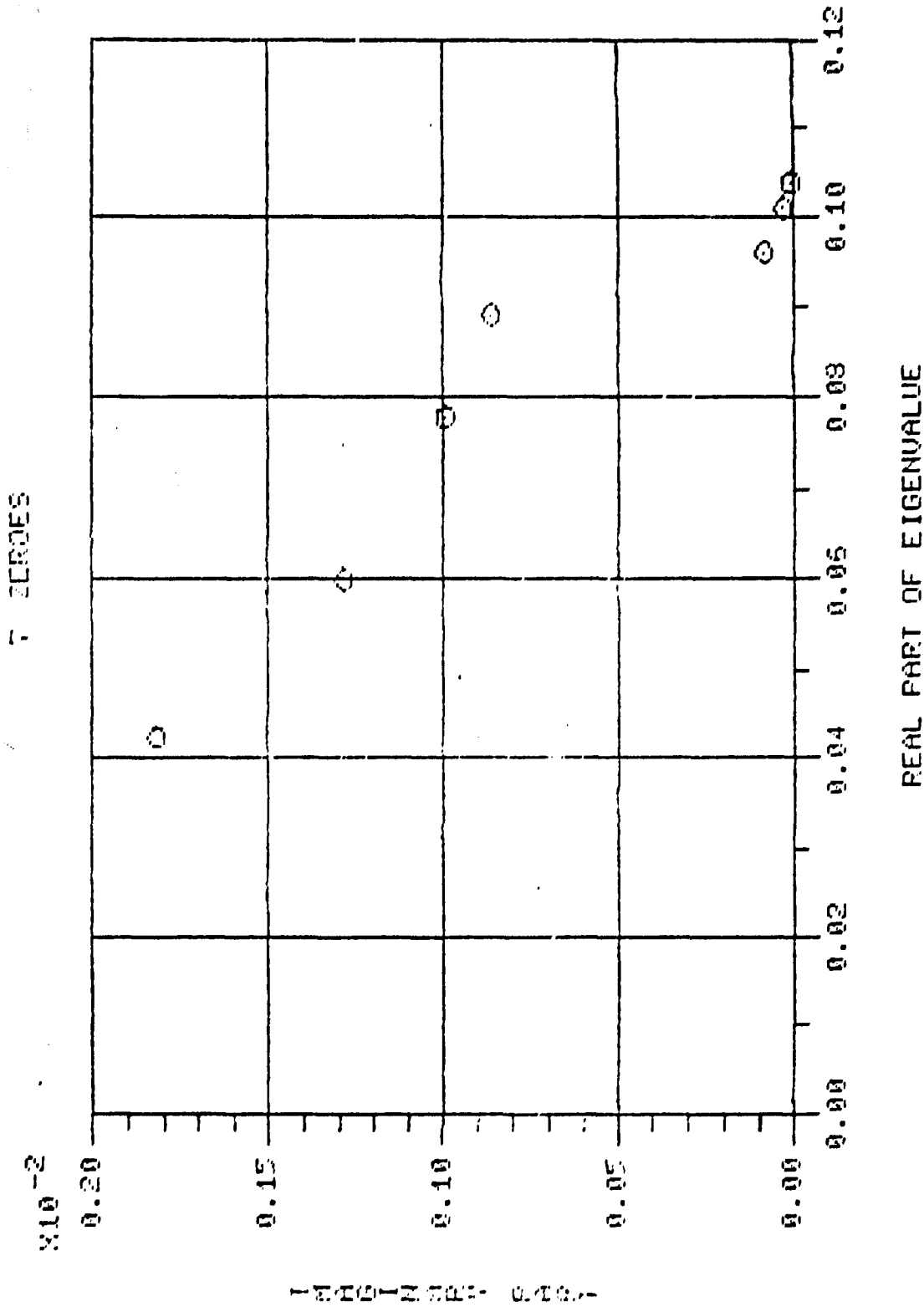
FIGURE 8. LOCATION OF THE COMPLEX EIGENVALUES FOR A 25 HZ SOURCE IN A WATER
COLUMN 200 METERS DEEP OVER A FLUID-LIKE SEMI-INFINITE BASEMENT
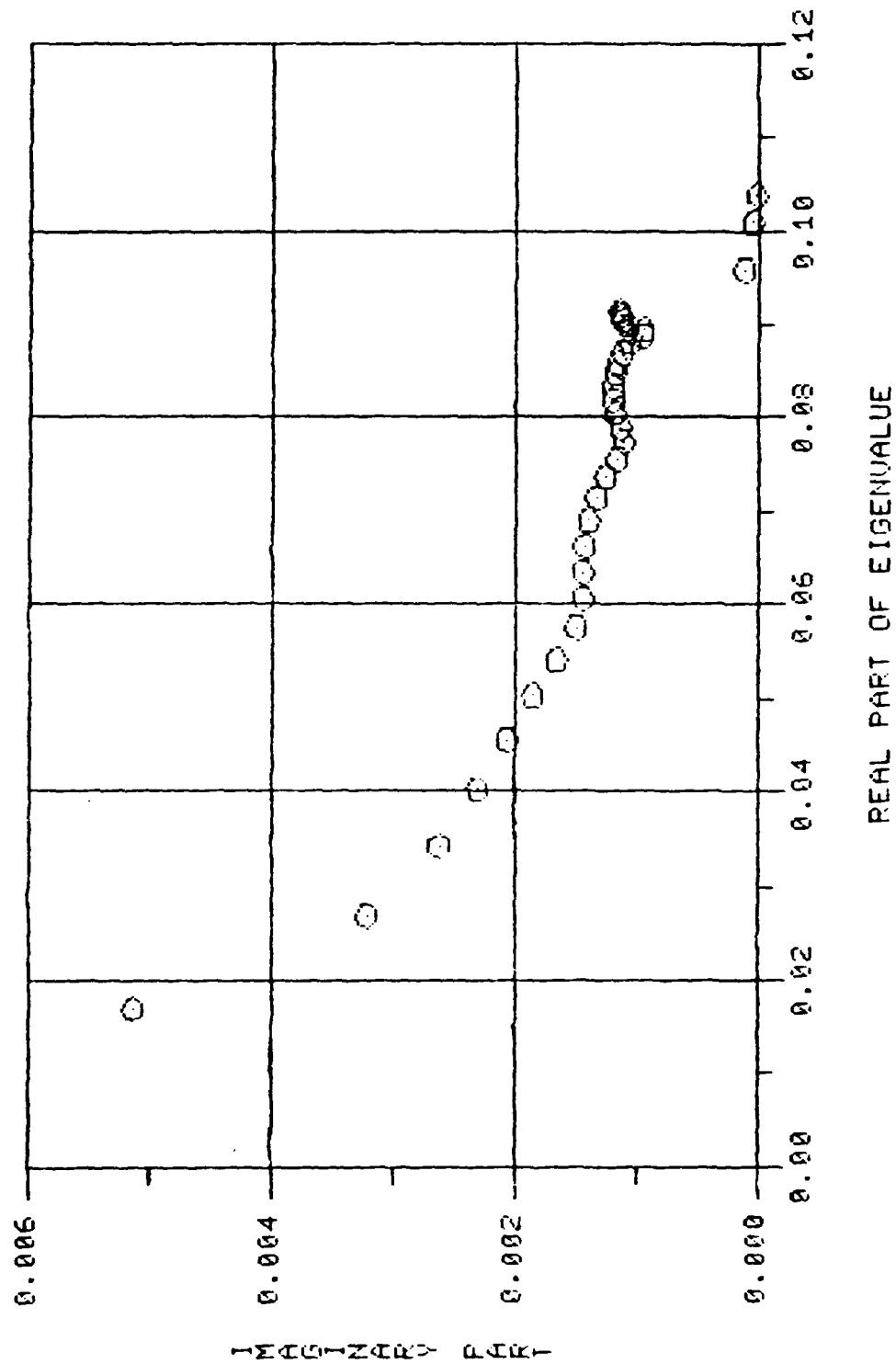
FIGURE 9.   LOCATION OF THE COMPLEX EIGENVALUES FOR A 25 HZ SOURCE IN A WATER
COLUMN 200 METERS DEEP OVER A FLUID-LIKE BASEMENT WITH A RIGID
BOUNDARY AT 1200 METERS
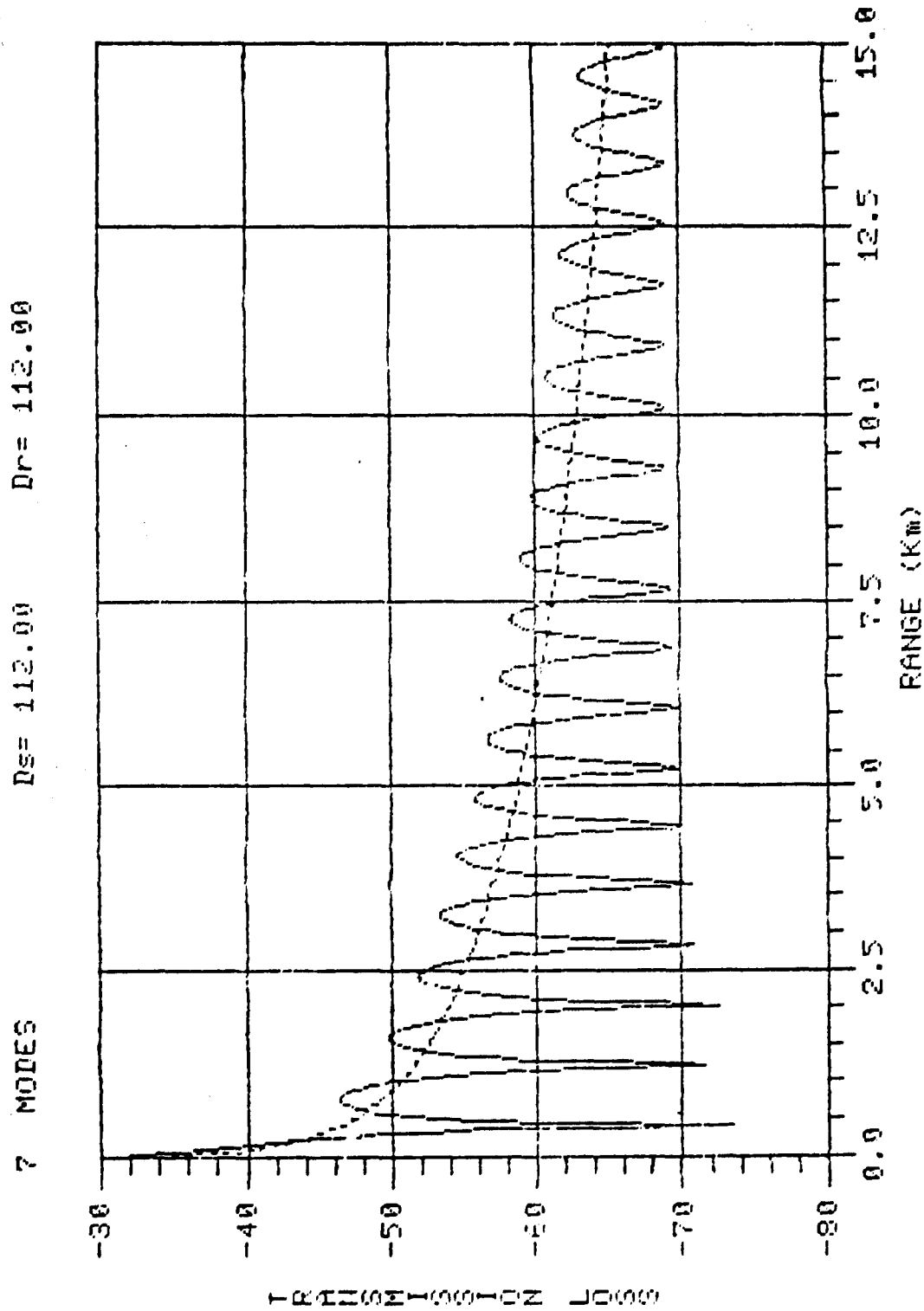
FIGURE 10. THE COHERENT (SOLID CURVE) AND INCOHERENT (DASH CURVE) TRANSMISSION LOSS VERSUS RANGE FOR A 25 HZ SOURCE IN A WATER COLUMN 200 METERS DEEP OVER A FLUID-LIKE SEMI-INFINITE BASEMENT (THE SOURCE AND RECEIVER DEPTH IS 112 METERS)
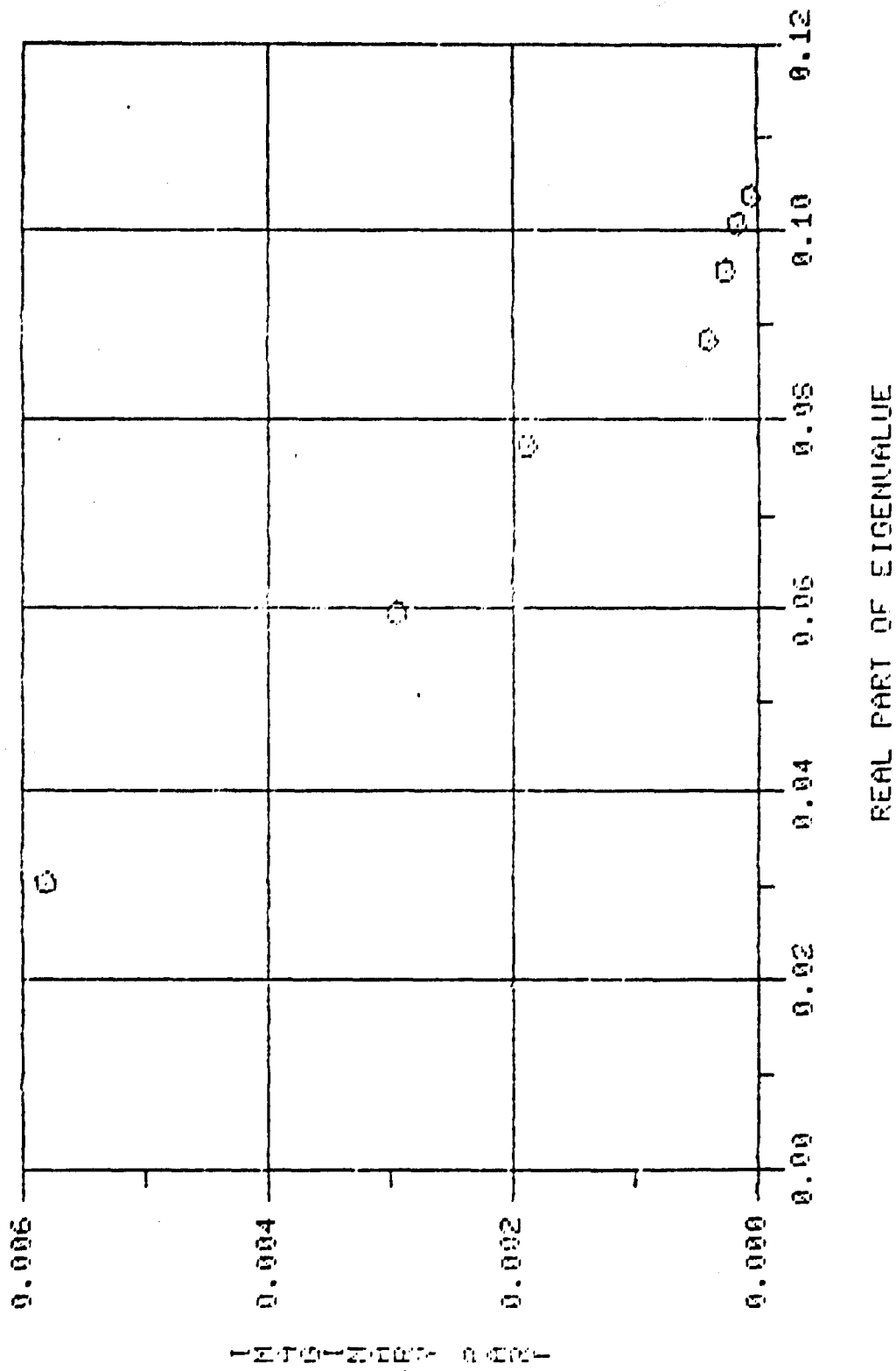
FIGURE 11. LOCATION OF THE COMPLEX EIGENVALUES FOR A 25 HZ SOURCE IN A WATER COLUMN 200 METERS DEEP OVER A SEMI-INFINITE SAND BASEMENT
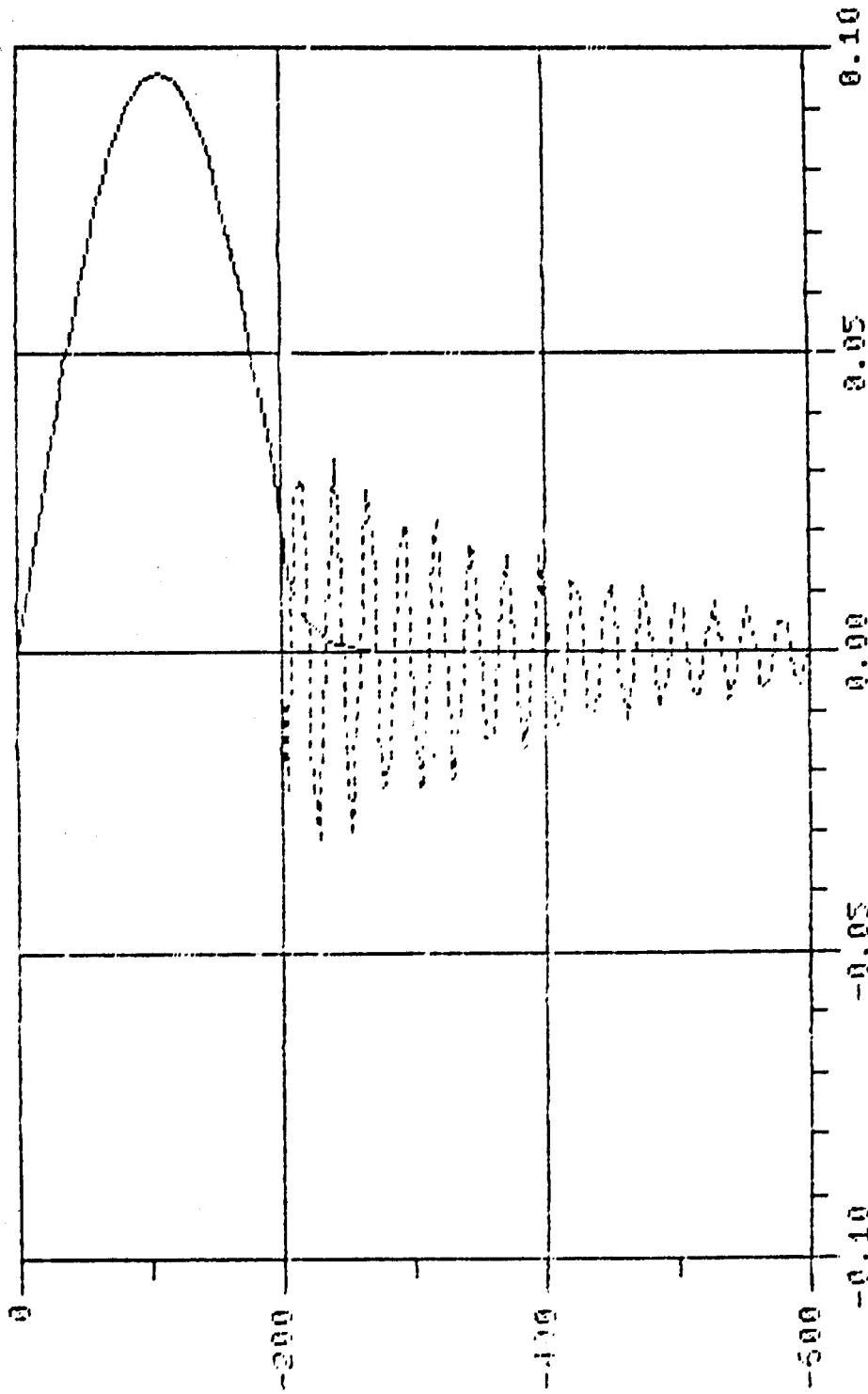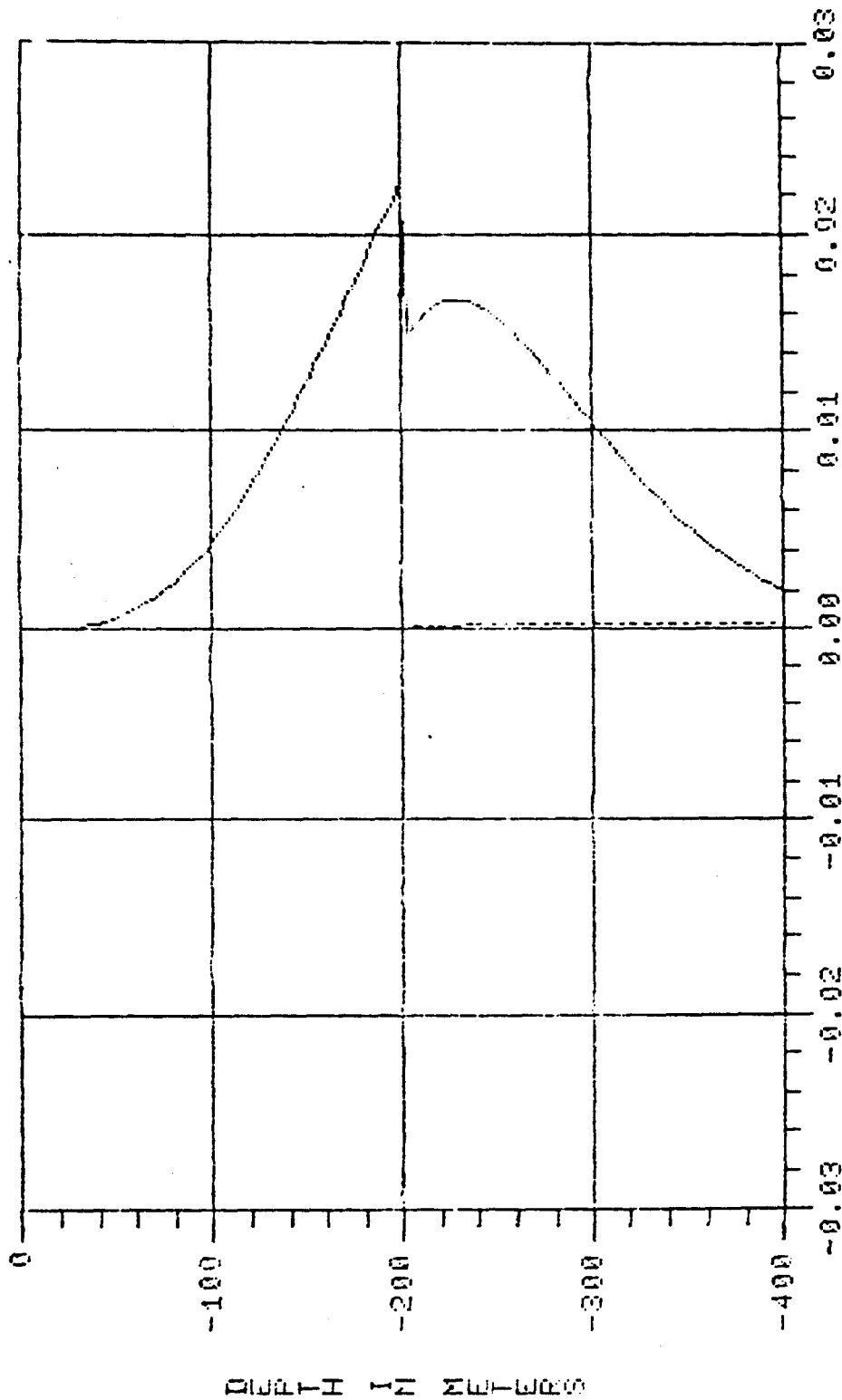
FIGURE 12. THE REAL PART OF THE FUNDAMENTAL MODE FOR A 25 HZ SOURCE IN A WATER COLUMN 200 METERS DEEP OVER A SEMI-INFINITE SAND BASEMENT (THE SOLID CURVE IS THE COMPRESSIONAL EIGENFUNCTION AND THE DASHED CURVE IS THE SHEAR EIGENFUNCTION)
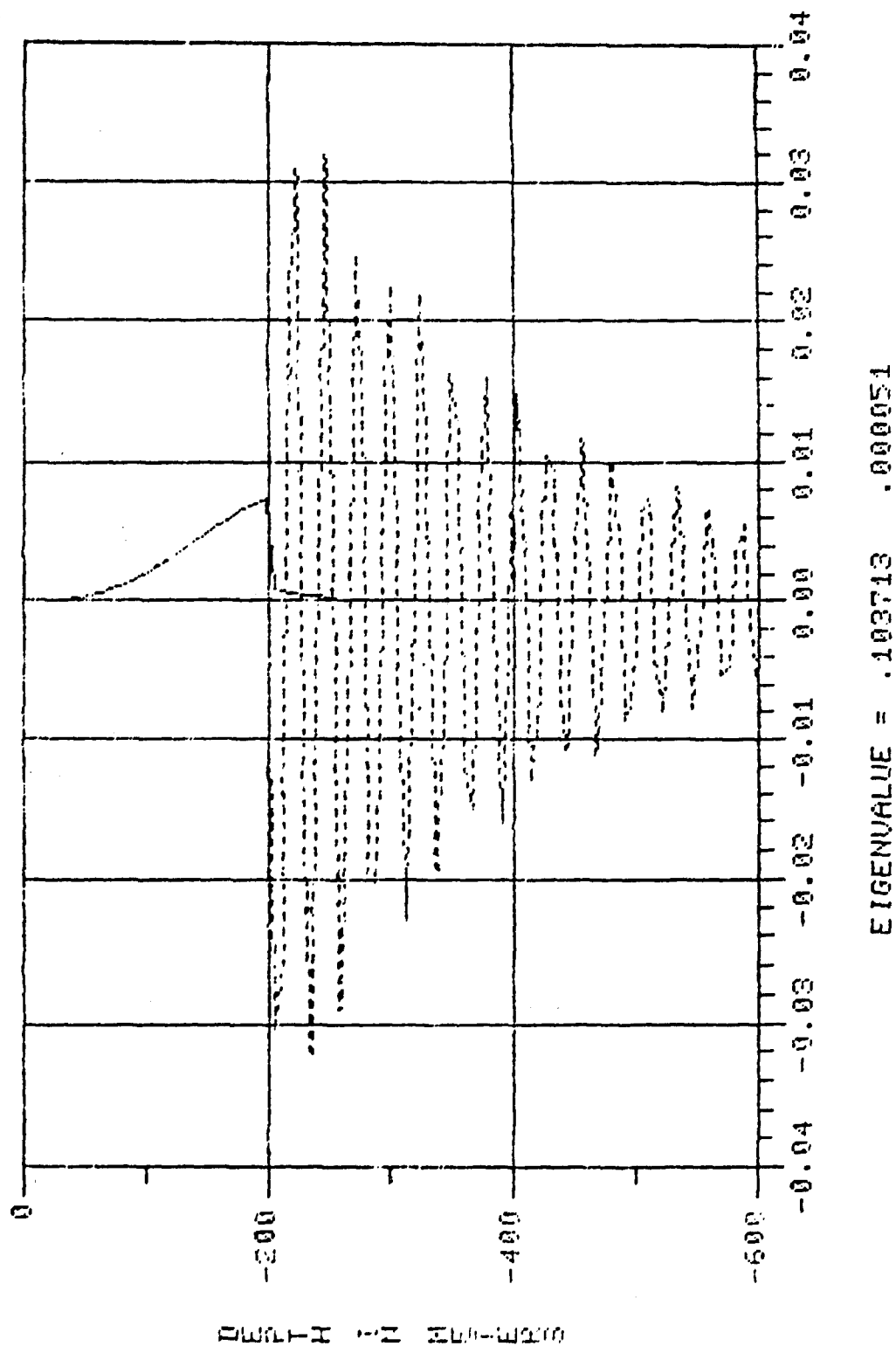
FIGURE 13. THE IMAGINARY PART OF THE FUNDAMENTAL MODE FOR A 25 HZ SOURCE IN A WATER COLUMN 200 METERS DEEP OVER A SEMI-INFINITE SAND BASEMENT (THE SOLID CURVE IS THE COMPRESSIONAL EIGENFUNCTION AND THE DASHED CURVE IS THE SHEAR EIGENFUNCTION)

FIGURE 14. THE REAL PART OF THE FIRST RADIATING MODE FOR A 25 HZ SOURCE IN A WATER COLUMN 200 METERS DEEP OVER A SEMI-INFINITE SAND BASEMENT (THE SOLID CURVE IS THE COMPRESSIONAL EIGENFUNCTION AND THE DASHED CURVE IS THE SHEAR EIGENFUNCTION)
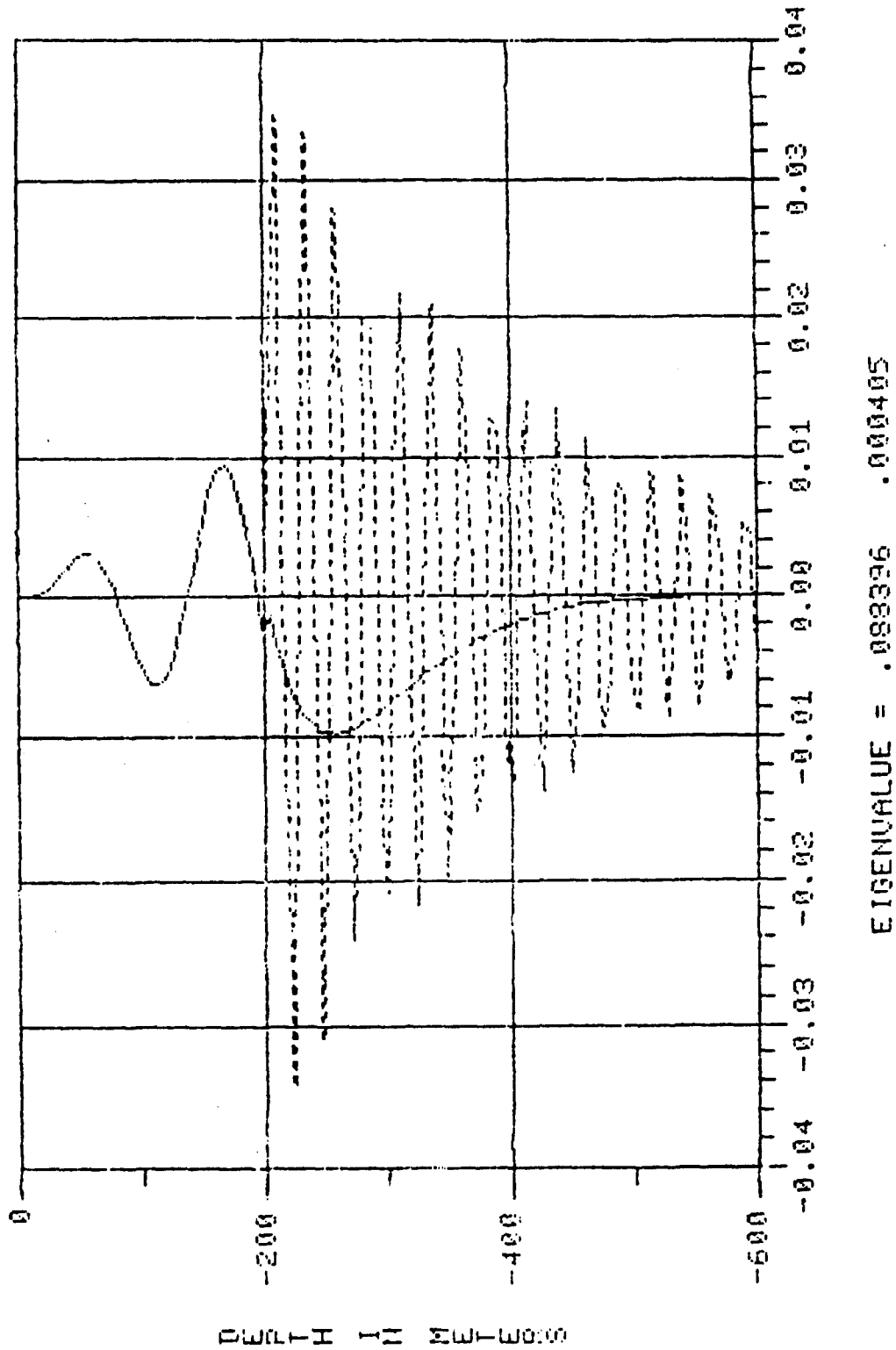
FIGURE 15. THE IMAGINARY PART OF THE FIRST RADIATING MODE FOR A 25 HZ SOURCE
IN A WATER COLUMN 200 METERS DEEP OVER A SEMI-INFINITE SAND
BASEMENT (THE SOLID CURVE IS THE COMPRESSIONAL EIGENFUNCTION AND
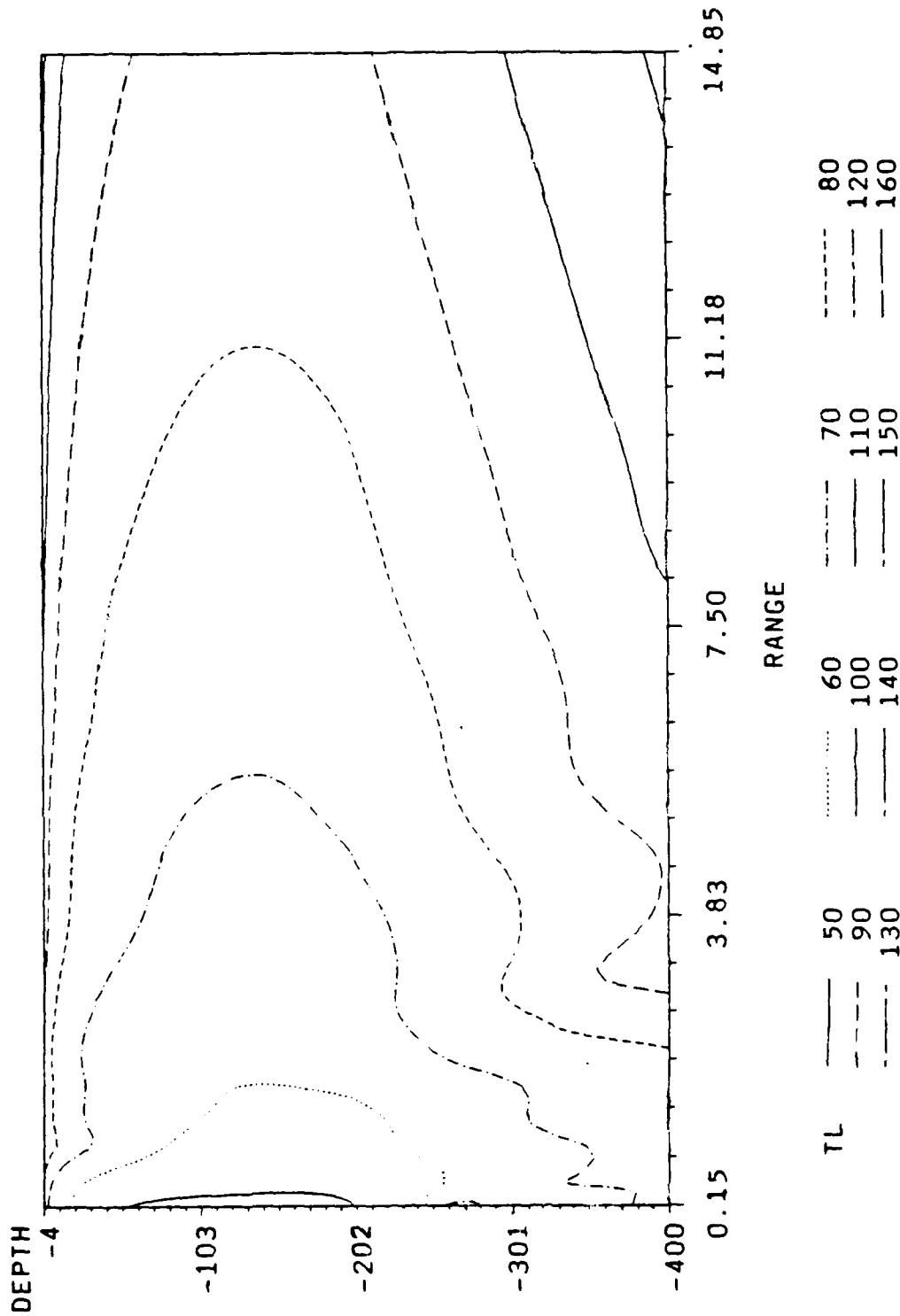THE DASHED CURVE IS THE SHEAR EIGENFUNCTION)
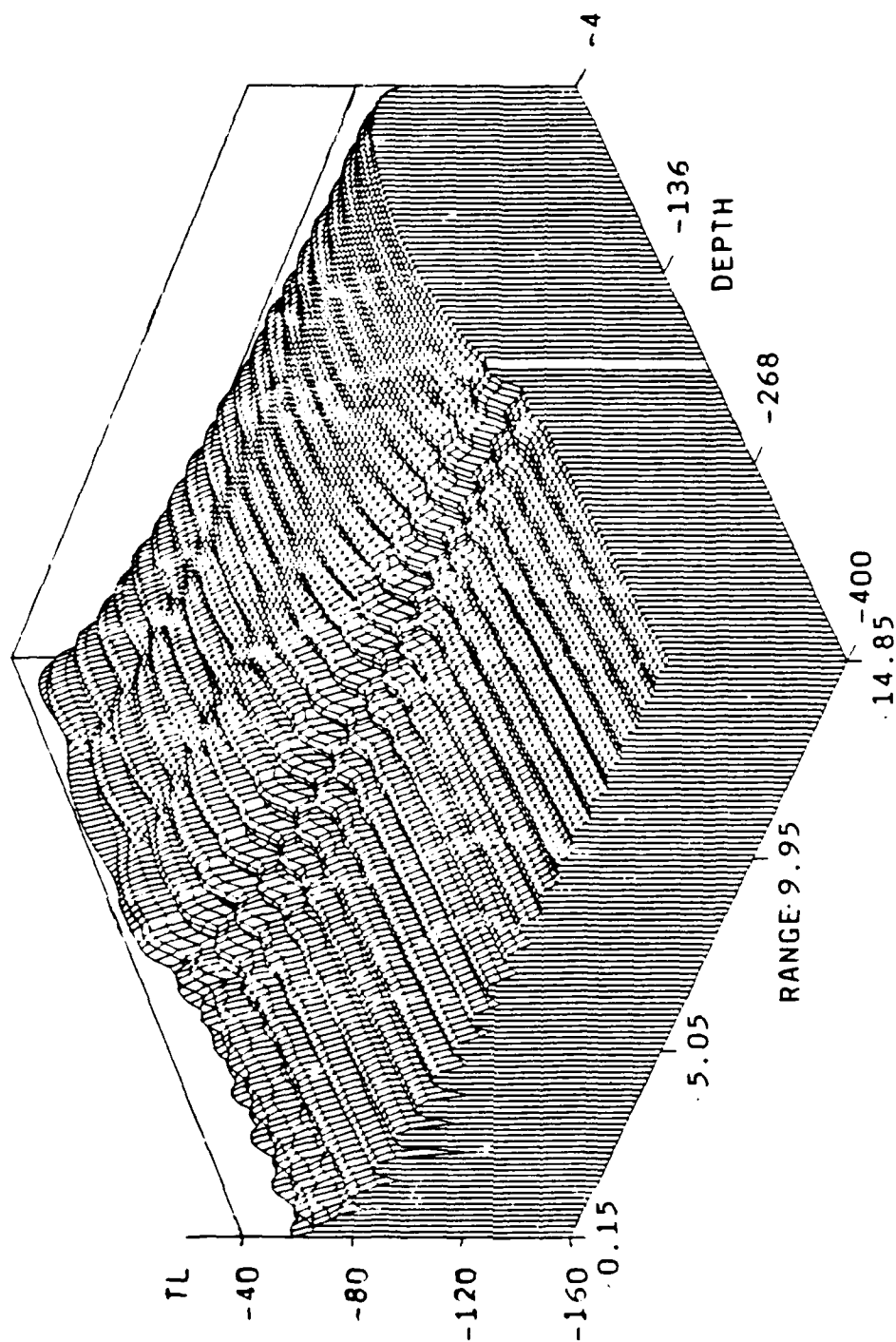
FIGURE 16. A THREE-DIMENSIONAL PLOT OF THE COHERENT TRANSMISSION LOSS (DB) AS A FUNCTION OF RANGE (KM) AND DEPTH (M) FOR A 25 HZ SOURCE AT 112 M DEPTH IN A 200 M WATER COLUMN OVER A SEMI-INFINITE SAND BASEMENT (ALL SEVEN MODES WERE USED)
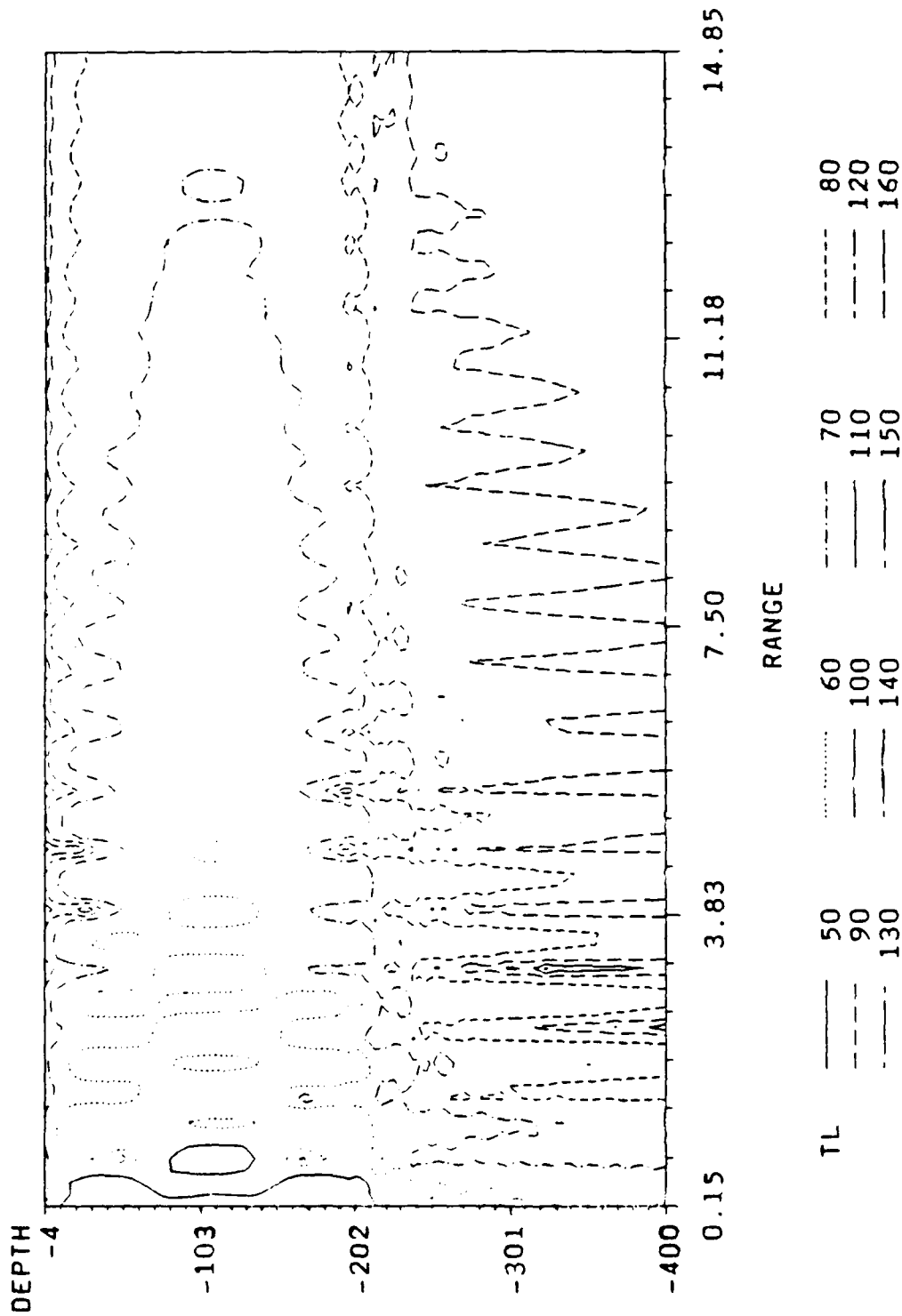
FIGURE 17. A CONTOUR PLOT OF THE COHERENT TRANSMISSION LOSS (DB) AS A FUNCTION OF RANGE (KM) AND DEPTH (M) FOR A 25 HZ SOURCE AT 112 M DEPTH IN A 200 M WATER COLUMN OVER A SEMI-INFINITE SAND BASEMENT (ALL SEVEN MODES WERE USED)

FIGURE 18. LOCATION OF THE COMPLEX EIGENVALUES FOR A 25 HZ SOURCE IN A WATER COLUMN 200 METERS DEEP OVER A SEMI-INFINITE CLAY-SILT BASEMENT
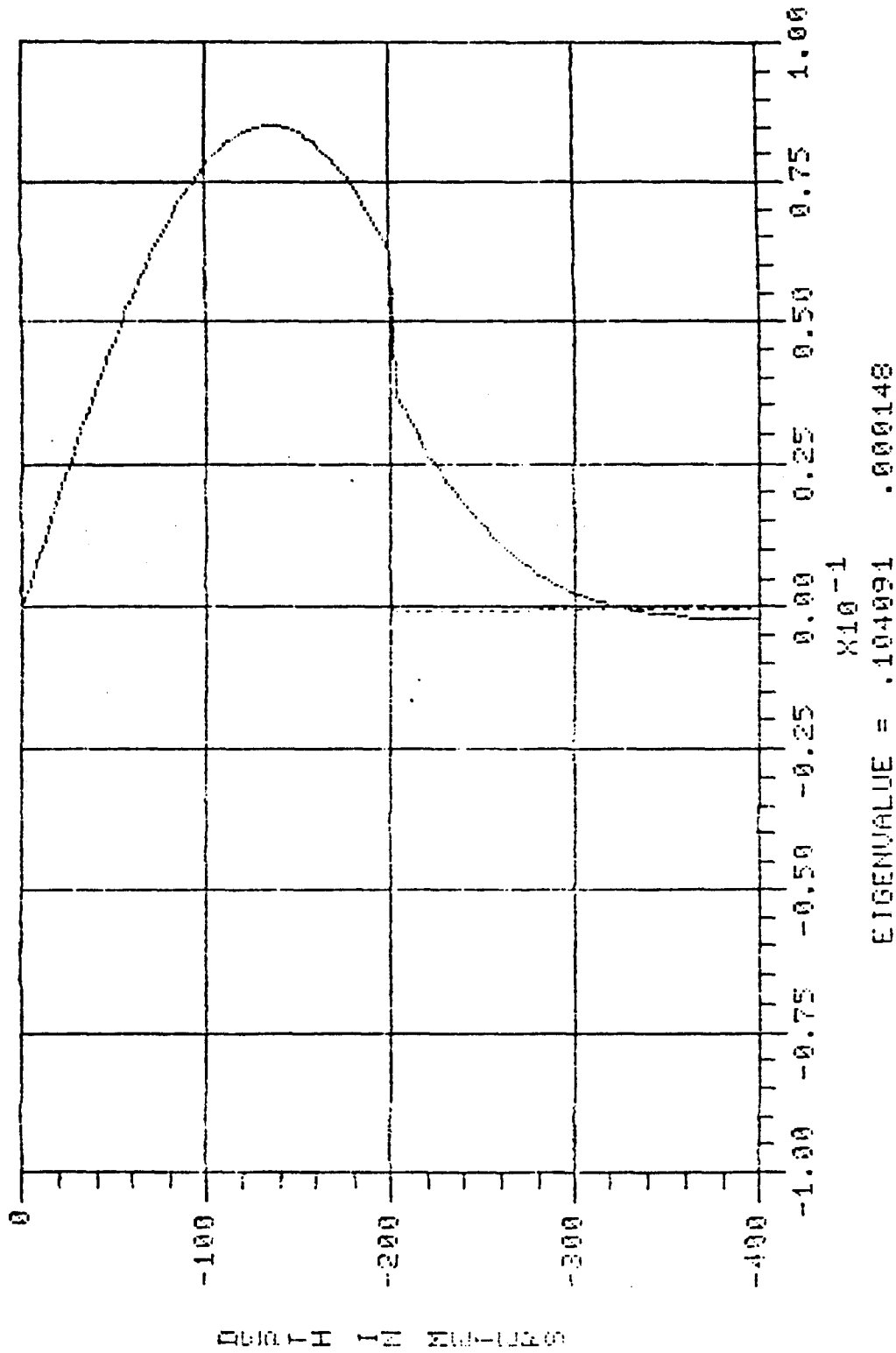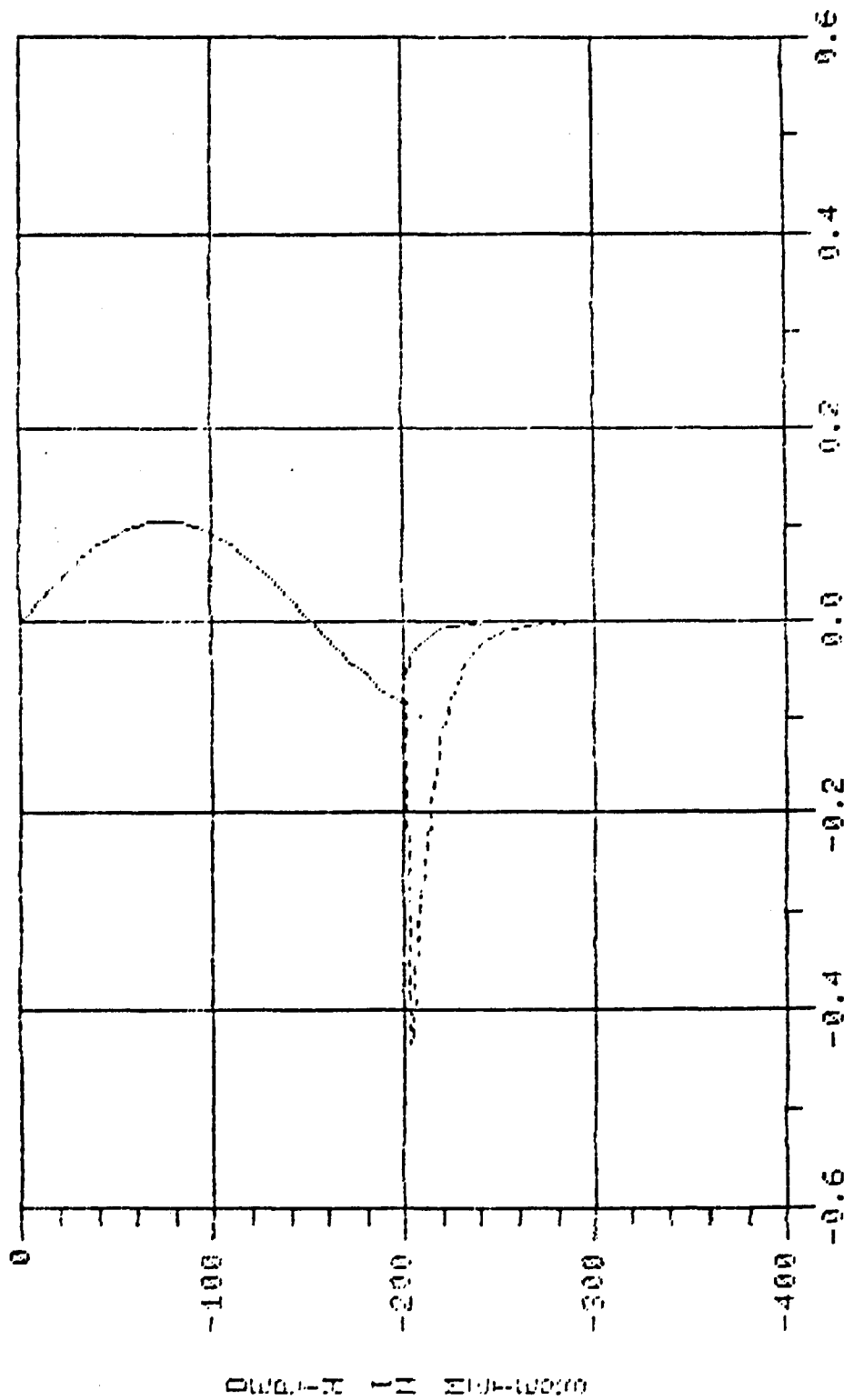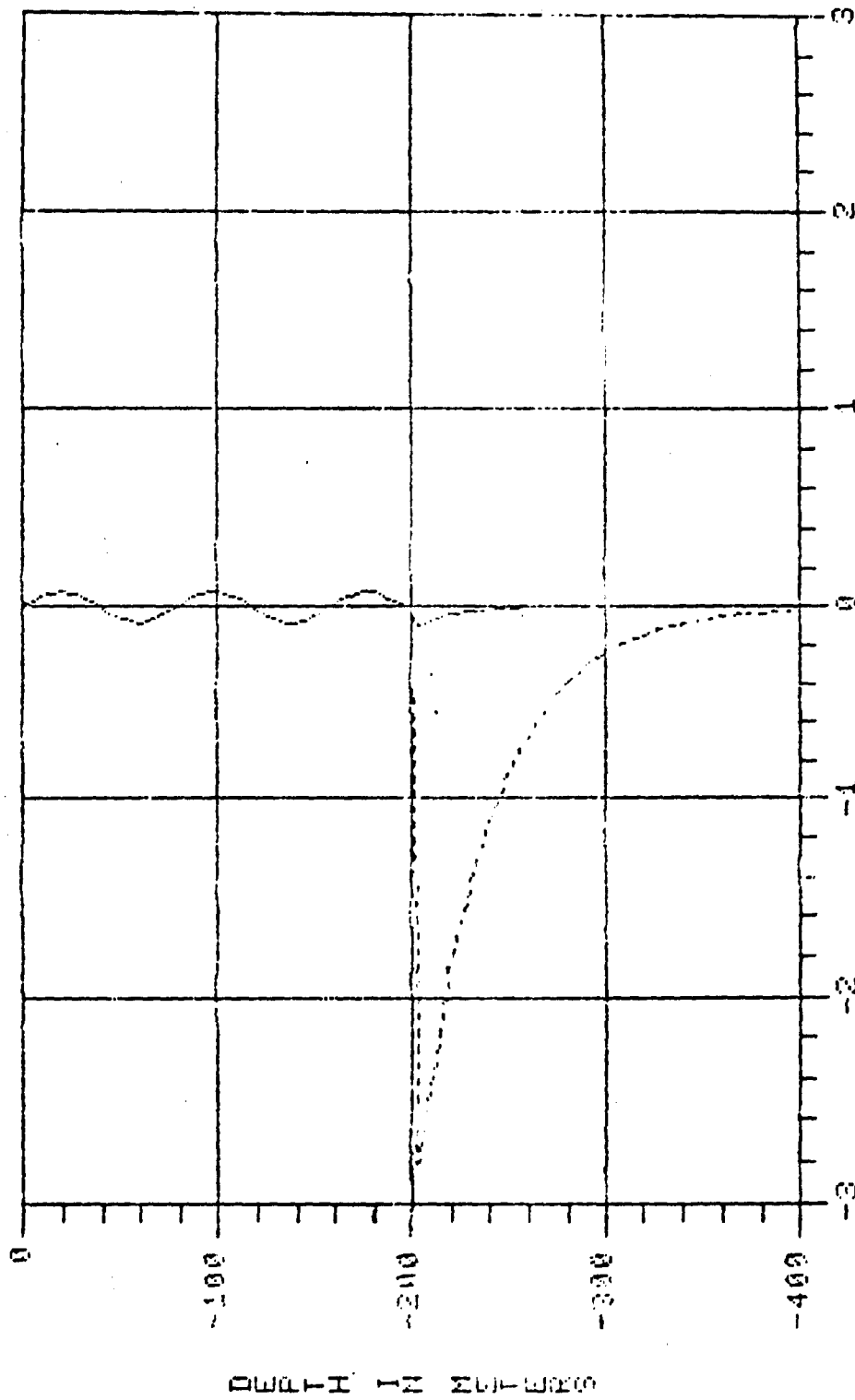
FIGURE 19. THE REAL PART OF THE FUNDAMENTAL MODE FOR A 25 HZ SOURCE IN A WATER COLUMN 200 METERS DEEP OVER A SEMI-INFINITE CLAY-SILT BASEMENT (THE SOLID CURVE IS THE COMPRESSIONAL EIGENFUNCTION AND THE DASHED CURVE IS THE SHEAR EIGENFUNCTION)

FIGURE 20. THE IMAGINARY PART OF THE FUNDAMENTAL MODE FOR A 25 HZ SOURCE IN A
WATER COLUMN 200 METERS DEEP OVER A SEMI-INFINITE CLAY-SILT
BASEMENT (THE SOLID CURVE IS THE COMPRESSIONAL EIGENFUNCTION AND
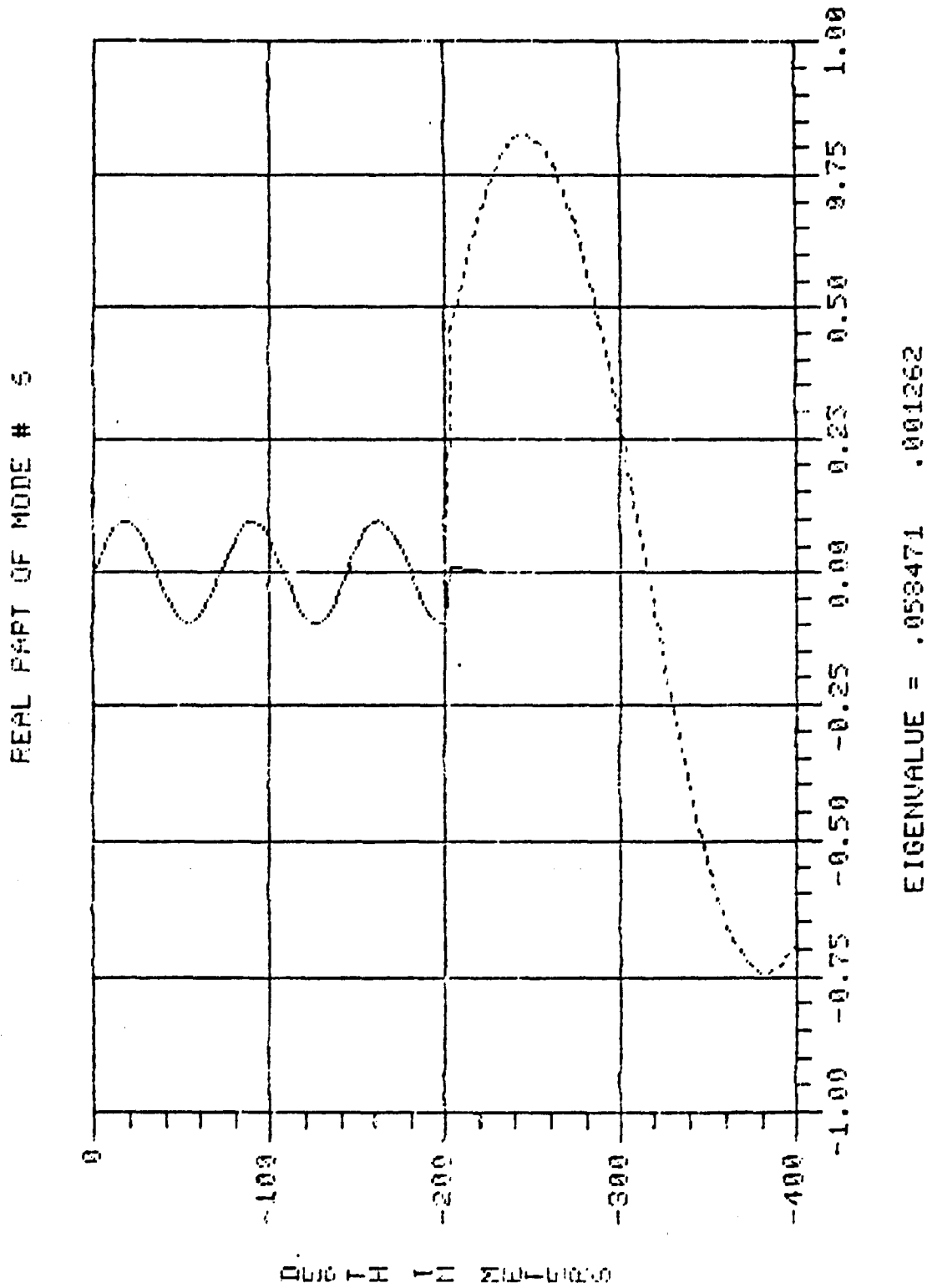THE DASHED CURVE IS THE SHEAR EIGENFUNCTION)
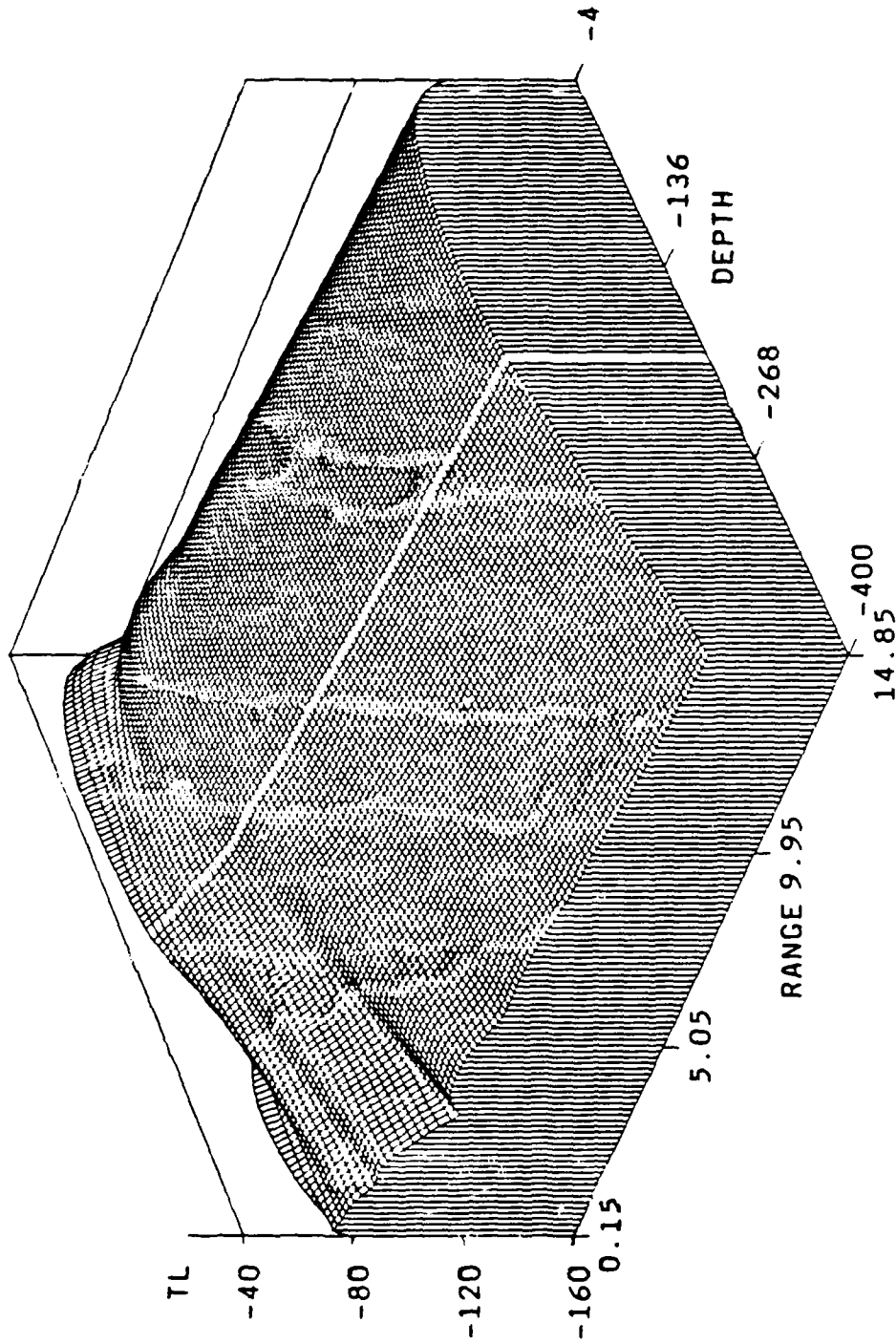
FIGURE 21. A THREE-DIMENSIONAL PLOT OF THE COHERENT TRANSMISSION LOSS (DB) AS A FUNCTION OF RANGE (KM) AND DEPTH (M) FOR A 25 HZ SOURCE AT 112 M DEPTH IN A 200 M WATER COLUMN OVER A SEMI-INFINITE CLAY-SILT BASEMENT (ALL SEVEN MODES WERE USED)

FIGURE 22. A CONTOUR PLOT OF THE COHERENT TRANSMISSION LOSS (DB) AS A FUNCTION OF RANGE (KM) AND DEPTH (M) FOR A 25 HZ SOURCE AT 112 M DEPTH IN A 200 M WATER COLUMN OVER A SEMI-INFINITE CLAY-SILT BASEMENT (ALL SEVEN MODES WERE USED)
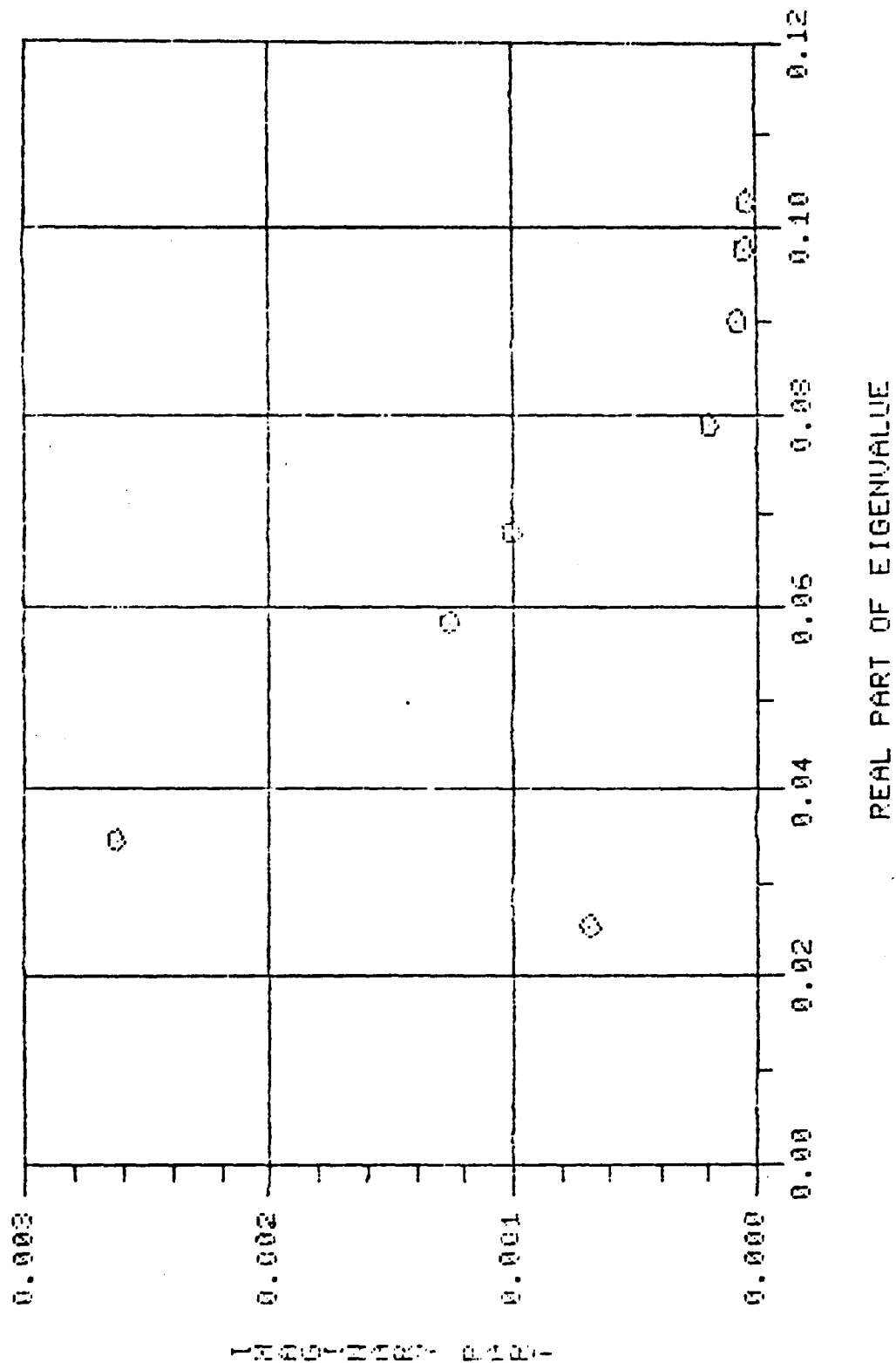
FIGURE 23. LOCATION OF THE COMPLEX EIGENVALUES FOR A 25 HZ SOURCE IN A WATER COLUMN 200 METERS DEEP OVER A SEMI-INFINITE BASALT BASEMENT

FIGURE 24. THE REAL PART OF THE FUNDAMENTAL MODE FOR A 25 HZ SOURCE IN A
WATER COLUMN 200 METERS DEEP OVER A SEMI-INFINITE BASALT BASEMENT
(THE SOLID CURVE IS THE COMPRESSIONAL EIGENFUNCTION AND THE DASHED
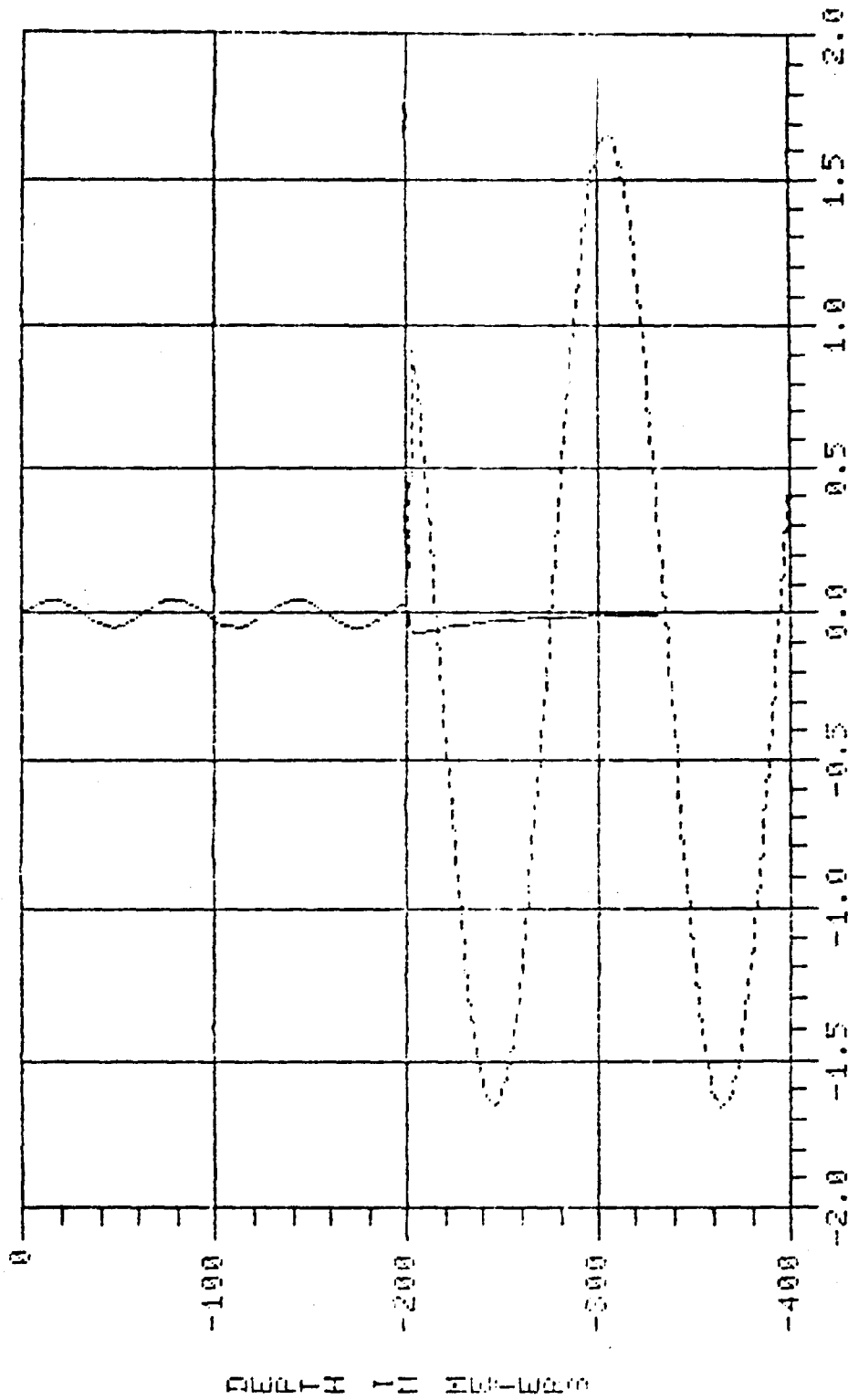CURVE IS THE SHEAR EIGENFUNCTION)
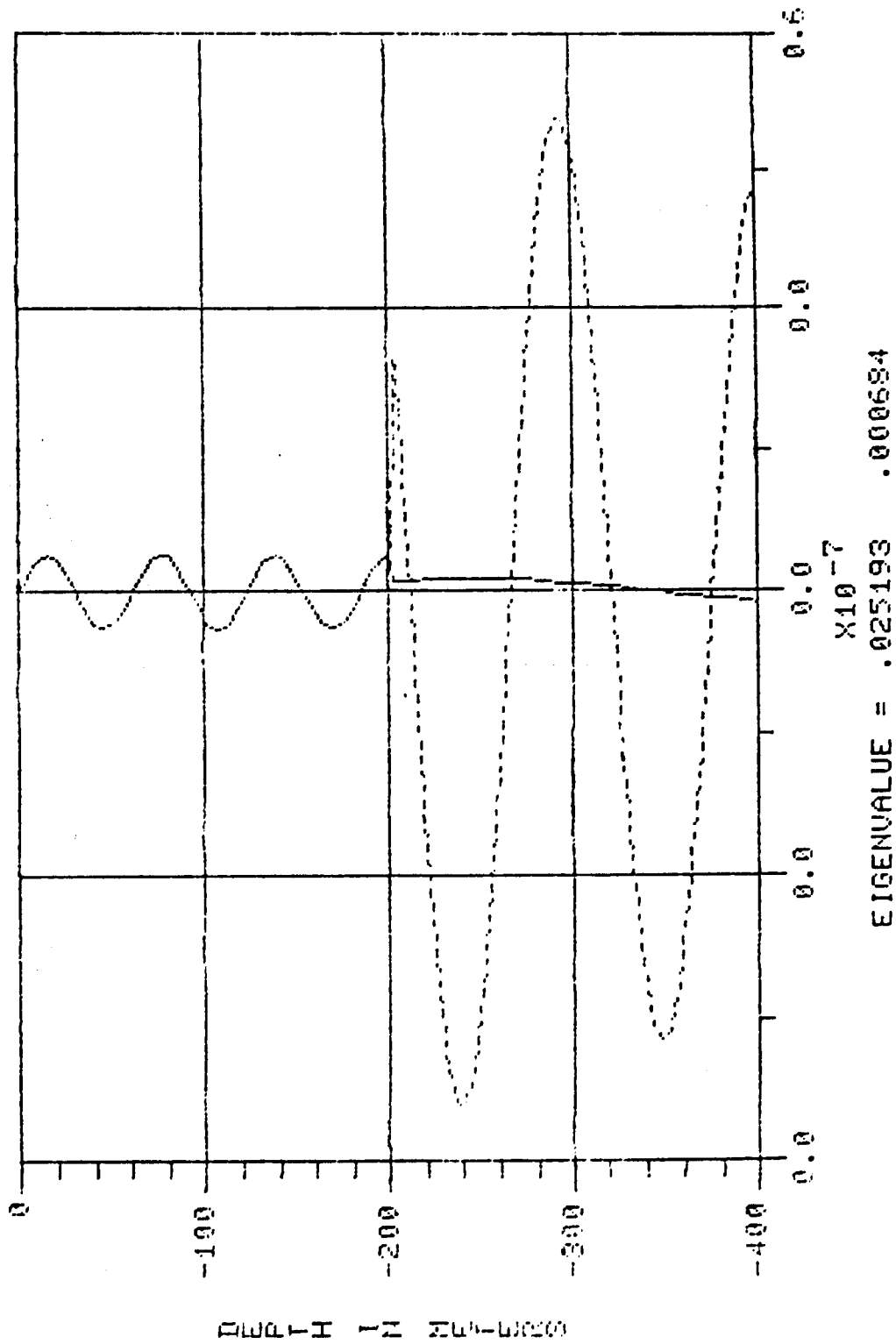
REAL PART OF MODE # 5

EIGENVALUE = .067887   .001003

FIGURE 25.   THE REAL PART OF THE FIFTH MODE FOR A 25 HZ SOURCE IN A WATER COLUMN 200 METERS DEEP OVER A SEMI-INFINITE BASALT BASEMENT (THE SOLID CURVE IS THE COMPRESSIONAL EIGENFUNCTION AND THE DASHED CURVE IS THE SHEAR EIGENFUNCTION)

FIGURE 26. THE REAL PART OF THE SIXTH MODE FOR A 25 HZ SOURCE IN A WATER COLUMN 200 METERS DEEP OVER A SEMI-INFINITE BASALT BASEMENT (THE SOLID CURVE IS THE COMPRESSIONAL EIGENFUNCTION AND THE DASHED CURVE IS THE SHEAR EIGENFUNCTION)

FIGURE 27. THE REAL PART OF THE SEVENTH MODE FOR A 25 HZ SOURCE IN A WATER COLUMN 200 METERS DEEP OVER A SEMI-INFINITE BASALT BASEMENT (THE SOLID CURVE IS THE COMPRESSIONAL EIGENFUNCTION AND THE DASHED CURVE IS THE SHEAR EIGENFUNCTION)

122

FIGURE 28. THE REAL PART OF THE LAST MODE FOR A 25 HZ SOURCE IN A WATER COLUMN 200 METERS DEEP OVER A SEMI-INFINITE BASALT BASEMENT (THE SOLID CURVE IS THE COMPRESSIONAL EIGENFUNCTION AND THE DASHED CURVE IS THE SHEAR EIGENFUNCTION)
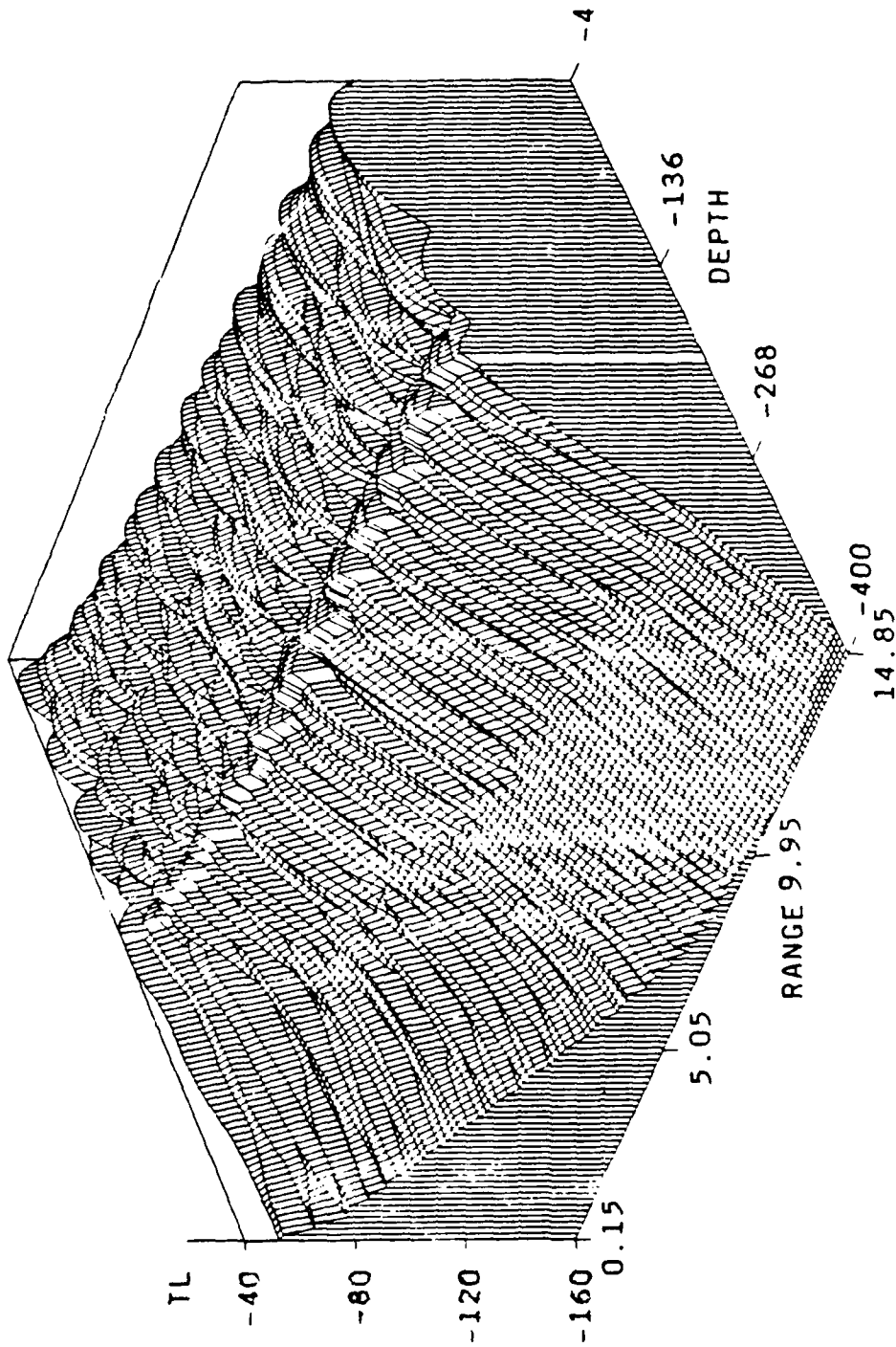
FIGURE 29. A THREE-DIMENSIONAL PLOT OF THE COHERENT TRANSMISSION LOSS (DB) AS A FUNCTION OF RANGE (KM) AND DEPTH (M) FOR A 25 HZ SOURCE AT 112 M DEPTH IN A 200 M WATER COLUMN OVER A SEMI-INFINITE BASALT BASEMENT (ALL EIGHT MODES WERE USED)
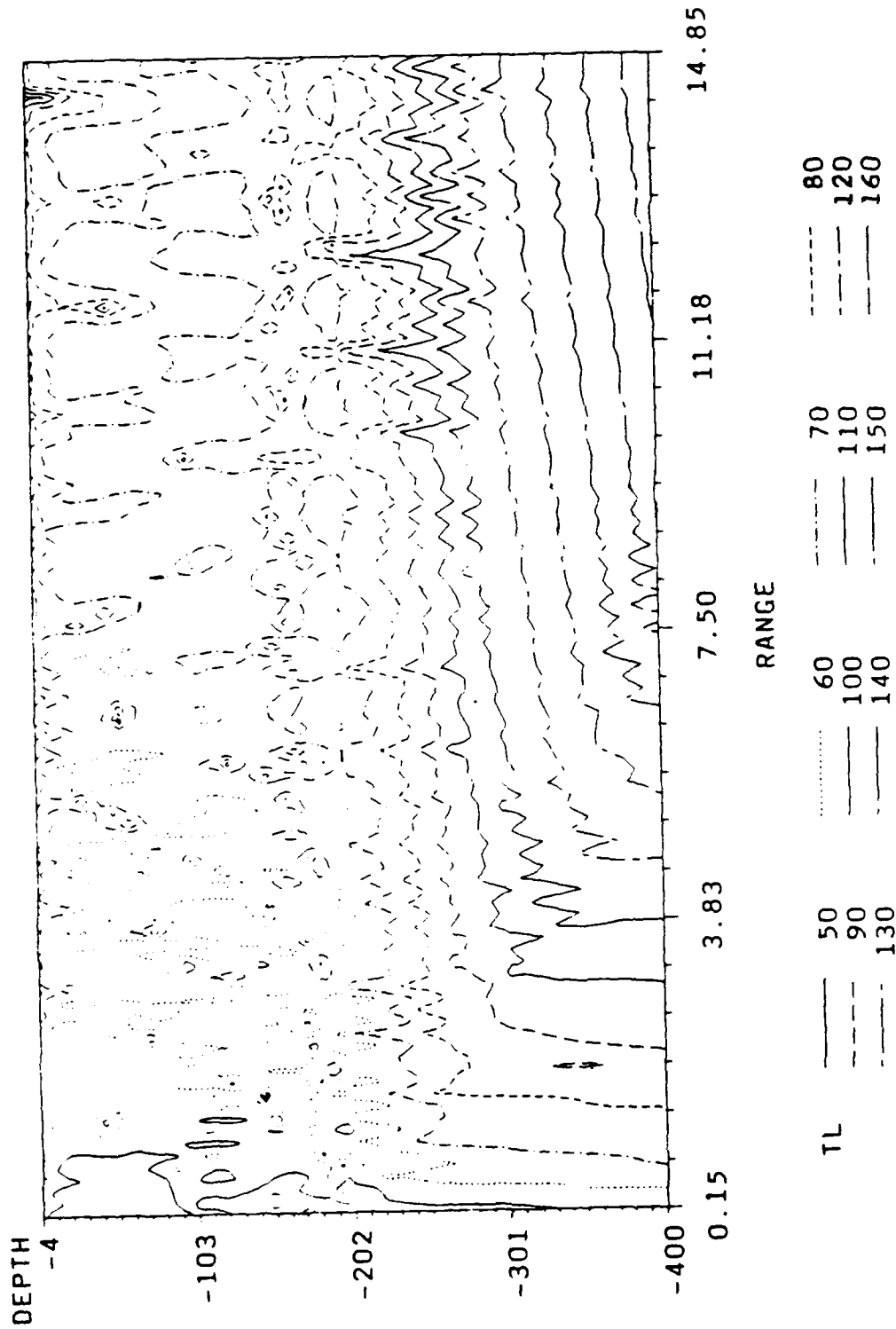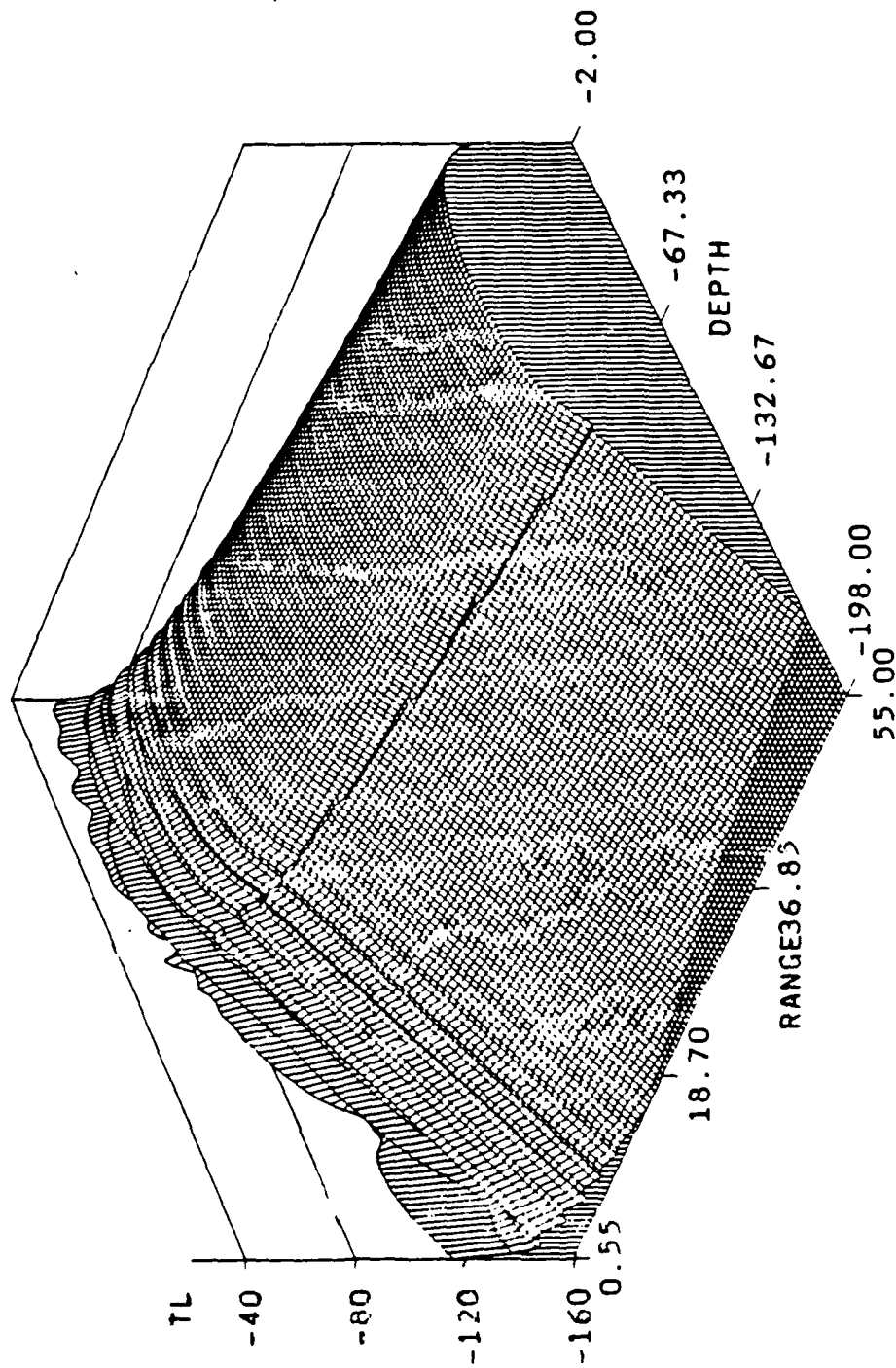
FIGURE 30. A CONTOUR PLOT OF THE COHERENT TRANSMISSION LOSS (DB) AS A
FUNCTION OF RANGE (KM) AND DEPTH (M) FOR A 25 HZ SOURCE AT 112 M
DEPTH IN A 200 M WATER COLUMN OVER A SEMI-INFINITE BASALT BASEMENT
(ALL EIGHT MODES WERE USED)

FIGURE 31. A THREE-DIMENSIONAL PLOT OF THE COHERENT TRANSMISSION LOSS (DB) AS A FUNCTION OF RANGE (KM) AND DEPTH (M) FOR A 128 HZ SOURCE AT 38 M DEPTH IN A SLIGHTLY RANGE-DEPENDENT (DOWN-SLOPE) WATER COLUMN OVER A SEMI-INFINITE CHALK BASEMENT (TEN MODES WERE USED)
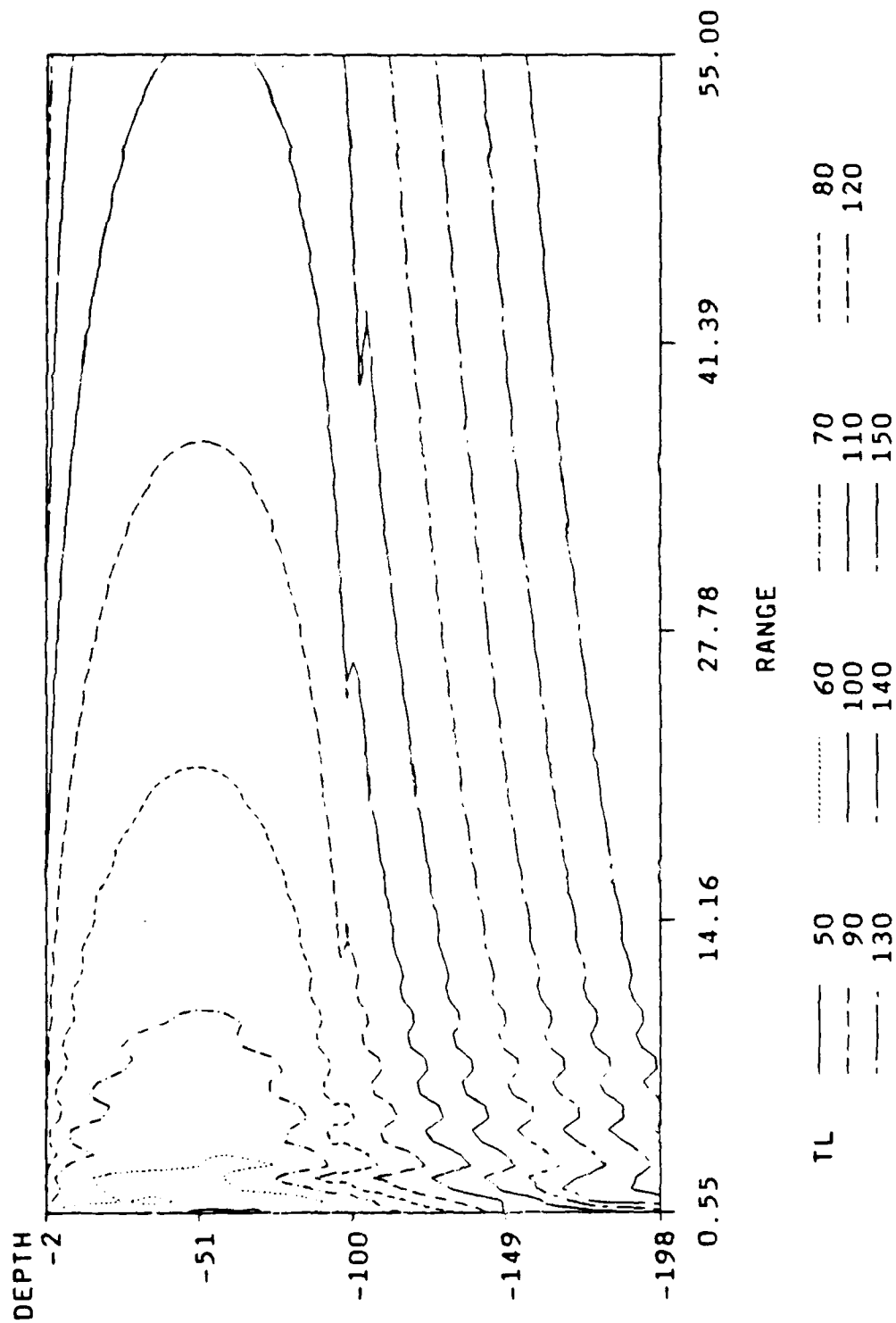
FIGURE 32. A CONTOUR PLOT OF THE COHERENT TRANSMISSION LOSS (DB) AS A FUNCTION OF RANGE (KM) AND DEPTH (M) FOR A 128 HZ SOURCE AT 38 M DEPTH IN A SLIGHTLY RANGE-DEPENDENT (DOWN-SLOPE) WATER COLUMN OVER A SEMI-INFINITE CHALK BASEMENT (TEN MODES WERE USED)
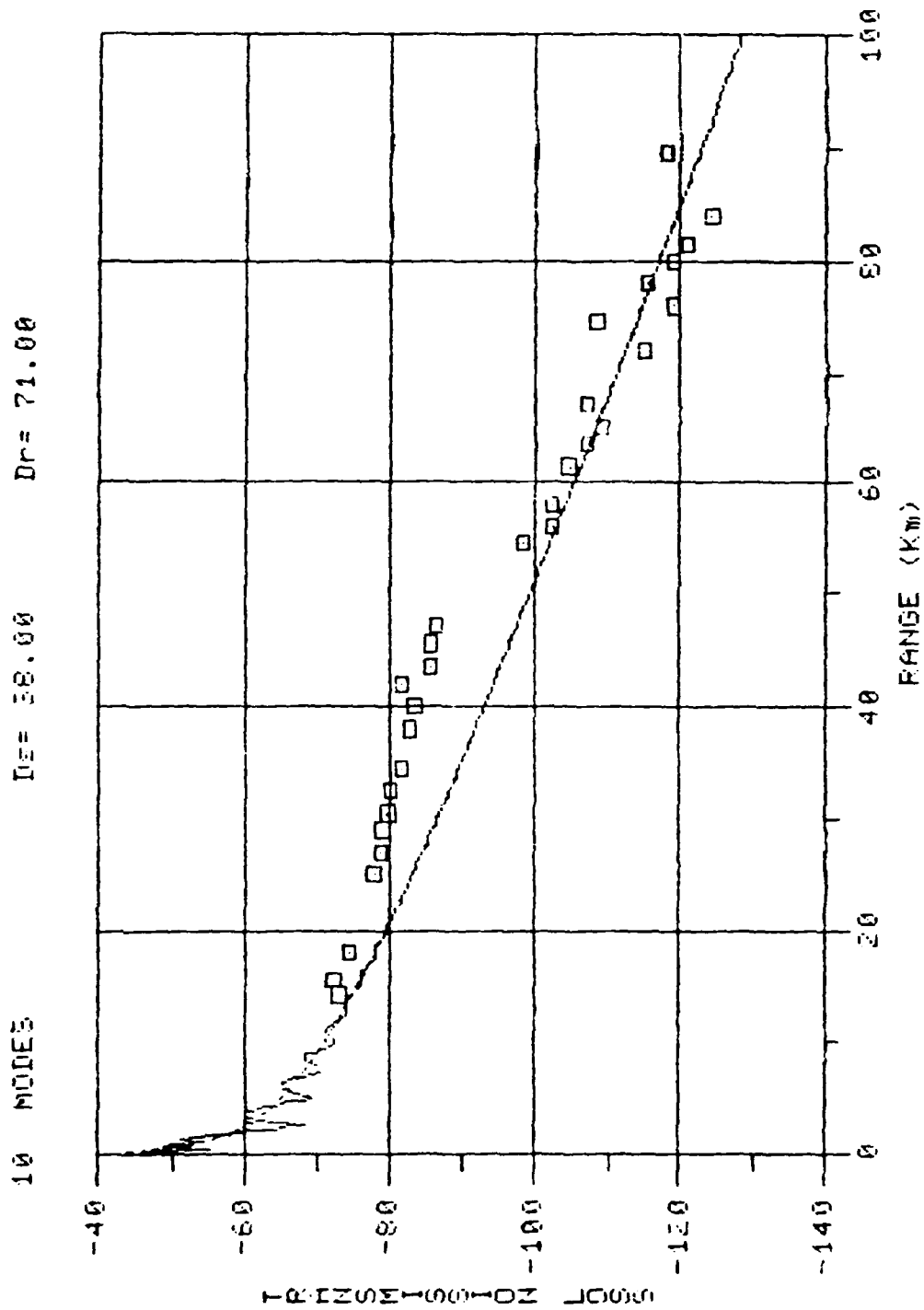
FIGURE 33. COMPARISON WITH EXPERIMENTAL MEASUREMENTS FOR A 128 HZ SOURCE IN A SLIGHTLY RANGE-DEPENDENT (DOWN-SLOPE) WATER COLUMN OVER A SEMI-INFINITE CHALK BASEMENT
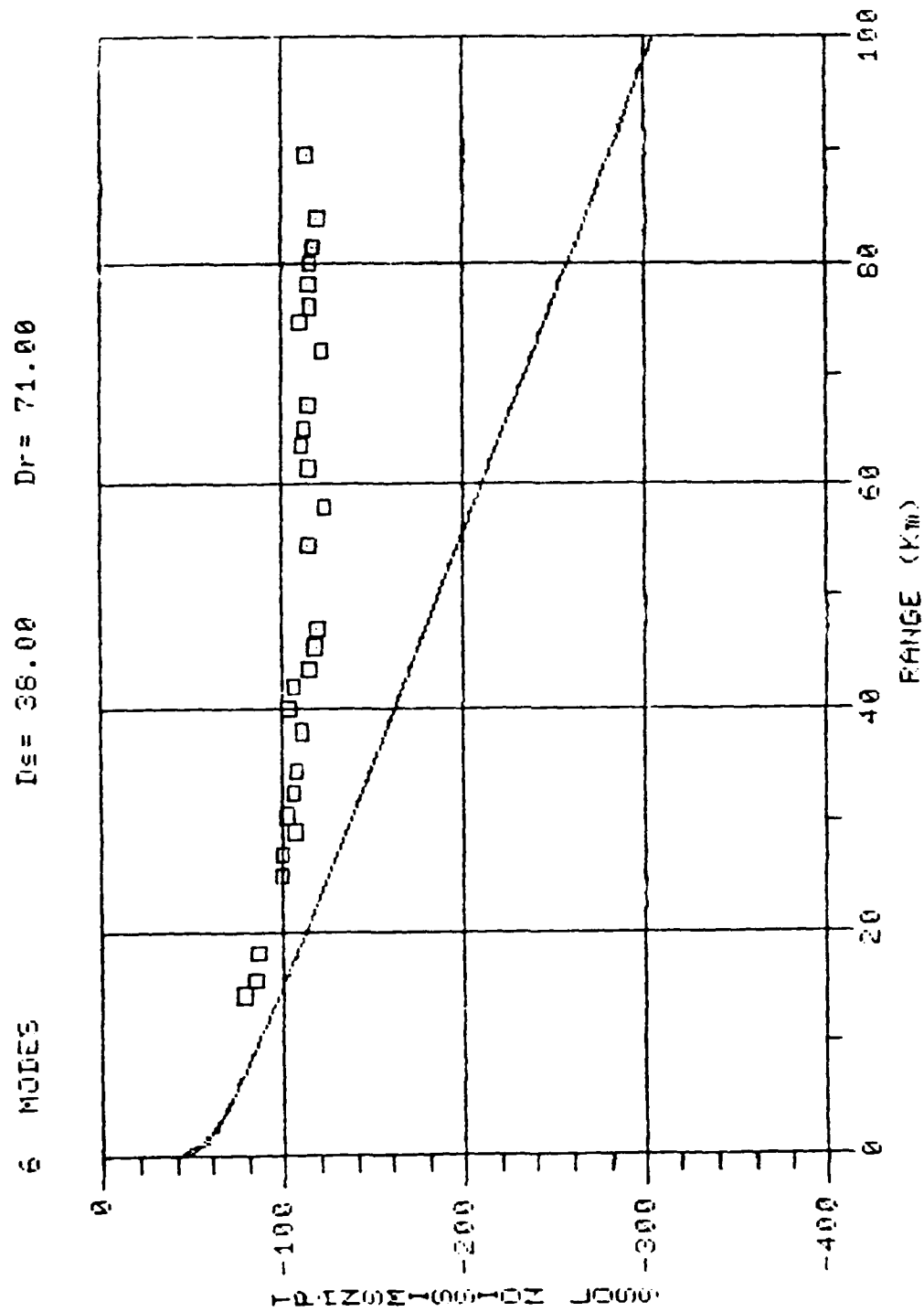
FIGURE 34.   COMPARISON WITH EXPERIMENTAL MEASUREMENTS FOR A 64 HZ SOURCE IN A
SLIGHTLY RANGE-DEPENDENT (DOWN-SLOPE) WATER COLUMN OVER A
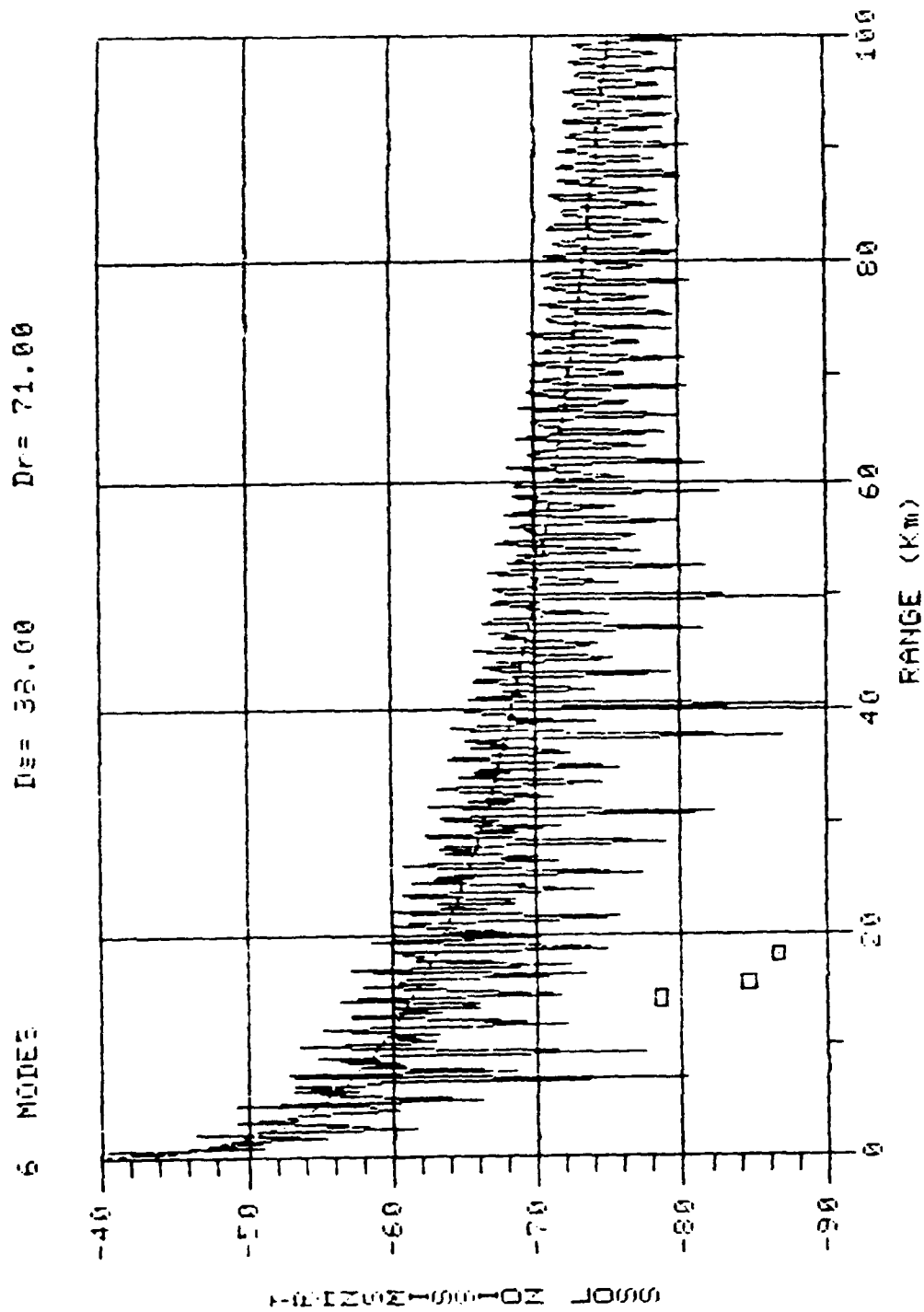SEMI-INFINITE CHALK BASEMENT

FIGURE 35. COMPARISON WITH EXPERIMENTAL MEASUREMENTS FOR A 64 HZ SOURCE IN A SLIGHTLY RANGE-DEPENDENT (DOWN-SLOPE) WATER COLUMN OVER A SEMI-INFINITE "CHALK" BASEMENT WITH A NEGLIGIBLE SHEAR SPEED (THE SOLID CURVE IS THE COHERENT TRANSMISSION LOSS AND THE DASHED CURVE IS THE INCOHERENT TRANSMISSION LOSS)
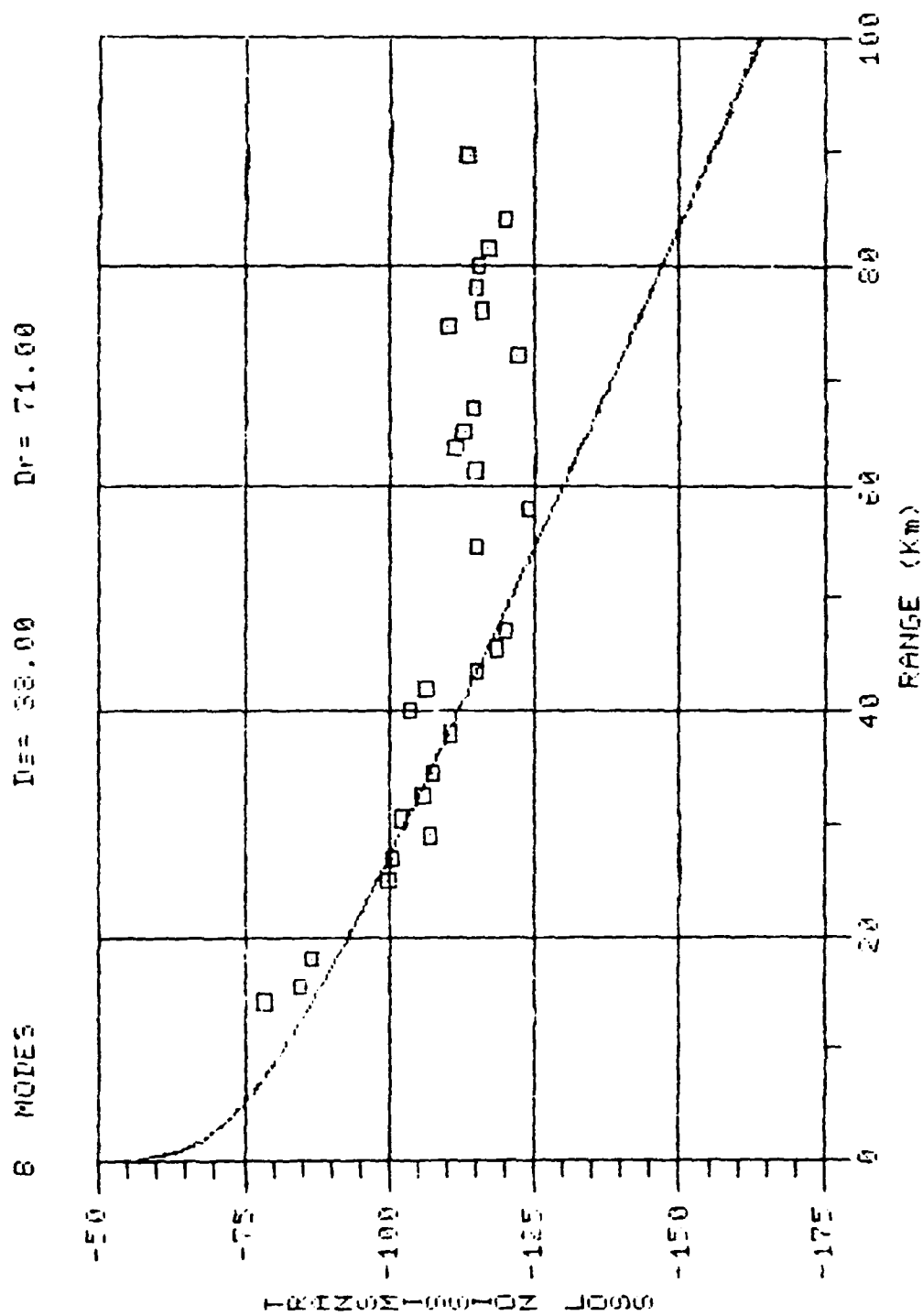
FIGURE 36. COMPARISON WITH EXPERIMENTAL MEASUREMENTS FOR A 64 HZ SOURCE IN A SLIGHTLY RANGE-DEPENDENT (DOWN-SLOPE) WATER COLUMN OVER A CHALK SEDIMENT AND A SEMI-INFINITE BASALT BASEMENT (THE CHALK-BASALT INTERFACE IS LOCATED 240 M DEEP TO OBTAIN THE BEST FIT)
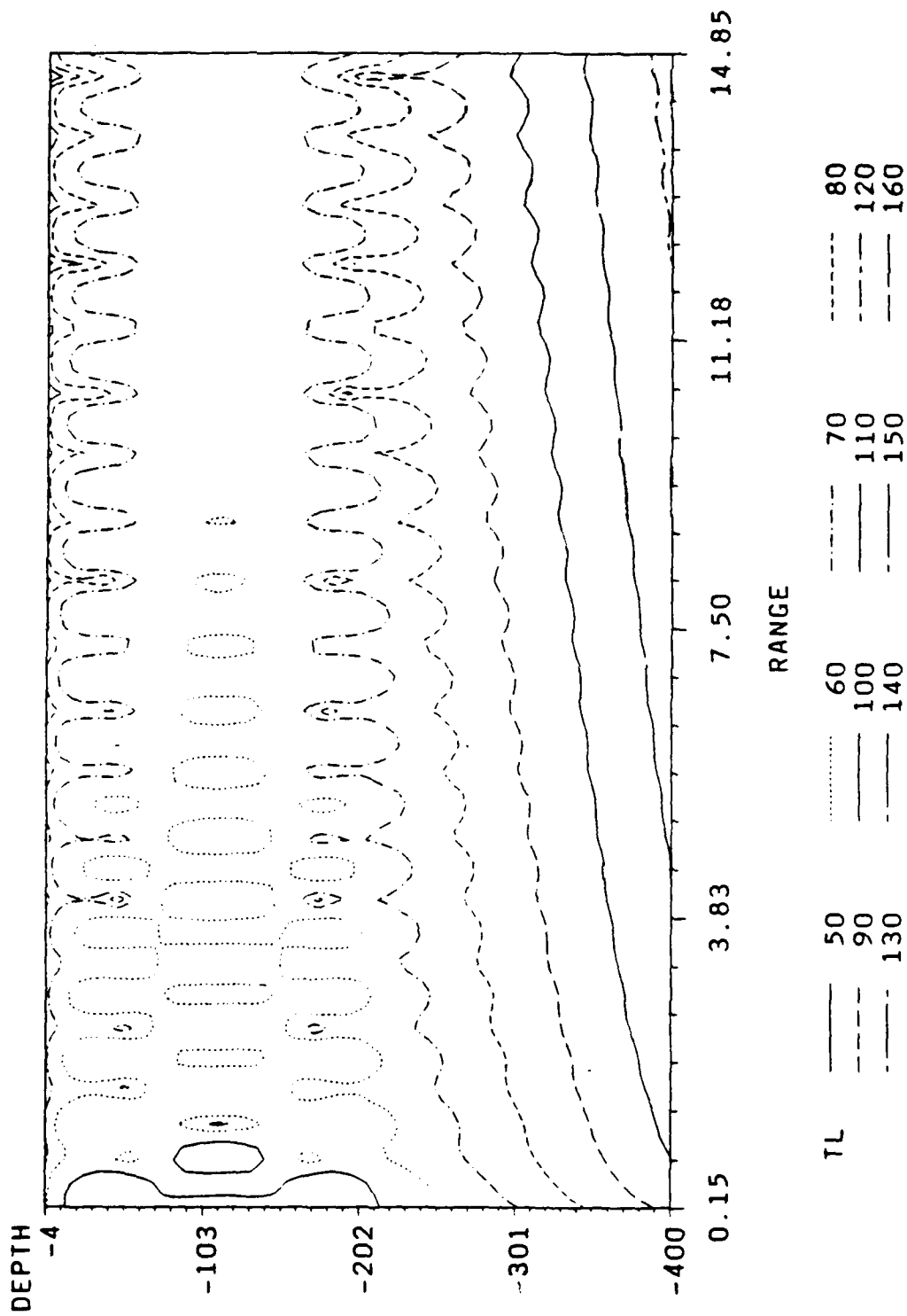
FIGURE 37. A CONTOUR PLOT OF THE COHERENT TRANSMISSION LOSS (DB) AS A FUNCTION OF RANGE (KM) AND DEPTH (M) FOR A 25 HZ SOURCE AT 112 M DEPTH IN A 200 M WATER COLUMN OVER A SEMI-INFINITE FLUID-LIKE BASEMENT (ALL SEVEN MODES WERE USED)

FIGURE 38.   A THREE-DIMENSIONAL PLOT OF THE COHERENT TRANSMISSION LOSS (DB) AS A FUNCTION OF RANGE (KM) AND DEPTH (M) FOR A 25 HZ SOURCE AT 112 M DEPTH IN A 200 M WATER COLUMN OVER A SEMI-INFINITE FLUID-LIKE BASEMENT (ALL SEVEN MODES WERE USED)
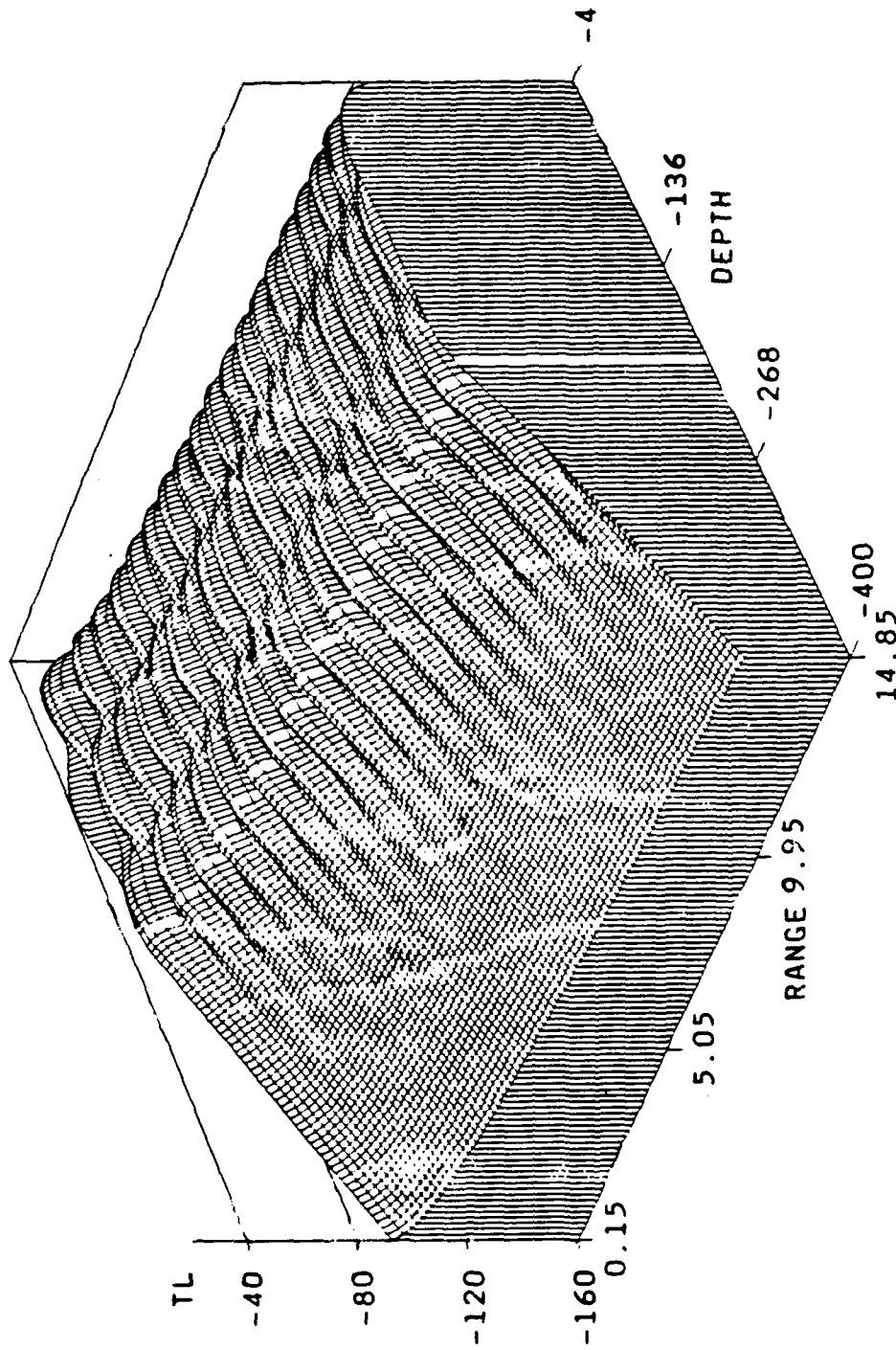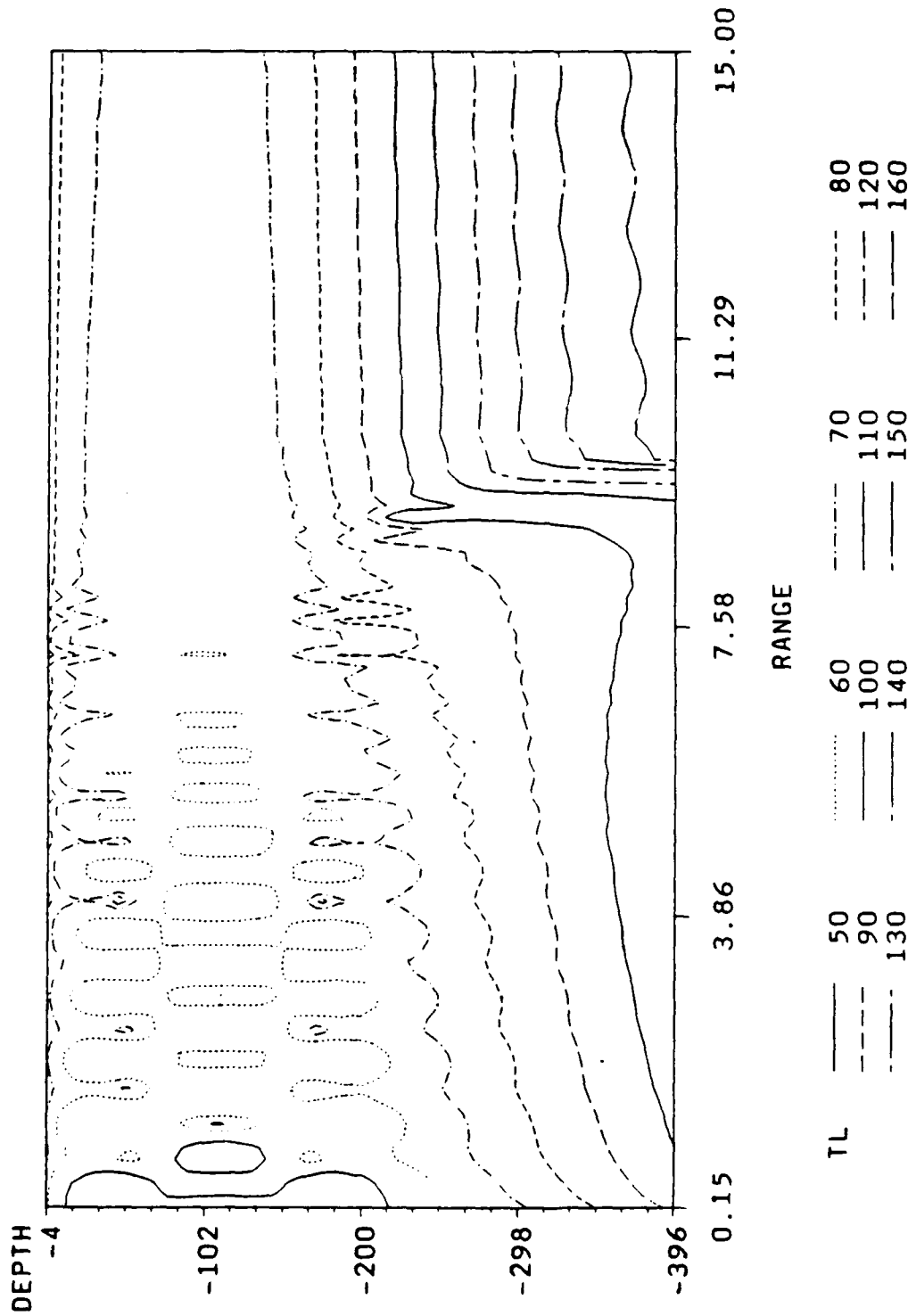
FIGURE 39.   A CONTOUR PLOT OF THE COHERENT TRANSMISSION LOSS (DB) AS A
FUNCTION OF RANGE (KM) AND DEPTH (M) FOR A 25 HZ SOURCE AT 112 M
DEPTH IN AN UP-SLOPE WATER COLUMN WITH A 0.57 DEGREE SLOPE OVER A
SEMI-INFINITE FLUID-LIKE BASEMENT (THE FIRST THREE MODES WERE USED
AND THE WAVE GUIDE WAS DIVIDED INTO 50 SEGMENTS)

FIGURE 40. A THREE-DIMENSIONAL PLOT OF THE COHERENT TRANSMISSION LOSS (DB) AS A FUNCTION OF RANGE (KM) AND DEPTH (M) FOR A 25 HZ SOURCE AT 112 M DEPTH IN AN UP-SLOPE WATER COLUMN WITH A 0.57 DEGREE SLOPE OVER A SEMI-INFINITE FLUID-LIKE BASEMENT (THE FIRST THREE MODES WERE USED AND THE WAVE GUIDE WAS DIVIDED INTO 50 SEGMENTS)
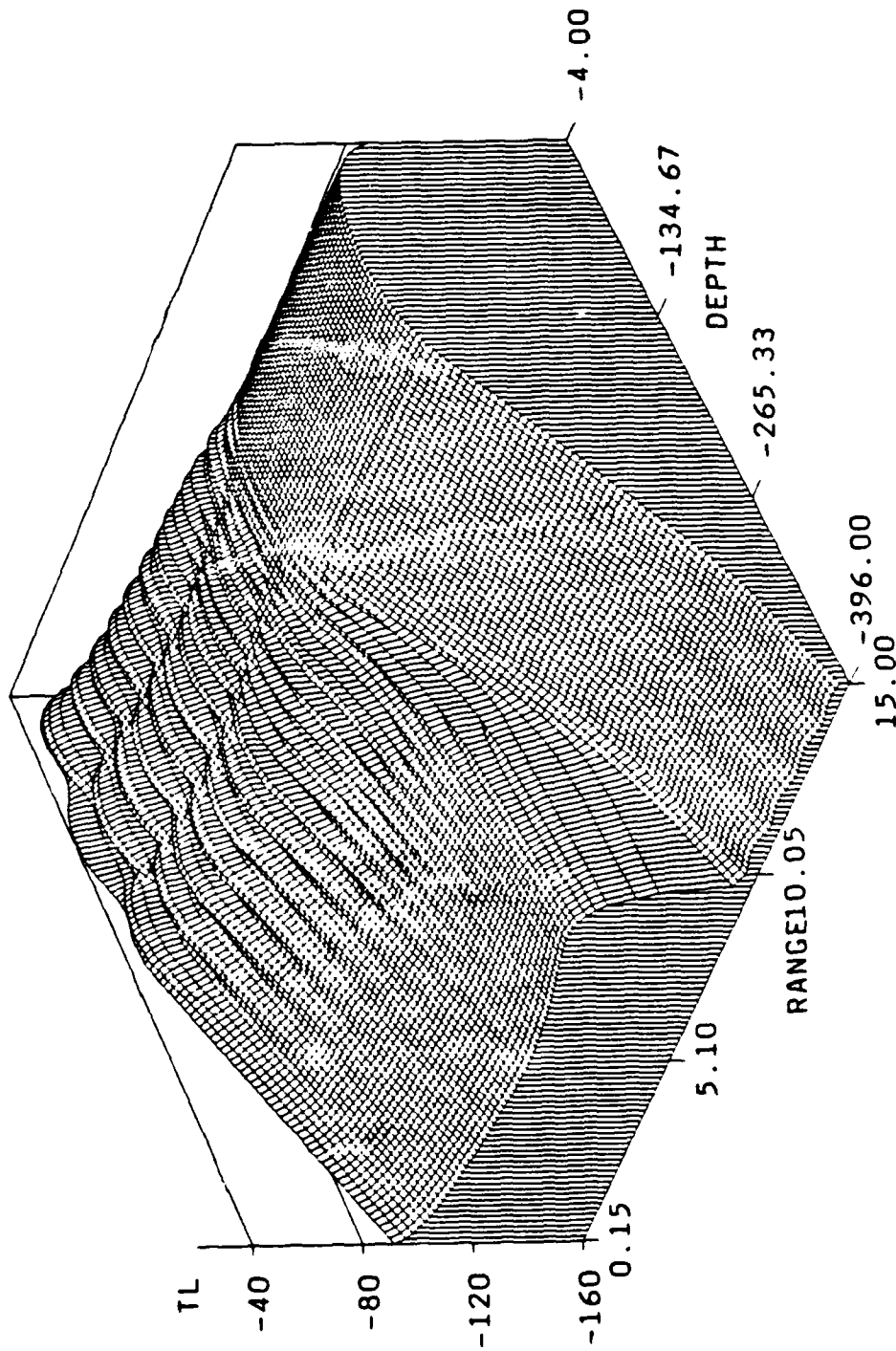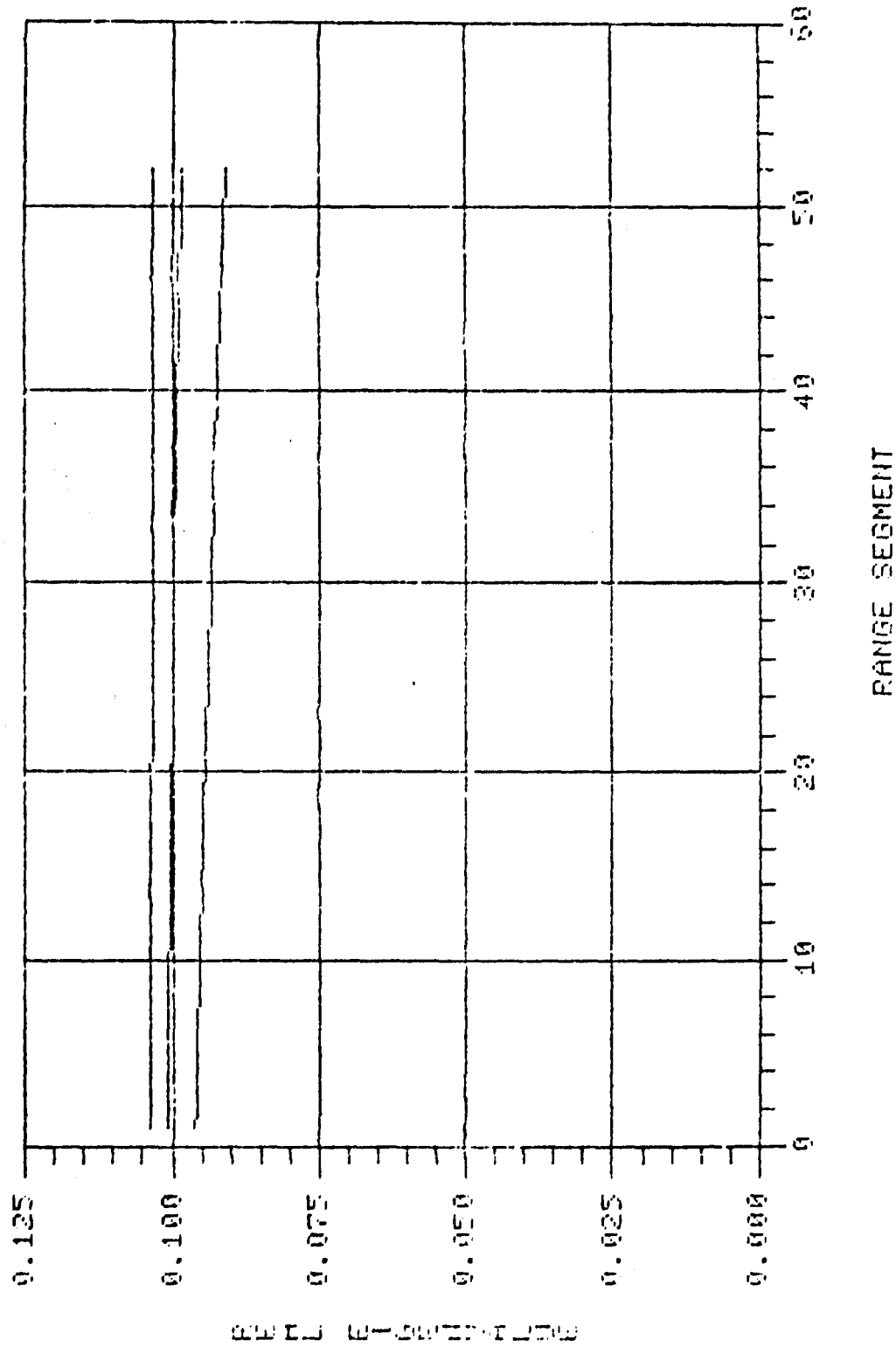
FIGURE 41. THE REAL COMPONENT OF THE FIRST THREE EIGENVALUES AS A FUNCTION OF THE RANGE SEGMENT NUMBER FOR A 25 HZ SOURCE IN AN UP-SLOPE WATER COLUMN WITH A 0.57 DEGREE SLOPE OVER A SEMI-INFINITE FLUID-LIKE BASEMENT
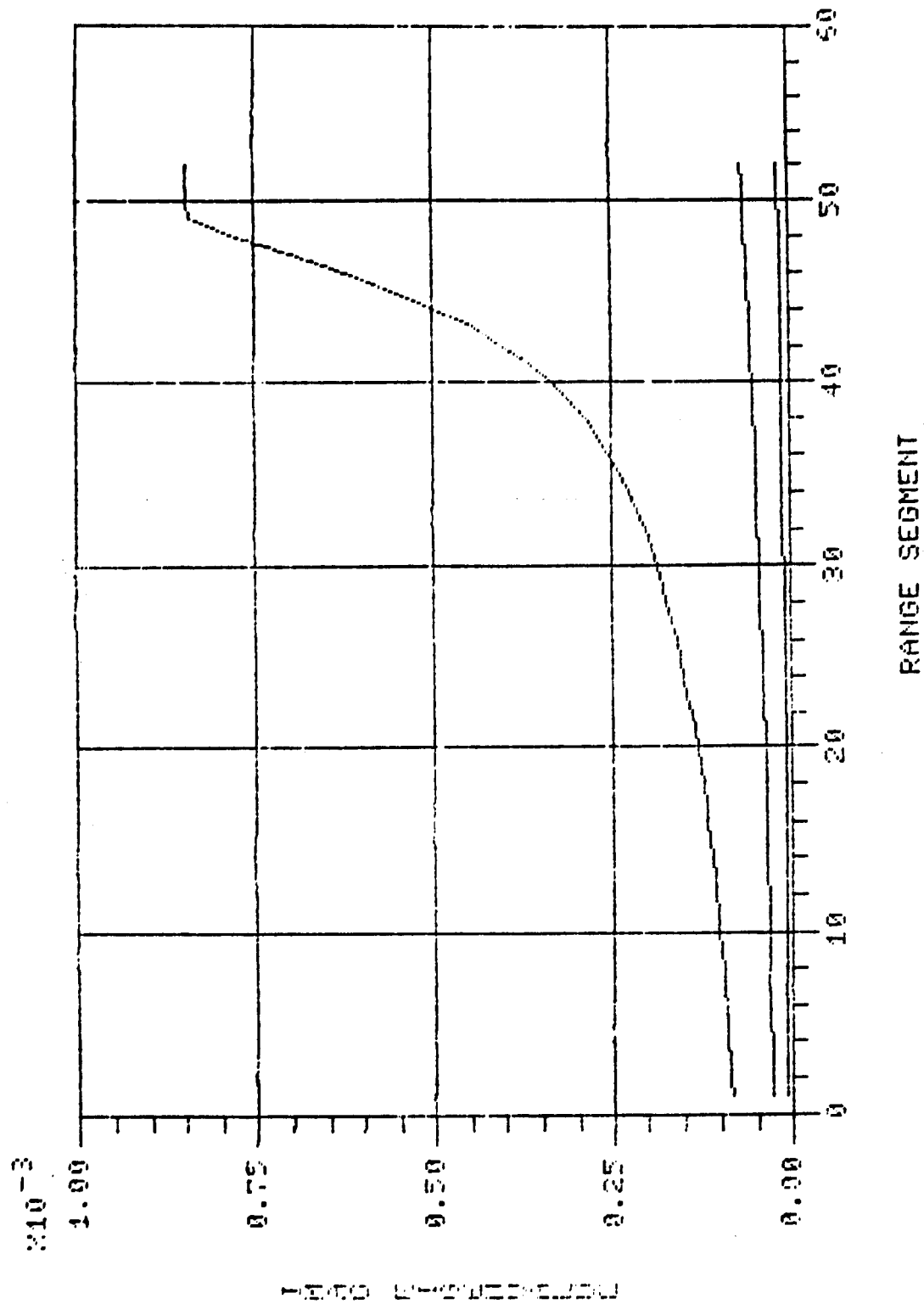
RANGE SEGMENT

FIGURE 42. THE IMAGINARY COMPONENT OF THE FIRST THREE EIGENVALUES AS A FUNCTION OF THE RANGE SEGMENT NUMBER FOR A 25 HZ SOURCE IN AN UP-SLOPE WATER COLUMN WITH A 0.57 DEGREE SLOPE OVER A SEMI-INFINITE FLUID-LIKE BASEMENT
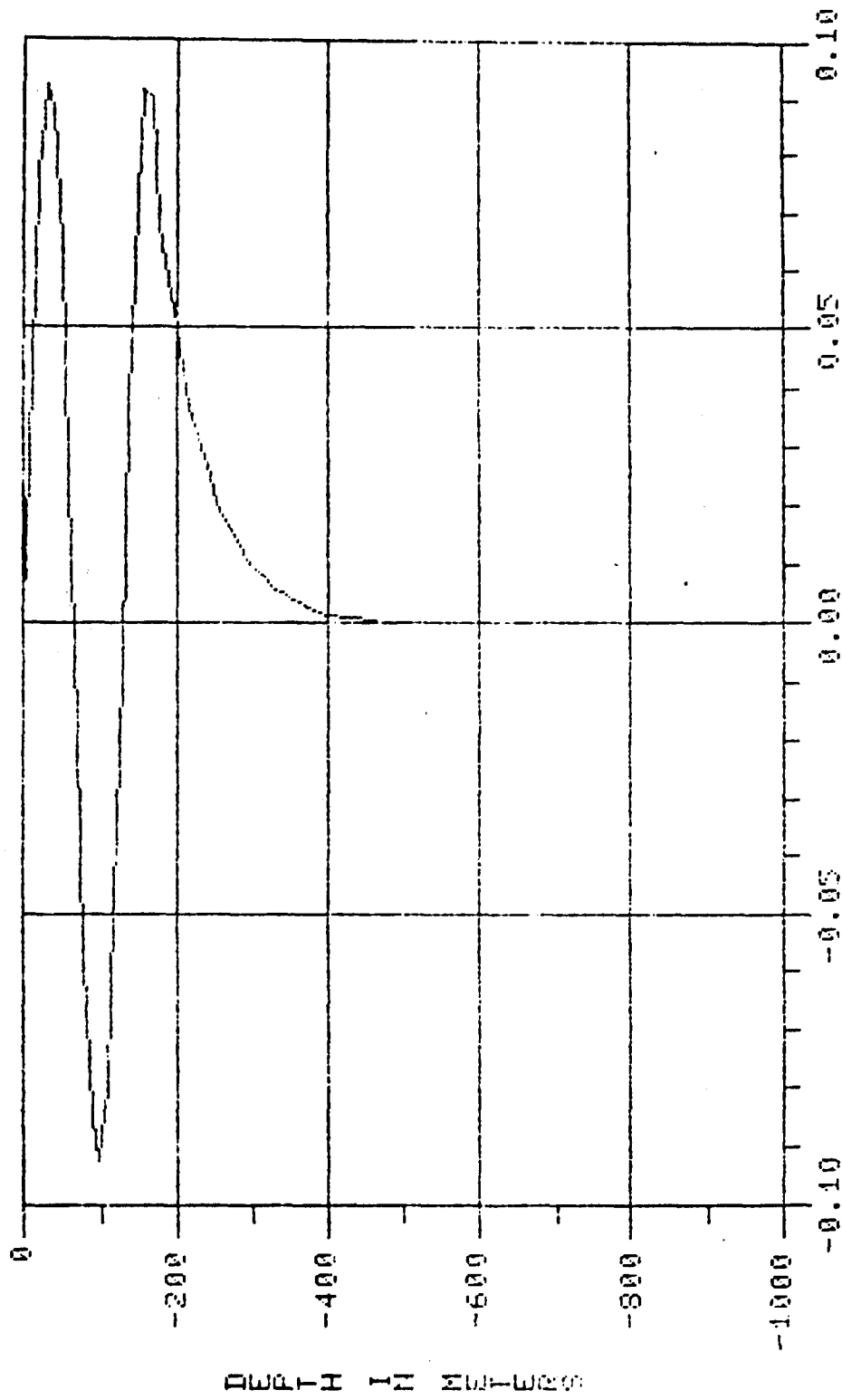
FIGURE 43. THE REAL PART OF THE THIRD DEPTH FUNCTION FOR A 25 HZ SOURCE IN A 170 M WATER COLUMN OVER A FLUID-LIKE SEMI-INFINITE BASEMENT
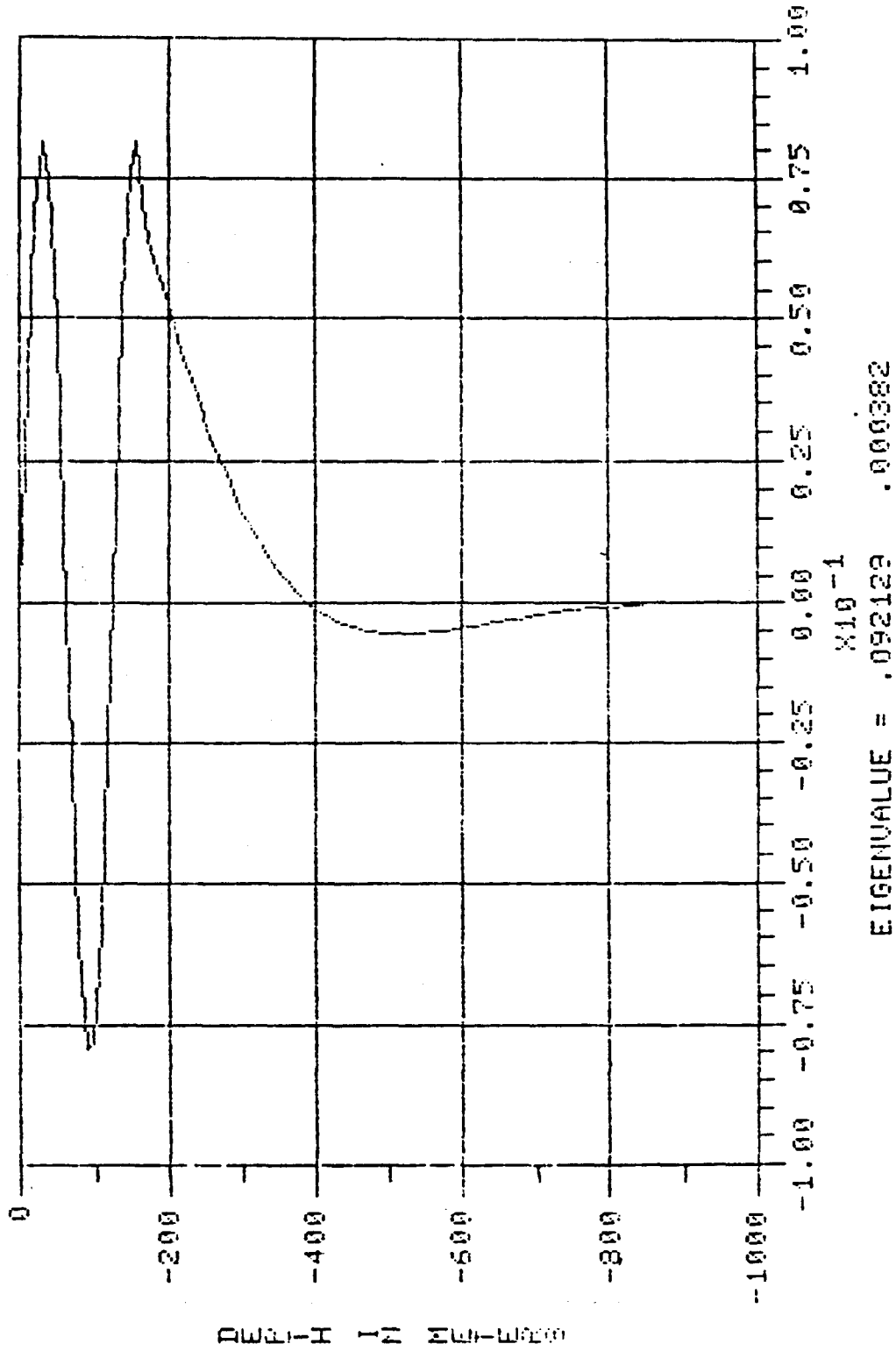
FIGURE 44. THE REAL PART OF THE THIRD DEPTH FUNCTION FOR A 25 HZ SOURCE IN A
160 M WATER COLUMN OVER A FLUID-LIKE SEMI-INFINITE BASEMENT
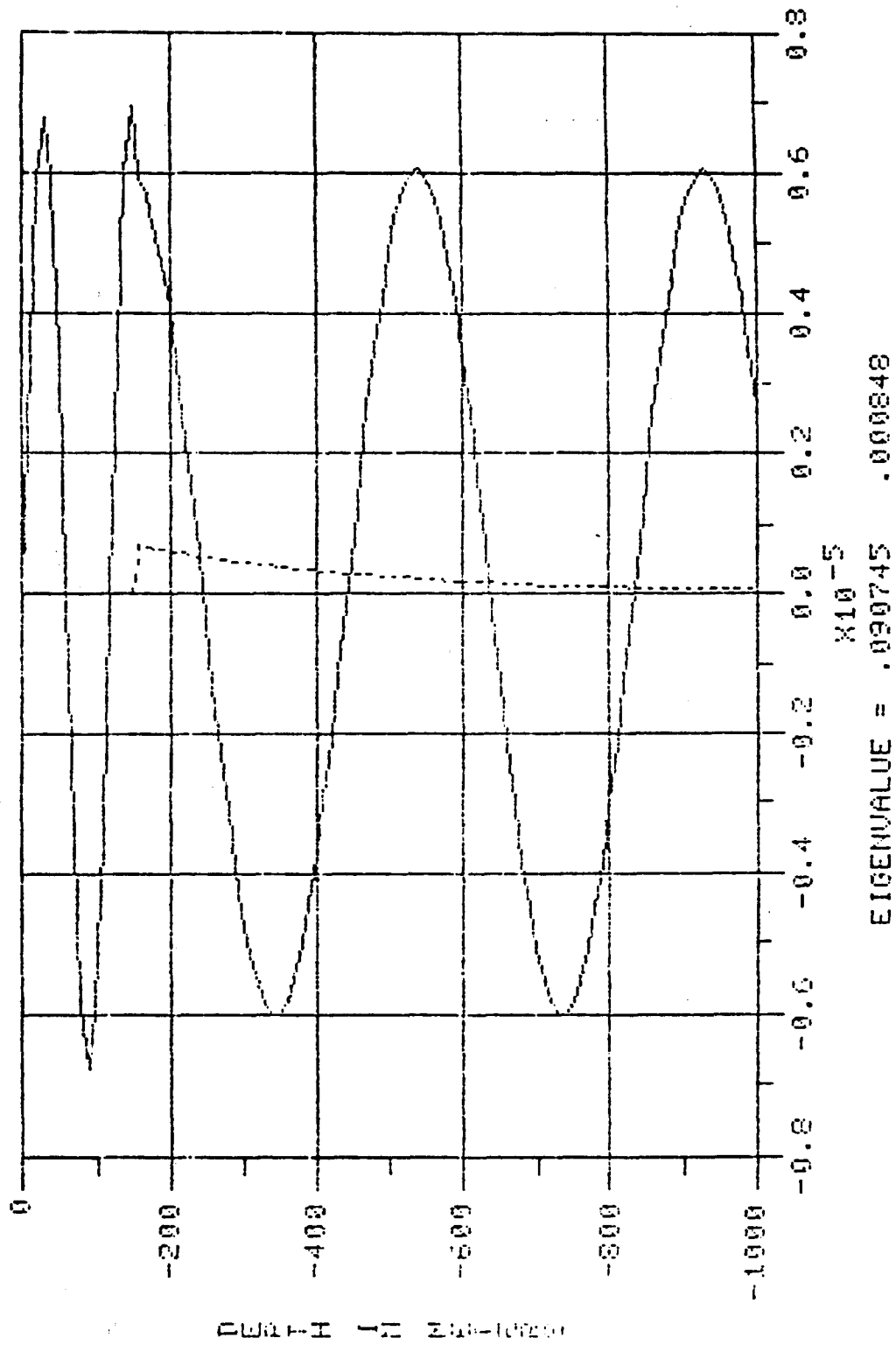
FIGURE 45. THE REAL PART OF THE THIRD DEPTH FUNCTION FOR A 25 HZ SOURCE IN A
150 M WATER COLUMN OVER A FLUID-LIKE SEMI-INFINITE BASEMENT
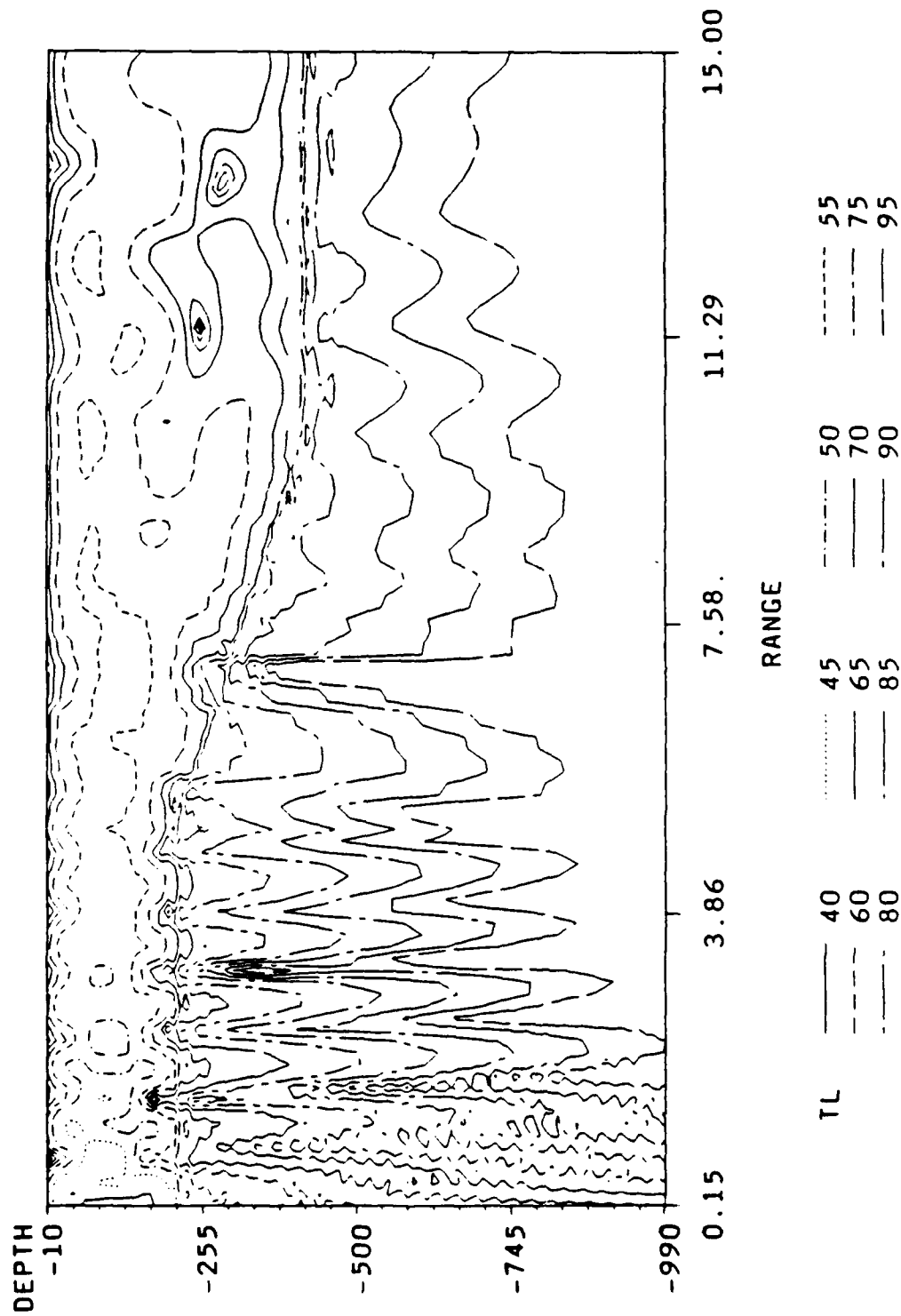
FIGURE 46.   A CONTOUR PLOT OF THE COHERENT TRANSMISSION LOSS (DB) AS A FUNCTION OF RANGE (KM) AND DEPTH (M) FOR A 25 HZ SOURCE AT 112 M DEPTH IN A WATER COLUMN WITH SOUND SPEED GRADIENT OF 0.125 S^{-1} AND A BOTTOM SLOPE OF -2.29 OVER A SEMI-INFINITE SAND BASEMENT (SEVEN MODES WERE USED AND THE WAVE GUIDE WAS DIVIDED INTO 50 SEGMENTS)
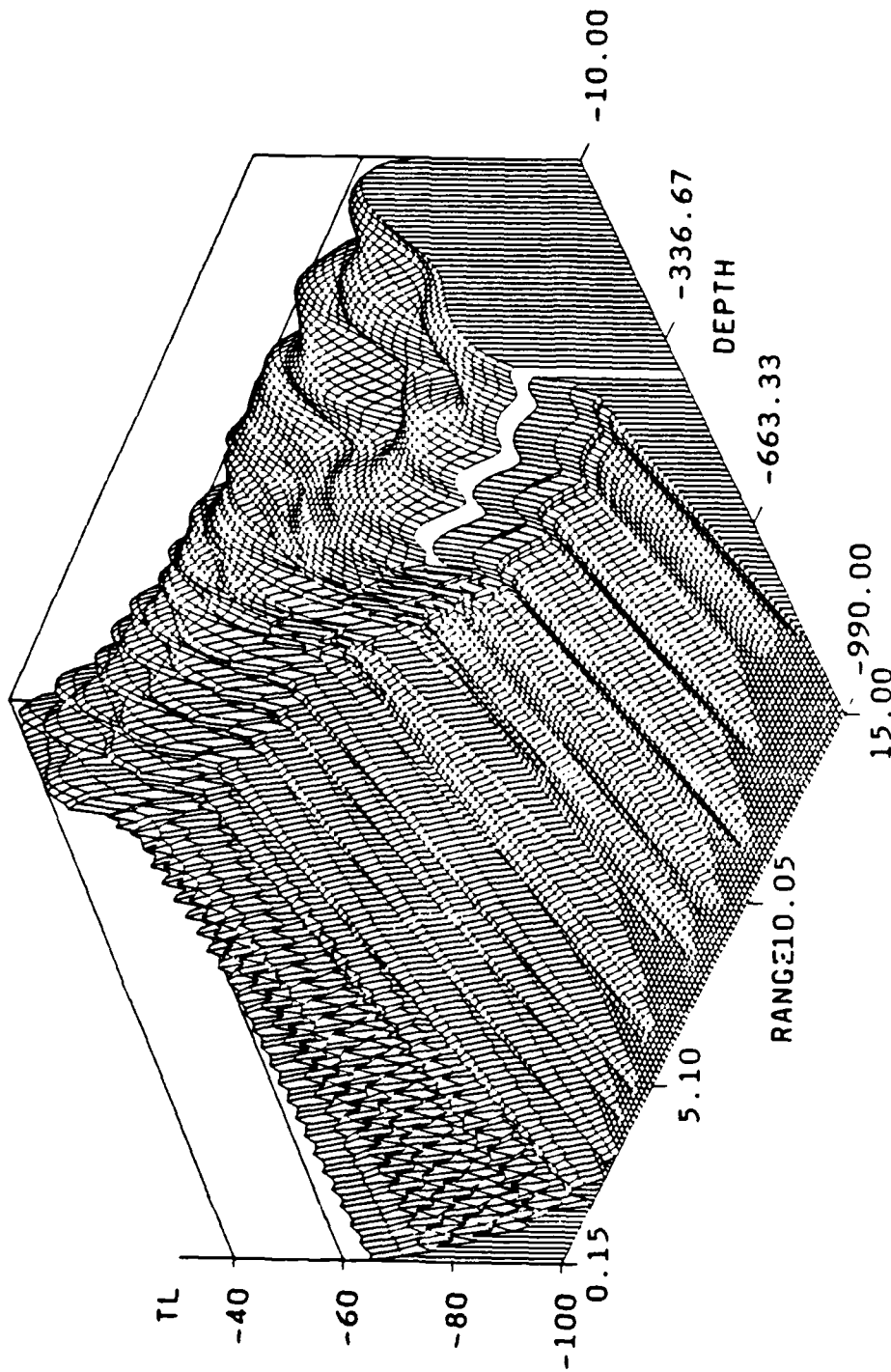
FIGURE 47.   A THREE-DIMENSIONAL PLOT OF THE COHERENT TRANSMISSION LOSS (DB) AS A FUNCTION OF RANGE (KM) AND DEPTH (M) FOR A 25 HZ SOURCE AT 112 M DEPTH IN A WATER COLUMN WITH SOUND SPEED GRADIENT OF 0.125 s^{-1} AND A BOTTOM SLOPE OF -2.29 OVER A SEMI-INFINITE SAND BASEMENT (SEVEN MODES WERE USED AND THE WAVE GUIDE WAS DIVIDED INTO 50 SEGMENTS)

TABLE 1.   GEO-ACOUSTIC PROPERTIES OF THE VARIOUS SEDIMENTS

Bottom Type	Density (gm/cc)	Compressional speed (m/s)	Compressional attenuation (dB/kHz-m)	Shear speed (m/s)	Shear attenuation (dB/kHz-m)
Fluid-like	1.15	1704.5	0.29	1.0	1.00
Clay-Silt	1.60	1515.0	0.50	100.0	1.00
Sand	2.00	1800.0	0.70	600.0	1.50
Basalt	2.60	5250.0	0.20	2500.0	0.50
Chalk	2.20	3200.0	0.10	1000.0	1.00

TABLE 2.   COMPARISON OF THE CALCULATED REAL PART OF THE TRAPPED EIGENVALUES

Mode#	Rigid Model	Soft Model	Perturbation	Exact Model
1	0.1044248	0.1035350	0.1041654	0.1040583
2	0.1020346	0.0998963	0.1012651	0.1014331
3	0.0970778	0.0935177	0.0963706	0.0960692
4	0.0891272	0.0837758		
5	0.0772641	0.0692656		
6	0.0591806	0.0456463		
7	0.0232692			

REFERENCES

1. Jackson, J. D., Classical Electrodynamics, Second Edition, John Wiley & Sons, New York, NY, 1975, pp. 290-292.

2. Urick, R. J., Principles of Underwater Sound for Engineers, Second Edition, McGraw-Hill, New York, NY, 1975.

3. Thompson, W., "Transmission of Elastic Waves Through a Stratified Medium," Journal of Applied Physics, Vol. 21, 1950, pp. 89 93.

4. Achenbach, J. D., Wave Propagation in Elastic Solids, North-Holland, 1973.

5. Folds, D. L. and Loggins, C. D., "Transmission and Reflection of Ultrasonic Waves in Layered Media," Acoustical Society of America Journal, Vol. 62, 1977, pp. 1102-1109.

6. Jackins, P. D. and Gaunaurd, G. C., "Resonance Acoustic Scattering from Stacks of Bonded Elastic Plates," Acoustical Society of America Journal, Vol. 80, 1986, pp. 1762-1776.

7. Pekeris, C. L., "Theory of Explosive Sound in Shallow Water," in Propagation of Sound in the Ocean, Vol. , 1948, pp. 1-177.

8. Staal, P., "Acoustic Propagation Measurements with a Bottom Mounted Array," in Acoustics and the Sea-Bed, Bath University Press, United Kingdom, 1983.

9. Zhou, J., Zhang, X., and Rogers, P., "Effects of Frequency Dependence of Sea-Bottom Attenuation on the Optimum Frequency for Acoustic Propagation in Shallow Water," Acoustical Society of America Journal, Vol. 82, 1987, pp. 287-292.

10. Gershfeld, D. and Eller, A., "Geometric Considerations in Determining the Optimum Frequency of Acoustic Propagation in a Shallow Water Waveguide," Acoustical Society of America Journal, Vol. 78, 1985, pp. 632-641.

11. Ellis, D. D. and Chapman, D. M. F., "A Simple Shallow Water Propagation Model Including Shear Wave Effects," Acoustical Society of America Journal, Vol. 78, 1985, pp. 2087-2095.

REFERENCES (Cont.)

12. Ellis, D. D. and Chapman, D. M. F., Modelling of Shear-Wave Related Acoustic Propagation on the UK Continental Shelf, Defence Research Establishment Atlantic Technical Memorandum 84/P, Nova Scotia, Canada, 1984.

13. Officer, C. B., Introduction to the Theory of Sound Transmission With Application to the Ocean, McGraw-Hill, New York, NY, 1958.

14. Pedersen, M. A., "Acoustic Intensity Anomalies Introduced by Constant Velocity Gradients," Acoustical Society of America Journal, Vol. 33, 1961, pp. 465-474.

15. Brekhovskikh, L. M., Waves in Layered Media, Second Edition, Academic Press, New York, NY, 1980.

16. Tappert, F. D., "The Parabolic Approximation Method," in Wave Propagation and Underwater Acoustics, Springer-Verlag, NY, 1977.

17. Jensen, F. B. and Kuperman, W. A., "Sound Propagation in a Wedge-shaped Ocean with a Penetrable Bottom," Acoustical Society of America Journal, Vol. 67, 1980, pp. 1564-1566.

18. Lee, D. and Botseas, G., IFD: An Implicit Finite-Difference Computer Model for Solving the Parabolic Equation, NUSC TR 6659, CT, 1982.

19. Tappert, F. D. and Lee, D., "A Range Refracted Parabolic Equation," Acoustical Society of America Journal, Vol. 76, 1984, pp. 1797-1803.

20. McDaniel, S., "Propagation of Normal Mode in the Parabolic Approximation," Acoustical Society of America Journal, Vol. 57, 1975, pp. 307-311.

21. Etter, P. and Flum R., A Survey of Underwater Acoustic Models and Environmental-Acoustic Data Bases, ASWR-SO-115, ASW Systems Project Office, Sep 1980.

22. Etter, P., "Underwater Acoustic Modeling Techniques," Shock and Vibration Digest, Jan 1984, pp. 17-23.

23. Landers, T. and Claerbout, J., "Numerical Calculations of Elastic Waves in Laterally Inhomogeneous Media," Geophysical Journal, Vol. 77, 1972, pp. 1476-1483.

24. McCoy, J., "A Parabolic Theory of Stress Wave Propagation through Inhomogeneous Linearly Elastic Solids," Applied Mechanics Journal, Vol. 44, 1977, pp. 462-468.

25. Hudson, J., "A Parabolic Approximation for Elastic Waves," Wave Motion, Vol. 2, 1980, pp. 207-214.

REFERENCES (Cont.)

26. Corones, J., DeFacio, B., and Krueger, R., "Parabolic Approximations to the Time-Independent Elastic Wave Equation," _Mathematical Physics Journal_, Vol. 24, 1982, pp. 577-586.

27. Wales, S. and McCoy, J., "A Comparison of Parabolic Wave Theories for Linearly Elastic Solids," _Wave Motion_, Vol. 5, 1983, pp. 99-113.

28. Schmidt, H., _SAFARI: Seismo-Acoustic Fast field Algorithm for Range-Independent environments_, SACLANTCEN Report SR-113, Sep 1988.

29. Porter, M. and Reiss, E., "A Numerical Method for Ocean-Acoustic Normal Modes," _Acoustical Society of America Journal_, Vol. 76, 1984, pp. 244-252.

30. Porter, M. and Reiss, E., "A Numerical Method for Bottom Interacting Ocean Acoustic Normal Modes," _Acoustical Society of America Journal_, Vol. 77, 1985, pp. 1760-1767.

31. Pierce, A., "Extension of the Method of Normal Modes to Sound Propagation in an Almost-Stratified Medium," _Acoustical Society of America Journal_, Vol. 37, 1965, pp. 19-27.

32. Pierce, A., "Parametric Solution of the Dispersion Relation for Guided Sound Propagation in Shallow Water," _Acoustical Society of America Journal_, Vol. 39, 1966, pp. 1139-1141.

33. McDaniel, S., "Coupled Power Equations for Cylindrical Spreading Waves," _Acoustical Society of America Journal_, Vol. 60, 1976, pp. 1285-1289.

34. McDaniel, S., "Mode Conversion in Shallow-Water Sound Propagation," _Acoustical Society of America Journal_, Vol. 62, 1977, pp. 320-325.

35. McDaniel, S., "Calculation of Mode Conversion Rates," _Acoustical Society of America Journal_, Vol. 63, 1978, pp. 1372-1374.

36. Evans, R. B., "A Coupled Mode Solution for Acoustic Propagation in a Waveguide with Stepwise Depth Variations of a Penetrable Bottom," _Acoustical Society of America Journal_, Vol. 74, 1983, pp. 188-195.

37. Evans, R. B. and Gilbert, K. E., "The Periodic Extension of Stepwise Coupled Modes," _Acoustical Society of America Journal_, Vol. 77, 1985, pp. 983-988.

38. Evans, R. B., "The Decoupling of Stepwise Coupled Modes," _Acoustical Society of America Journal_, Vol. 80, 1986, pp. 1414-1418.

39. Graves, R. D., Nagl, A., Überall, H., and Zarur, G. L., "Range-Dependent Normal Modes in Underwater Sound Propagation: Application to the Wedge-Shaped Ocean," _Acoustical Society of America Journal_, Vol. 58, 1975, pp. 1171-1177.

REFERENCES (Cont.)

40. Graves, R. D., Nagl, A., Überall, H., and Zarur, G. L., "Normal Modes in a Sound Channel with Range Dependent Parabolic Sound Speed Profile," Acustica, Vol. 39, 1978, pp. 173-181.

41. Nagl, A., Chwieroth, F. S., Zarur, G. L., and Überall, H., A FORTRAN Code for the Calculation of Sound Propagation in a Range Dependent Ocean, Vols. I and II, Dept. of Physics, The Catholic University of America, Wash., D.C., 1979.

42. Miller, J. F., Nagl, A., and Überall, H., "Sound Propagation in a Range-Dependent Shallow Ocean with a Bottom containing Vertical Sound Speed Gradients," in Progress in Underwater Acoustics, Merklinger, H., Plenum Press, New York, NY, 1985, pp. 533-540.

43. Miller, J. F., Nagl, A., and Überall, H., "Upslope Sound Propagation through the Bottom of a Wedge-Shaped Ocean Beyond Cutoff," Acoustical Society of America Journal, Vol. 79, 1986, pp. 562-565.

44. Miller, J. F., Collins, M. D., Ali, H., Arvelo, J. I., Nagl, A., and Überall, H., "Sound Penetration into a Sloping Ocean Floor," FASE Conference, Spain, Jun 1987.

45. Collins, M. D., Ali, H., Authement, M., Nagl, A., Überall, H., Miller, J. F., and Arvelo, J. I., "Low-Frequency Sound Interaction with a Sloping, Refracting Ocean Bottom," IEEE Ocean Engineering Journal, Vol. 13, Oct 1988, pp. 235-244.

46. Press, W. H., Flannery, B. P., Teukolsky, S. A., and Vetterling, W. T., Numerical Recipes, Cambridge University Press, New York, NY, 1986, pp. 269-273.

47. IMSL User's Guide, Version 1.0, Vol. 2, Apr 1987, p. 767.

48. Morris, A. H., NSWC Library of Mathematics Subroutines, NSWC TR 90-21, Jan 1990, NSWC, Dalgren, VA, p. 353.

49. Skudrzyk, E., The Foundations of Acoustics, Springer-Verlag, New York, NY, 1971.

50. Hamilton, E., "Geoacoustic Modeling of the Sea Floor," Acoustical Society of America Journal, Vol. 68, 1980, pp. 1313-1340.

51. Boyles, C. A., Acoustic Waveguides: Applications to Oceanic Science, Wiley & Sons, New York, NY, 1984.

52. Aki, K. and Richards, P. G., Quantitative Seismology, Theory and Methods, W. H. Freeman & Co., New York, NY, 1980.

53. Miller, J. F., Range-Dependent Normal-Mode Calculations of Acoustic Propagation in the Ocean including Effects of Layered-bottom Penetration, Ph.D. Dissertation, Catholic University of America, 1985.

REFERENCES (Cont.)

54. Abramowitz, M. and Stegun, I. A., _Handbook of Mathematical Functions_, National Bureau of Standards, 1964, pp. 446-450.

55. Gordon, R. G., "New Method for Constructing Wavefunctions for Bound States and Scattering," _Chemical Physics Journal_, Vol. 51, 1968, pp. 14-25.

56. Gordon, R. G., "Quantum Scattering Using Piecewise Analytic Solutions," _Mathematical Physics Journal_, Vol. 9, 1968, pp. 81-109.

57. Schulten, Z., Anderson, D. G. M., and Gordon, R. G., "An Algorithm for the Evaluation of the Complex Airy Functions," _Computational Physics Journal_, Vol. 31, 1979, pp. 60-75.

58. Jensen, F. B., "Wave Theory Modeling: A Convenient Approach to CW and Pulse Propagation Modeling in Low-Frequency Acoustics," _IEEE Ocean Engineering Journal_, Vol. 13, Oct 1988, pp. 186-197.

59. Chapman, N. R., Stinson, K., Levy, S., Cabrera, J., and Oldenburg, D. W., "Estimation of the Elastic Properties of Seafloor Sediments by Inversion of Precritical Reflection Data," _IEEE Ocean Engineering Journal_, Vol. 13, Oct 1988, pp. 215-221.

60. Ellis, D. D., _A Two-Ended Shooting Technique for Calculating Normal Modes in Underwater Acoustic Propagation_, DREA Report 85/105, Sep 1985, Nova Scotia, Canada.

61. Werby, M. F. and Tango, G. J., "Characterization of Average Geoacoustic Bottom Properties from Expected Propagation behavior at Very Low Frequencies (VLF) using a Towed Array Simulation," _Ocean Seismo-Acoustics_, Plenum Press, New York, NY, Jun 1985, pp. 881-889.

62. Otsubo, H., Ohta, K., and Ozati, S., "Normal-Mode Solution in the Ocean with Absorbing Bottom Sediments which have a Sound-Speed Gradient," _Acoustical Society of Japan Journal_, Vol. 1, 1980, pp. 47-57.

63. Viktorov, I. A., _Rayleigh and Lamb Waves_, Plenum Press, New York, NY, 1967.

64. Überall, H., "Surface Waves in Acoustics," _Physical Acoustics_, Vol. 10, Academic Press, New York, NY, Mason, W. P. and Thurston, R. N., Eds., 1973, pp. 1-60.

65. Jackins, P. D., Gaunaurd, G. C., and Arvelo, J. I., "Resonance Reflections from a Stratified Ocean Bottom," _Acoustical Society of America Journal_, Vol. 80, 1986, p. 116.

66. Hamilton, E., "Sound Velocity as a Function of Depth in Marine Sediments," _Acoustical Society of America Journal_, Vol. 78, 1985, p. 1348.

REFERENCES (Cont.)

67. Hamilton, E., "Sound Velocity Gradients in Marine Sediments," Acoustical Society of America Journal, Vol. 65, 1979, p. 909.

68. Hamilton, E., "Shear-Wave Velocity versus Depth in Marine Sediments: A Review," Geophysics, Vol. 41, 1976, p. 985.

69. Hamilton, E., "Sound Attenuation as a Function of Depth in the Sea Floor," Acoustical Society of America Journal, Vol. 59, 1976, p. 528.

70. Hamilton, E., "Attenuation of Shear Waves in Marine Sediments," Acoustical Society of America Journal, Vol. 60, 1976, p. 334.

71. Hamilton, E., "Geoacoustic Modeling of the Sea Floor," Acoustical Society of America Journal, Vol. 68, 1980, p. 1313.

72. Shirley, D. and Hampton, L., "Shear-Wave Measurements in Laboratory Sediments," Acoustical Society of America Journal, Vol. 63, 1978, p. 607.

73. Brunson, B. and Johnson, R., "Laboratory Measurements of Shear Wave Attenuation in Saturated Sand," Acoustical Society of America Journal, Vol. 68, 1980, p. 1371.

74. Kuperman, W. and Ingenito, F., "Attenuation of the Coherent Component of Sound Propagation in Shallow Water with Rough Boundaries," Acoustical Society of America Journal, Vol. 61, 1977, pp. 1178-1187.

DISTRIBUTION

	Copies		Copies
Office of Naval Research Attn: Code 1122 800 N. Quincy St., BCT#1 Arlington, VA 22217	1	Defense Advanced Research Project Agency 1400 Wilson Blvd. Arlington, VA 22209	1
Naval Underwater Systems Center Attn: Library New London, CT 06320	1	Defense Technical Information Center Cameron Station Alexandria, VA 22314	12
Superintendent Naval Postgraduate School Attn: Library Monterrey, CA 93940	1	Library of Congress Attn: Gift and Exchange Division Washington, DC 20540	4
Naval Underwater Systems Center Attn: Library Newport, RI 02841-5047	1	Internal Distribution: E231 E232	2 3
Naval Ocean Systems Center Attn: Library San Diego, CA 92152	1	E342 (GIDEP) R04 (C. Dickinson) U (B. Gay) U02 (J. Goeller)	1 1 1 1
Naval Air Development Center Attn: Library Warminster, PA 18974	1	U04 (M. Stripling) U20 (C. Kalivretenos) U202 (T. Ballard) U25 (J. Sherman)	1 1 1 1
Naval Coastal Systems Center Attn: Library Panama City, FL 32401	1	U25 (D. Watts) U25 (J. Arvelo) U25 (S. Hebbert)	1 10 1
Naval Research Laboratory Attn: Library Washington, DC 20390	1		
Naval Sea Systems Command Attn: Library Washington, DC 20362	1		